Chapter 8
Field Injection Operations and Monitoring of the Injected CO_2

Auli Niemi, Jacob Bensabat, Peter Bergmann, Christopher Juhlin, Alexandru Tatomir, Iulia Ghergut, Martin Sauter, Barry Freifeld, Larry Myer, Christine Doughty, Axel Liebscher, Stefan Lüth, Sonja Martens, Fabian Möller, Cornelia Schmidt-Hattenberger and Martin Streibel

Abstract Monitoring the fate of the injected CO_2 and possible associated effects, such as hydro-mechanical and chemical effects in the target reservoir and its surroundings, is essential for safe operation of a storage facility. In this chapter, we shall first provide an overview of the technologies available and used for monitoring of CO_2. We shall then proceed to describe specific methods and finally present some important case studies that will demonstrate the use of the discussed monitoring technologies under specific field settings.

A. Niemi (✉) · C. Juhlin
Department of Earth Sciences, Uppsala University, Villavägen 16, 75236 Uppsala, Sweden
e-mail: auli.niemi@geo.uu.se

C. Juhlin
e-mail: christopher.juhlin@geo.uu.se

J. Bensabat
Environmental and Water Resources Engineering Inc., P.O. Box 6770, 31067 Haifa, Israel
e-mail: jbensabat@ewre.com

P. Bergmann · A. Liebscher · S. Lüth · S. Martens · F. Möller · C. Schmidt-Hattenberger · M. Streibel
Helmholtz Centre Potsdam, GFZ German Research Centre for Geosciences, Section Geological Storage, Telegrafenberg, Potsdam 14473, Germany
e-mail: alieb@gfz-potsdam.de

A. Liebscher
e-mail: alieb@gfz-potsdam.de

S. Lüth
e-mail: alieb@gfz-potsdam.de

S. Martens
e-mail: sonja.martens@gfz-potsdam.de

F. Möller
e-mail: fabian.moeller@gfz-potsdam.de

C. Schmidt-Hattenberger
e-mail: cornelia.schmidt-hattenberger@gfz-potsdam.de

A. Niemi et al. (eds.), *Geological Storage of CO_2 in Deep Saline Formations*,
Theory and Applications of Transport in Porous Media 29,
DOI 10.1007/978-94-024-0996-3_8

8.1 Background on Monitoring

Monitoring the fate of the injected CO_2 and possible associated effects, such as hydro-mechanical and chemical effects in the target reservoir and its surroundings, is essential for safe operation of a storage facility. NETL (2012) report on 'Best Practices for Monitoring, Verification and Accounting of CO_2 Stored in Deep Geological Formations' divides monitoring in three sub-groups, according to the domain where the monitoring is taking place and defines them as follows:

Atmospheric monitoring aims at measuring CO_2 density and flux in the atmosphere, to detect any possible leaks. The tools that are used are optical CO_2 sensors, atmospheric tracers and eddy covariance (EC) flux measurements.

Near-surface monitoring measures CO_2 and its effects in the zone ranging from the top of the soil down to the shallow groundwater. Tools include geochemical monitoring (in soil, vadose zone and shallow groundwater), surface displacement monitoring tools and ecosystem stress (e.g. changes in vegetation due to increased CO_2 fluxes) monitoring tools. The latter two are commonly measured by satellite-based remote sensing tools.

Subsurface monitoring where tools are used to detect and quantify the injected CO_2 in the subsurface, as well as the related effects of e.g. seismic activity, as well as to detect faults and fractures. The monitoring tools include well logging, downhole monitoring, fluid sampling including tracer analysis, seismic imaging, high-precision gravity methods and electrical techniques.

NETL (2012) also gives thorough discussions, general as well as case-specific, concerning these methods and their benefits and challenges. Here we will only present the summary tables, giving the description, benefits and challenges for each

A. Tatomir · I. Ghergut · M. Sauter
Angewandte Geologie, Universität Göttingen, Goldschmidtstr. 3, 37077 Göttingen, Germany
e-mail: alexandru.tatomir@geo.uni-goettingen.de

I. Ghergut
e-mail: iulia.ghergut@geo.uni-goettingen.de

M. Sauter
e-mail: Martin.Sauter@geo.uni-goettingen.de

B. Freifeld · L. Myer · C. Doughty
Lawrence Berkeley National Laboratory, 1 Cyclotron Road, Berkeley, CA 94720, USA
e-mail: bmfreifeld@lbl.gov

L. Myer
e-mail: lmyerco2@gmail.com

C. Doughty
e-mail: cadoughty@lbl.gov

Table 8.1 Summary of atmospheric monitoring techniques (adapted from NETL 2012)

Monitoring Technique	Description, benefits, and challenges
Optical CO_2 sensors	Description: sensors for measurement of CO_2 in air
	Benefits: relatively inexpensive and portable
	Challenges: difficult to distinguish release from natural variations and to provide continuous measurements over large areas
Atmospheric tracers	Description: natural and injected chemical compounds monitored in air to detect CO_2 released to the atmosphere
	Benefits: used as a proxy for CO_2, when direct observation of a CO_2 release is not adequate. Also used to track potential CO_2 plumes
	Challenges: In some cases, analytical equipment is not available onsite, and samples need to be analyzed offsite. Background/baseline levels need to be established
Eddy covariance	Description: flux measurement technique to measure atmospheric CO_2 at a specified height above the ground surface
	Benefits: can provide continuous data, averaged over both time and space, over a large area.
	Challenges: specialized equipment and robust data processing required. Natural variability in CO_2 flux may mask the signal

methodology, Table 8.1 is for the atmospheric monitoring, Table 8.2 for the near-surface monitoring and Table 8.3 for the subsurface monitoring. It should be noted that these tables do not include monitoring in off-shore situations where monitoring at seabed is also included, such as in the case of the Sleipner site.

Carbon Sequestration Leadership Forum (CSLF 2013) summarizes the monitoring techniques used in some major storage projects (Table 8.4). Inspection shows that practically all sites monitor well-head pressure and temperature. After that, most used are seismic surveys (2D/3D), downhole pressure and temperature monitoring, fluid sampling and observation wells. Several sites have also seismic downhole (VSP, Crosshole) monitoring, InSAR, soil gas sampling, and atmospheric CO_2 measurements. Microseismic observations and tracers are used in five cases. Other methods are used in four or fewer of the listed projects.

International Energy Agency Greenhouse Gas Control (IEAGHG 2013) reviews a number of test injection projects, summarizes the experiences and based on them, gives suggestions for best practices. Data from altogether 45 small scale projects and 43 large scale projects were compiled. The monitoring techniques used in the small scale projects are summarized in Table 8.5. The method classification somewhat differs from the one used by CSLF above. Inspection of the data in Table 8.5 shows that in these smaller scale, more research oriented projects, reflection seismic, downhole seismic, pressure logging and coring is used in 100 % of the projects. Almost all projects (90 %) use also thermal logging, wireline logging, geological model and reservoir modeling, and 80 % uses some type of geochemical analysis. These are followed by groundwater monitoring (70 %),

Table 8.2 Summary of near-surface monitoring techniques (adapted from NETL 2012)

Monitoring technique	Description, benefits, and challenges
Geochemical monitoring in the soil and vadose zone	Description: sampling of soil gas for CO_2, natural chemical tracers, and introduced tracers. Measurements are made with sensors inserted into the soil and/or with opaque flux accumulation chambers placed on the soil surface
	Benefits: soil-gas measurements detect elevated CO_2 concentrations above background levels and provide indications of releases. Tracers aid in identification of native versus injected CO_2. Opaque flux chambers can quickly and accurately measure local CO_2 fluxes from soil to air
	Challenges: significant effort for null result. Relatively late detection of release. Considerable effort is required to avoid cross-contamination of tracer samples. Flux chambers provide measurements for a limited area
Geochemical monitoring of shallow groundwater	Description: geochemical sampling of shallow groundwater above CO_2 injection zone to demonstrate integrity of freshwater formations. Chemical analyses may include pH, alkalinity, electrical conductivity, carbon, hydrogen, oxygen, and tracers
	Benefits: mature technology, samples collected with shallow monitoring wells. Early detection may be possible
	Challenges: significant effort for null result. Carbon isotopes are difficult to interpret due to complex dynamics of carbonate dissolution in shallow formations
Surface displacement monitoring (includes remote sensing)	Description: monitor surface deformation caused by reservoir pressure changes associated with CO_2 injection. Measurements made with satellite-based radar (SAR/InSAR) and surface- and subsurface-based tiltmeters and GPS instruments. Data allow modeling of injection-induced fracturing and volumetric change in the reservoir
	Benefits: highly precise measurements over a large area (100 km $\times$ 100 km) can be used to track pressure changes in the subsurface associated with plume migration. Tiltmeter technology is mature, and has been used successfully for monitoring steam/water injection and hydraulic fracturing in oil and gas fields. GPS measurements complement InSAR and tiltmeter data
	Challenges: InSAR methods work well in locations with level terrain, minimal vegetation, and minimal land use, but must be modified for complex terrain/varied conditions. Tiltmeters and GPS measurements require surface/subsurface access and remote data collection

(continued)

Table 8.2 (continued)

Monitoring technique	Description, benefits, and challenges
Ecosystem stress monitoring (includes remote sensing)	Description: satellite imagery, aerial photography, and spectral imagery are used to measure vegetative stress resulting from elevated CO_2 in soil or air
	Benefits: Imaging techniques can cover large areas. Vegetative stress is proportional to soil CO_2 levels and proximity to CO_2 release
	Challenges: Detection only possible after sustained CO_2 emissions have occurred. Shorter duration release may not be detectable. Natural variations in site conditions make it difficult to establish reliable baseline. Changes not related to CO_2 release can lead to false positives

Table 8.3 Summary of sub-surface monitoring techniques (adapted from NETL 2012)

Monitoring technique	Description, benefits, and challenges
Well logging tools	Description: mature technology used to monitor the wellbore and near-wellbore environment. Logs include porosity, density, acoustic, optical, gamma ray, resistivity imaging, borehole diameter logging, and pulsed neutron capture
	Benefits: easily deployed technology used to detect wellbore release and changes in near-wellbore fluid or formation composition
	Challenges: area of investigation limited to near the wellbore. Sensitivity of tool to fluid change may vary. Some tools are not sensitive to dissolved or mineralized CO_2. Workover fluids may affect log results
Downhole monitoring tools	Description: technology used to monitor CO_2 injection, reservoir conditions, wellbore conditions, CO_2 breakthrough at observation wells; also used to differentiate between CO_2 and brine
	Benefits: indirect and direct measurements of CO_2 transport. Pressure sensors useful for monitoring wellbore mechanical integrity and detecting CO_2 releases. Downhole temperature monitoring data could be used as inputs for history-matching simulation models. Flow meters monitor fluid flow conditions throughout the injection site
	Challenges: sensors need to have little drift over a long time span. Sensors and meters require specific calibrations to conform to regulations
Subsurface fluid sampling and tracer analysis	Description: technology used to monitor changes in the composition of fluids at observation wells and for characterizing CO_2 transport, reactions, dissolution, and subsurface dispersion
	Benefits: Provides information on fluid geochemistry, CO_2 transport properties, and CO_2 saturation to estimate mass balances and distribution of CO_2 in the subsurface
	Challenges: cannot image CO_2 migration and release directly. Only near-well fluids are measured

(continued)

Table 8.3 (continued)

Monitoring technique	Description, benefits, and challenges
Seismic methods	Description: reflection seismic uses acoustic properties of geologic formations and pore fluids to image geologic layers and plume migration in the subsurface. Passive seismic detects microseismic events in the subsurface and can provide information on fluid movement in a formation
	Benefits: reflection seismic is useful for time-lapse monitoring of a CO_2 plume, and possibly for out-of-zone CO_2 migration indicating a release. Borehole seismic (crosswell, VSP) surveys can provide high-resolution imaging of the plume near the wellbore. Passive seismic can be used to detect natural and induced seismicity, to map faults and fractures in the injection zone and adjacent horizons, and to track the migration of the fluid pressure front during and after injection
	Challenges: geologic complexity and a noisy recording environment can degrade or attenuate surface seismic data. Two-dimensional seismic surveys may not detect out-of-plane migration of CO_2. Borehole seismic methods require a wellbore for monitoring, and careful planning is required to integrate these with other surveys. Microseismic monitoring detects fracturing and faulting events that may result from CO_2 injection, but a comprehensive knowledge of reservoir geomechanical properties is needed to properly interpret these events
Gravity	Description: use of gravity to monitor changes in density of fluid resulting from injection of CO_2
	Benefits: fluid density changes due to CO_2 releases or CO_2 dissolution can be detected, unlike seismic methods, which do not identify dissolved CO_2
	Challenges: limited detection and resolution unless gravimeters are located just above reservoir, which significantly increases cost. Noise and gravity variations (tides, drift) need to be eliminated to interpret gravity anomalies due to CO_2

atmospheric monitoring and observation well (60 %). Clearly different from the projects summarized in Table 8.4 that also includes large-scale industrial projects, none of these smaller test injections used InSAR according to this survey. The IEAGHG also gives a full list of monitoring techniques, but does not specify their use in various projects. The full list of individual monitoring techniques can be found on IEAGHG CO_2 Monitoring Technique Data Base.

In the following chapters we will discuss in more detail some essential monitoring techniques (Sects. 8.2, 8.3 and 8.4) as well as case studies, including monitoring experiences from some major large scale industrial projects (Sect. 8.5)

Table 8.4 Monitoring techniques used in some CO_2 injection projects (CSLF 2013)

Monitoring technology	Sleipner	Weyburn	In Salah	Snøhvit	K12-B	Otway	Ketzin	Decatur	Quest	Lacq	Aquistore
Seismic surface (2D/3D)	+	+	+	+		+	+	+	+		+
Seismic surface (3C/9C)		+									
Seismic downhole		+				+	+	+	+		+
Electrical surface	+						+				
Electrical downhole		+					+		+		
Gravity surface/seabed	+	+									+
Tiltmeters			+								+
Satellite interferometry (InSAR)		+	+				+	+	+		+
Downhole P, T		+		+	+	+	+	+	+	+	+
Continuous downhole temperature							+		+	+	
Acoustic seabed imaging	+			+							
Acoustic water column imaging	+										
Geophones								+			
Water column chemistry	+										
Seabed video (ROV/AUV)	+										
Soil gas		+	+			+	+	+		+	+
Surface gas flux		+	+			+		+		+	
Passive CO_2 detectors			+			+					
Ecosystem and biomarkers	+		+	+						+	
Microseismic (passive seismic)		+	+			+	+			+	

(continued)

Table 8.4 (continued)

Monitoring technology	Sleipner	Weyburn	In Salah	Snøhvit	K12-B	Otway	Ketzin	Decatur	Quest	Lacq	Aquistore
Observation wells		+	+		+	+	+	+	+		+
Tracers		+	+		+		+		+		
Microbiology			+				+				
Wireline logs			+		+		+				
Fluid samples		+	+		+	+	+	+	+	+	+
Atmospheric CO_2 mobile/spatial		+	+			+		+	+	+	
Atmospheric CO_2 flux tower		+	+			+				+	
Well head pressure	+	+	+	+	+	+	+	+	+	+	+
Temperature	+	+	+	+	+	+	+	+	+	+	+
Well integrity monitoring (EMIT, PMIT)					+				+		
Downhole camera log					+		+				

Table 8.5 Monitoring technologies used in 18 small-scale projects in saline aquifers as summarized by IEAGHG (adapted from IEAGHG 2013)

Monitoring technology	Percentage of projects using	Monitoring technology	Percentage of projects using
Downhole seismic	100	Thermal logging	90
Groundwater monitoring	70	Wireline logging	90
Soil monitoring	40	Observation well	60
Atmospheric monitoring	60	Geochemical	80
Biological monitoring	20	InSAR	0
Tracer analysis	40	Reservoir modeling	90
Electromagnetic	20	Coring	100
Gravity	0	Reflection seismic	100
Pressure logging	100	Geological model	90

as well as small-scale, more scientifically motivated projects Frio and Ketzin (Sects. 8.6 and 8.7).

8.2 Geophysical Methods

Peter Bergmann and Christopher Juhlin

8.2.1 Overview of Geophysical Methods

Geophysical methods allow for imaging of physical subsurface properties and provide an opportunity for the monitoring of geological CO_2 storage. The objective of any geophysical site monitoring is the development of a baseline model and following changes within it in space and time. Comprehensive site models contain information about the present geometrical structures and composition, such as rock types and pore fluids. Since these models are always simplified representations of reality, they also contain inherent uncertainties.

In order to correctly describe the evolution of these models, they continuously need to be updated with elementary models that are provided by individual survey techniques. This implies that a combination of different geophysical methods are a

prerequisite for monitoring the different properties of the models at a (as broad as possible) range of scales. Consequently, monitoring of geological CO_2 storage requires integrated multi-method concepts to allow for comprehensive site descriptions.

A vast number of reported studies underlines the capabilities of geophysical methods for subsurface monitoring. Although most of these studies have been carried out for near-surface hydrogeological purposes or hydrocarbon production, they are of great relevance for CO_2 storage monitoring since many of their methodical and practical aspects are similar. In addition, there are also a number of studies which address CO_2 storage monitoring in particular. The majority of these studies are based on ongoing/completed CO_2 injection projects, such as those located in Norway (Sleipner and Snøhvit), Canada (Weyburn), USA (Frio), Australia (Otway), Japan (Nagaoka), and Algeria (In Salah) and Germany (Ketzin).

These projects are located in diverse environments, concerning factors such as storage depth, reservoir system, reservoir use, pressure and temperature conditions. This variability also results in that different combinations of geophysical methods have been used for monitoring, most of which include seismics and borehole logging, but also electromagnetics and gravity surveying (e.g. Michael et al. 2010). All of these methods provide a certain range of resolution and sensitivity, underlining the importance of using a combination of methods. There are also cases where geophysical methods do not deliver sufficient information or even fail. Therefore, several research initiatives have been initiated (e.g. SACS, CO_2STORE, IEAGHG Monitoring Network, CASTOR, CO_2GeoNet, CO_2ReMoVe, CO_2 Capture Project) in order to compile the gained experiences into best-practice guidelines and to support the definition of regulatory frameworks. Interestingly, these initiatives consistently agree on that monitoring is indeed site-specific, but that is it always needs to be comprised of multi-method geophysical programs.

In this review we focus on two geophysical methods, seismic and geo-electric. Other methods, such as electromagnetic, gravity, passive seismic and InSar, may also be used, but currently it is mainly seismic and geo-electric methods that are being applied at CO_2 storage sites and, therefore, the focus is on these. Even within the fields of applied seismic and geo-electric there is significant research ongoing. The use of sparser arrays to reduce costs, permanent sources and sensors, active seismic interferometry, downhole methods (including fibreoptics) and advanced processing methods are all being tested and their use should eventually provide higher resolution images or allow larger volumes to be investigated without increased cost. Faults and other features can potentially be mapped in greater detail and better geological models produced. The ability to repeat measurements on shorter time scales than what is commonly done with, for example, 3D reflection seismic surveys may also help to better understand CO_2 plume evolution and allow better integration of geophysical results with hydrogeological modeling. However, in the present review we have chosen to focus on the basic principles behind seismic and geo-electric methods that are currently being employed. Furthermore, we refer to the Ketzin site (see Sect. 8.7) to illustrate how changes in physical properties will influence the geophysical response. Note that all CO_2 storage sites

will most likely have site specific rock properties and that thorough investigations are required before making predictions on the seismic and geo-electric response at an individual site to CO_2 injection.

8.2.2 Seismic Methods

8.2.2.1 Theory

The basis of the reflection seismic method is the controlled activation and measurement of elastic wave fields. Waves which are reflected back to the surface convey information about geologic structures, since the reflections are due to discontinuities in elastic parameters (Fig. 8.1). Wave field properties that are valuable in this context are travel time, amplitude, frequency content, and phase. In the following, the focus will be on the amplitude, because it is the most important property that is monitored in time lapse surveys.

Assume that a compressional wave (P-wave) hits a layer with the wavefront perpendicular to the boundary (normal incidence, $\theta = 0$ in Fig. 8.1), the amplitude coefficients for reflection and transmission are given by (e.g. Kearey et al. 2002)

$$R = \frac{V_2\rho_2 - V_1\rho_1}{V_2\rho_2 + V_1\rho_1} \quad T = \frac{-2\,V_1\rho_1}{V_2\rho_2 + V_1\rho_1} \tag{8.2.1}$$

Here, V_1, V_2 and ρ_1, ρ_2 denote the P-wave velocities and densities in the upper and lower layer, respectively. In this nomenclature, the wave is propagating from within the first layer towards the second layer. The normal incidence assumption implies that a source and a receiver are located on the surface of the first layer at identical position (zero-offset). The receiver will then measure the amplitude of the reflected wave at the zero-offset two-way-traveltime (TWT), which corresponds to the wave propagating forward and backward along the same ray path.

Typically, seismic acquisition is performed at finite offset ($\theta \neq 0$ in Fig. 8.1), which gives rise to two implications: First, forward and backward propagation of a reflected wave will occur along different ray paths. Consequently, the travel time

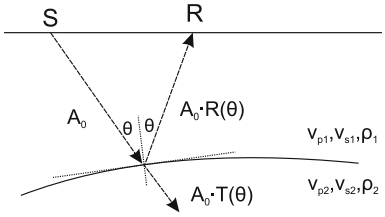

Fig. 8.1 Schematic illustration of a wave propagating from a source location S to a receiver location R after being reflected at an interface. A_0 denotes the amplitude of the wave impinging the interface. R(θ) and T(θ) denote the proportions of A_0 that are reflected and transmitted, respectively

will likely differ from that of a zero-offset ray. Assuming an isotropic medium with horizontal or moderately dipping layers, the onset time of a reflection will be increasing with increasing source-receiver offset. The offset-traveltime relation can then be approximated by hyperbolic functions which define the normal moveout (NMO) of the reflection onsets (Yilmaz 2001). Secondly, acquisition at finite offsets leads to reflections at non-normal incidence, which makes it necessary to consider R for an arbitrary angle of incidence θ. Most often, such a case leads to conversion of P-waves to (vertically polarized) shear waves (S-waves), which implies an equation system that requires knowledge of the P-wave velocities in the upper and lower layers (Vp_1, Vp_2) and the respective S-wave velocities (Vs_1, Vs_2) in order to calculate the reflection and transmission coefficients. The reflection and transmission angles are determined by Snell's law. Respective amplitudes are specified by the Zoeppritz equations (Zoeppritz 1919), which can be derived from the requirement of continuity of displacement and stress at the reflecting interface. Application of the Zoeppritz equations has now become common practice to analyze for so-called amplitude-versus-offset (AVO), or amplitude-versus-angle (AVA), responses to quantitatively assess the elastic properties of the media (Castagna and Backus 1993). Due to the inherent complexity of the Zoeppritz equations, a number of approximations have been introduced to allow for more convenient calculations (e.g. Aki and Richards 1980; Bortfeld 1961; Shuey 1985; Wang 1999). Aki and Richards (1980) presented the following 3-term approximation for layers with small contrasts in elastic properties (see Mavko et al. 2003).

$$R_{pp}(\theta) \approx A + B\sin^2(\theta) + C\tan^2(\theta)\sin^2(\theta) \tag{8.2.2}$$

In the following, only the P-wave reflection from an incident P-wave is discussed, the most common seismic wave that is recorded, and which is indicated by the notation R_{pp}. The angular reflection coefficients A, B and C are (Mavko et al. 2003)

$$A = \frac{1}{2}\left(\frac{\Delta V_p}{\langle V_p \rangle} + \frac{\Delta \rho}{\langle \rho \rangle}\right) \tag{8.2.3}$$

$$B = \frac{1}{2}\frac{\Delta V_p}{\langle V_p \rangle} - 2\left(\frac{V_s}{Vp}\right)^2\left(\frac{\Delta \rho}{\langle \rho \rangle} + \frac{\Delta V_s}{\langle V_s \rangle}\right) \tag{8.2.4}$$

$$C = \frac{1}{2}\frac{\Delta V_p}{\langle V_p \rangle} \tag{8.2.5}$$

with the following contrasts and averages across the interface

$$\Delta V_p = Vp_2 - Vp_1 \quad \langle V_p \rangle = \frac{Vp_1 + Vp_2}{2} \tag{8.2.6}$$

$$\Delta V_s = Vs_2 - Vs_1 \quad \langle V_s \rangle = \frac{Vs_1 + Vs_2}{2} \tag{8.2.7}$$

$$\Delta \rho = \rho_2 - \rho_1 \quad \langle \rho \rangle = \frac{\rho_1 + \rho_2}{2} \tag{8.2.8}$$

A, B and C can be interpreted in terms of different angle ranges (Castagna and Backus 1993). The term A dominates at small angles (near-offsets) and approximates, again assuming small contrasts, the normal-incidence reflection coefficient (Mavko et al. 2003). The terms B and C dominate at intermediate and large angles (near the critical angle), respectively. In practice, C is often neglected, since common acquisition geometries provide reflection data mostly at small and intermediate angles. This leads to a linearized form of the equation, in which A is the so-called AVO intercept and B the AVO gradient.

Practical AVO analysis is most commonly carried out by crossplots of A and B, which are used to analyze background trends and search for deviations from them (Ross 2000). For example, the reservoir sandstone where CO_2 is stored at Ketzin shows lower wave velocities and density than the caprock mudstones (Norden et al. 2010), a fact that leads to a negative AVO gradient and a negative AVO intercept. This is also illustrated by the single interface reflection coefficients in Fig. 8.2. However, it is important to recognize that the Ketzin reservoir is of sub-wavelength thickness, which generally poses additional implications on the normal incidence amplitude (e.g. Gochioco 1991; Meissner and Meixner 1969; Widess 1973) and the AVO response (e.g. Bakke and Ursin 1998; Juhlin and Young 1993; Liu and Schmitt 2003). For instance, if the contrasts in elastic properties of reservoir and surrounding rocks increase the main assumption of the AVO equation becomes increasingly invalid. Moreover, the AVO response cannot adequately be approximated by the superposition of the reflections off the top of the layer and off the bottom of the layer only. In such a case interbed multiples and conversions also have to be taken into account (Meissner and Meixner 1969). Based on the Ketzin reservoir model of Kazemeini et al. (2010), Fig. 8.2 illustrates the difference in the AVA response for the reservoir represented by a single boundary and a sub-wavelength layer.

8.2.2.2 Seismic Rock Physics

Seismic wave velocities are governed by the elastic moduli of the rocks they propagate through and their density. The elastic moduli and densities correspond to the whole rock and depend both on the rock matrix properties as well as the properties of the fluids or gases filling the pore space. P-wave (V_p) and S-wave (V_s) velocities are governed by the bulk modulus, K, the shear modulus, G, and the density.

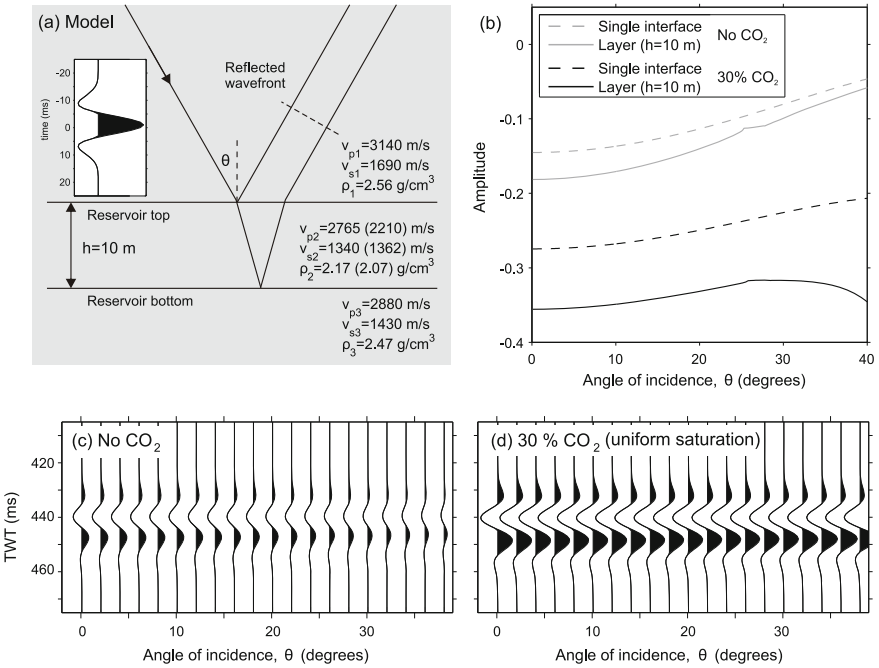

Fig. 8.2 Modeled AVA reflectivity of a thin layer with Ketzin reservoir parameters after Kazemeini et al. (2010) as input model. **a** The input model comprises a single layer representing the reservoir. Modeling was performed with the input model before CO_2 injection (values without brackets) and after CO_2 injection (bracketed values). **b** AVA response of the reservoir top as a single interface and as a layer of 10 m thickness. Thin layer amplitudes were computed with the method of Juhlin and Young (1993) using the 50 Hz Ricker wavelet shown in **a**. Computations include first-order multiples and conversions, and use the Aki-Richards approximation after Guy et al. (2003). **c**, **d** Modeled AVA response of the 10 m layer for the 50 Hz Ricker wavelet. Note that the traces in **a**, **c**, **d** are drawn to the same amplitude scale

$$V_p = \sqrt{\frac{K + \frac{4}{3}G}{\rho}} \tag{8.2.9}$$

$$V_s = \sqrt{\frac{G}{\rho}} \tag{8.2.10}$$

The bulk modulus is defined by the relative volume change caused by an omni-directional confinement pressure. The shear modulus is defined by the relative shear displacement when a shear force is applied (e.g. Lay and Wallace 1995). As there is no restoring force for liquids and gases, their shear modulus is zero.

Injection of CO_2 into porous reservoir rock containing saline fluids will result in the replacement of some of the saline fluid by CO_2. The injection will also increase the pressure in the reservoir. Leakage from a deeper storage formation to shallower levels will result in similar changes in reservoirs at shallower levels. The replacement of saline fluid by CO_2 is referred to as fluid substitution and there are two models for how this replacement affects seismic velocities. These are the uniform saturation model (Gassmann 1951) and the patchy saturation model (Mavko et al. 2003). In both models only the bulk modulus and the density will change due to the replacement of fluid by gas, while the shear modulus is unaffected. This implies that there is very little change in the S-wave velocity when CO_2 is injected into the reservoir, but there will be large changes in the P-wave velocity. However, increased pore pressure in the reservoir caused by the injection will result in a decrease in the effective stress and thereby a decrease in both the bulk and shear modulus of the rock. This difference in behavior between changes in gas saturation and pore pressure can potentially be monitored with seismic methods (e.g. Landrø 2001).

The uniform saturation model gives the following change in bulk modulus (Gassmann 1951):

$$K_{uni} = K_d + \frac{\left(1 - \frac{K_d}{K_m}\right)^2}{\frac{\Phi}{K_f} + \frac{1-\Phi}{K_m} - \frac{K_d}{K_{m^2}}}, \tag{8.2.11}$$

where K is the bulk modulus of a rock saturated with a frictionless fluid of bulk modulus K_f, K_d is the frame bulk modulus (air-saturated rock), K_m is the matrix bulk modulus of the same rock, and Φ is the porosity.

The bulk modulus K_f of a water/CO_2 mixture after the rock is flooded with CO_2 can be calculated using Wood's equation (Wood 1941),

$$\frac{1}{K_f} = \frac{S_w}{K_w} + \frac{1 - S_w}{K_{CO_2}}, \tag{8.2.12}$$

where K_w and K_{CO_2} are, respectively, the bulk moduli of brine and CO_2, and S_w is the brine saturation fraction. Wood's equation is based on the uniform stress assumption for fluid mixtures.

On a fine scale, the Gassmann model assumes homogeneous mixing of both phases. However, if mixing is heterogeneous on a coarse scale, a passing wave causes local pore-pressure differences. Assuming that the mixing can be described by geometric patches, which themselves are homogeneously saturated, there will be pressure exchange between nearby patches (Mavko et al. 2003). On a larger scale, wave-induced pore-pressure differences should average to an equilibrated value. At a seismic wave frequency f, these pore pressure heterogeneities will equilibrate for scales smaller than the critical diffusion length L_c (Mavko et al. 2003):

$$L_c \approx \sqrt{\frac{kK_f}{f\eta}} \tag{8.2.13}$$

with k denoting the rock permeability and η the fluid viscosity. If the patches are sufficiently small ($<L_c$), the pore-fluid mixture can be represented by a single effective fluid, which is then considered to be uniformly saturated. If the patches are larger than L_c spatial fluctuations will tend to persist during the passage of seismic waves, a state which is referred to as non-uniform or patchy saturation (Mavko and Mukerji 1998). Patchy saturation can for example be caused by "fingering" of pore-fluids, which might result from spatial variations in wettability, permeability or shaliness (Asveth 2009). Yet, it is possible to describe the individual patches by separate Gassmann models.

The patchy saturation model gives the following change in bulk modulus via the Hill equation (Berryman and Milton 1991; Hill 1963):

$$K_{pat} = \frac{1}{\frac{S_w}{K_0 + \frac{4}{3}G} + \frac{1-S_w}{K_{100} + \frac{4}{3}G}} \quad - \quad \frac{4}{3}G, \tag{8.2.14}$$

where K_0 and K_{100} are the whole rock bulk moduli for 0 % CO_2 saturation and 100 % CO_2 saturation, respectively. In both the uniform and patchy models the density of the saturated rock is given by

$$\rho = \rho_d + \Phi\rho_f, \tag{8.2.15}$$

where ρ and ρ_d are, respectively, the fluid-saturated and dry densities of the rock, and ρ_f is the pore fluid's density. For a mixture composed of water and CO_2 it is determined with an arithmetic average of the separate fluid phases:

$$\rho_f = S_w * \rho_w + S_{CO_2} * \rho_{CO_2}, \tag{8.2.16}$$

where ρ_f is the mixture density, ρ_W and ρ_{CO_2}, and S_W and S_{CO_2} are, respectively, the densities and volume fractions (saturation) of water and CO_2.

Values for the different parameters can either be determined through lab experiments or by theoretical formulas. An online program to calculate fluid properties based on Batzle and Wang (1992) is available at:

www.crewes.org/ResearchLinks/ExplorerPrograms/FlProp/FluidProp.htm

Changes in P-wave and S-wave velocities due to a pore pressure increase may be modeled with second order curves with empirical constants to be determined (Landrø 2001).

$$\Delta V_p = \left(l_\alpha \Delta P + m_\alpha \Delta P^2\right) V_p \tag{8.2.17}$$

$$\Delta V_s = \left(l_\beta \Delta P + m_\beta \Delta P^2\right) V_s \tag{8.2.18}$$

For a hypothetical leak from reservoir depth with accumulation of CO_2 at 300 m depth into a high porosity sandstone the velocities as a function of CO_2 saturation for the uniform and patchy models are plotted in Fig. 8.3 Note the large difference predicted for velocity depending upon which model is assumed. Note also that the S-wave velocity only increases slightly in both models, due to the decrease in density as CO_2 enters the rock. A similar plot for an increase in pore pressure is shown in Fig. 8.4. Note that at 300 m depth pore pressure changes more than 2 MPa are unlikely without fracturing the formations. At greater depth, pore pressure changes due to injection can be significant without fracturing the formations.

8.2.2.3 Time-Lapse Seismics

Reflection seismic based time-lapse methods are the heart of all geophysical monitoring methods in sedimentary environments and, therefore, a very brief outline of reflection seismic processing is given here. Typical processing procedures comprise three main steps: (1) data preprocessing, (2) stacking, and (3) seismic migration (e.g. Yilmaz 2001). (1) The preprocessing aims to extract the

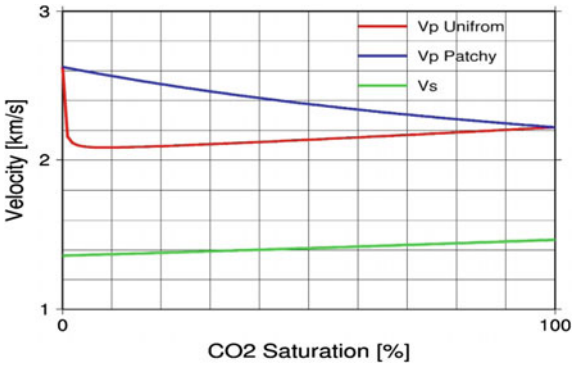

Fig. 8.3 P-wave and S-wave velocities for the uniform and patchy saturation models for a 30 % porosity sandstone at 300 m depth

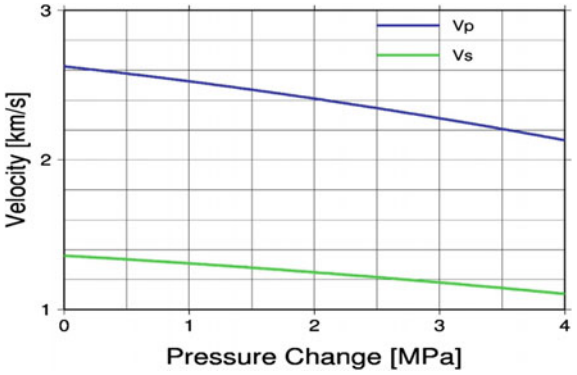

Fig. 8.4 P-wave and S-wave velocities as a function of increased pore pressure

relevant reflections out of the acquired seismograms. Common preprocessing steps are the muting and suppression (filtering) of undesired signals, deconvolution, and amplitude restoration. A further important step is the application of static corrections, which will be explained in more detail below. (2) Seismic stacking comprises resorting of traces into gathers and summation along time-offset trajectories which are defined by velocity model estimations. Most commonly, the traces are resorted into common-midpoint (CMP) gathers. Then, NMO corrections are applied on the basis of velocities that are extracted from velocity analyses in the CMP domain. These velocity analyses are typically carried out in alternation with residual static corrections until the velocity models sufficiently remove the NMO (Yilmaz 2001). Stacking is then completed with the summing of the NMO-corrected traces that belong to the same CMP gathers (Mayne 1962). The number of traces within a CMP gather is termed the fold, which is an indicator of the signal-to-noise improvement that can be obtained in the stacking procedure. Aside from the CMP stack there are also alternative stacking procedures, such as the methodically related common-reflection-element (CRE) stack (Gelchinsky 1988), multifocusing stack (Gelchinsky et al. 1999), or common-reflection-surface (CRS) stack (Jäger et al. 2001). (3) Seismic processing is typically finalized by migration which intends to relocate reflected energy to its true (temporal or spatial) position of origin. Seismic migration generally aims to overcome mis-positioning (e.g. image angle of dipping reflectors) and can be applied in the pre-stack or post-stack domain (see, e.g. Biondi 2006; Yilmaz 2001). In the latter case, migration is typically carried out in conjunction with dip-moveout (DMO) corrections before stacking, which then resembles a pre-stack migration scheme (Deregowski 1986).

The general objective of seismic processing is to modify acquired data into images that can be used for interpretation of subsurface structures. On this basis, time-lapse seismic aims for the detection of changes in the seismic response of the sub-surface by means of repeated data acquisition and processing. There are several metrics which are used to quantify the repeatability of seismic surveys, with the normalized-root-mean-square amplitude difference (NRMS) of (Kragh and Christie 2002) being the most commonly used. The NRMS of two traces a and b is given by

$$NRMS = 100\,\% \frac{RMS(a-b)}{0.5(RMS(a)+RMS(b))} \tag{8.2.19}$$

The NRMS measure ranges from 0 % for identical traces to 141 % for randomly uncorrelated traces, and up to 200 % for 180° out of phase traces (amplitude reversal). It is very sensitive to small changes between the two input traces, whether it is in the amplitude or phase (Domes 2010).

Beyond the impact of noise, there are a number of practical challenges to time-lapse seismic. In the case of onshore surveying, unforeseen acquisition obstacles usually occur. Although the fold reduction caused by these obstacles can be compensated for by relocating source and receiver locations (e.g. acquisition of data that will be binned into the same CMP bin at different offsets), a reduced experimental reproduction inevitably remains. Furthermore, wavelet reproducibility

may be limited. This is not only a matter of source technology, but also of source-ground coupling and changes in near-surface velocities (Kashubin et al. 2011). These complications need to be handled by cross-equalization of the frequency and phase characteristics (wavelet matching).

In addition, the seismic response also senses pressure changes (Eberhart-Phillips et al. 1989; Todd and Simmons 1972). It is obvious that time-lapse seismic interpretation for monitoring CO_2 injection must take this into consideration. In this context, Landrø (2001) introduced a method for discriminating the fluid and pressure response in time-lapse seismic data by exploiting the AVO response.

8.2.3 Geoelectric Methods

The geoelectric method, here also referred to as Electrical Resistivity Tomography (ERT), uses artificial electrical currents to investigate the distribution of electric resistivity within the subsurface. It serves as a complementary method to seismic methods, and its application to CO_2 storage monitoring is motivated by the expected change in rock resistivity when electrically well conductive brine is substituted by insulating CO_2 (Christensen et al. 2006; Nakatsuka et al. 2010).

8.2.3.1 Theory

Geoelectrics uses diffusive electric fields, as opposed to propagating wave fields as in most seismic applications, which obey Poisson's equation (e.g. Telford et al. 1990)

$$\nabla \cdot \left(\frac{1}{\rho} \nabla \Phi \right) = -I\delta(\vec{r} - \vec{r}_s) \tag{8.2.20}$$

It entails that electric current flow, I, is determined by the spatial arrangement of electrical sources (and sinks) as well as the distribution in electric resistivity ρ. Both factors specify the electric potential ϕ, to which the gradient of the current flow aligns. The right hand side of the equation places an infinitesimal source (represented by Dirac's delta) at r_s, releasing an electric current I. If this source would be located on a perfectly uniform half-space with a resistivity of ρ_0, the potential would be given by

$$\Phi(\vec{r}) = I \frac{\rho_0}{|\vec{r} - \vec{r}_s|} \tag{8.2.21}$$

A combination of current sources can be given by the superposition of their individual potential distributions. Due to the conservation of electric charge, the practical field experiment is typically carried out by a current circuit, which is

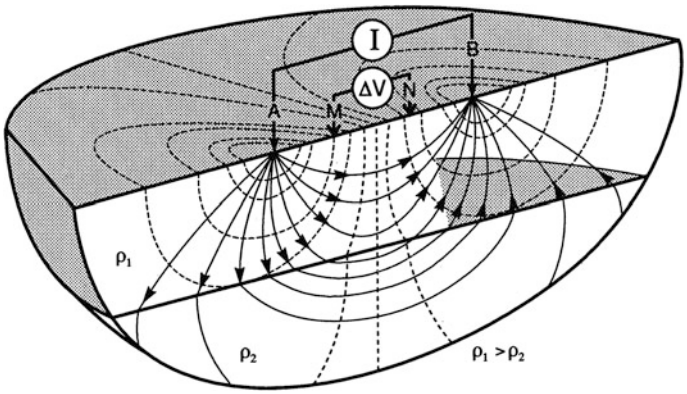

Fig. 8.5 Schematic illustration of a four-point electrode arrangement after Lange (1997). Current flow lines (*solid*) and equipotential lines (*dashed*) are given for a two-layer case with higher resistivity in the first layer

realized through a pair of current electrodes (A and B). An additional pair of potential electrodes (M and N) are used to measure spatial differences in ϕ, i.e. the electric voltage U. This so-called four-point layout is schematically illustrated in Fig. 8.5.

Geoelectric surveying is commonly performed by using multiple pairs of current electrodes and voltage electrodes with an aim to achieve a dense sampling of the imaging target. From the injected current I and the measured voltage, U, a resitance, R, can be calculated. This resistance has a strong dependence on the geometrical arrangement of the electrodes. Using a uniform half-space again, it is possible to compute geometrical correction factors, k, which convert readings of R into apparent resistivity values ρ_{app} by

$$k\frac{\Phi(\vec{r}_2)-\Phi(\vec{r}_1)}{I}=k\frac{U}{I}=kR=\rho_{app} \tag{8.2.22}$$

The apparent resistivity represents a weighted mean of the actual resistivity distribution $\rho(r)$. For ERT, the apparent resistivities provide the starting point for assessing the earth's true resistivity by means of inverse procedures. If the electrodes are placed on the surface, the geometric factor k is (e.g. Kearey et al. 2002)

$$k=\frac{4\pi}{\frac{1}{\overline{AM}}-\frac{1}{\overline{AN}}-\frac{1}{\overline{BM}}+\frac{1}{\overline{BN}}} \tag{8.2.23}$$

For current injections below the surface, e.g. electrodes in wells, the positions of the mirrored current electrodes A' and B' also have to be taken into account

$$k = \frac{4\pi}{\frac{1}{AM} + \frac{1}{A'M} - \frac{1}{AN} + \frac{1}{A'N} - \frac{1}{BM} + \frac{1}{B'M} - \frac{1}{BN} + \frac{1}{B'N}} \tag{8.2.24}$$

8.2.3.2 Geoelectric Rock Physics

Electrolytic ion transport is the most efficient conduction mechanism in fluid-filled sedimentary materials, in particular for those which are filled with highly saline brines. The efficiency of the ion transport is determined by the ion concentration in the fluid and the connectivity of the pores (Kirsch 2006). To first-order, porous sediments can be viewed as a composite system comprising the mineral matrix and the pore space. Similarly to the previous discussion, the pore-space may be filled with brine or CO_2 or a mixture of both. Since the electrical resistivity of most matrix-building minerals is high, their contribution to electric current flow is generally neglected. Using this assumption, the empirical Archie equation (Archie 1942) specifies the rock resistivity ρ with regard to the CO_2 saturation S_{CO_2} as

$$\rho = \frac{A\rho_w}{\phi^m (1 - S_{CO_2})^n} \tag{8.2.25}$$

where ϕ now denotes the rock porosity and ρ_w the resistivity of the initially present brine. The porosity exponent m reflects the pore geometry, compaction and insulation effects due to possible pore-space cementation. The saturation exponent n accounts for the presence of non-conductive fluid in the pore space. The factor A reflects the current component being conducted through the matrix. Since A, m, and n are purely empirical parameters, they need to be determined on an experimental or statistical basis. In situations where such a basis is not given, estimates often have to be made from literature values. For instance, the saturation exponent n is reported to be in the range of 1.715 for unconsolidated sediments up to 2.1661 for sandstones (Lee 2011). The porosity exponent m is reported to vary between 1.8 and 2.1 for sediments (Waxman and Thomas 1974).

Archie-based resistivity models make two crucial assumptions: First, the pore-space mixture of brine and CO_2 is substituted with a virtual equivalent fluid. Electric current flow, however, is affected by complicated geometrical considerations, such as shape and connectivity of the pores and the spatial distribution of these fluids within the pores. For example, Han et al. (2009) reported for fluid saturations <0.2, that the resistivity measured on clay-free sandstone can be notably lower than that predicted by Archie's law. They attributed this observation to liquid films that cover the rock grains and maintain considerable electric current flow even for very low fluid saturations. Secondly, the Archie equation assumes that electric current flow takes place solely within the pore-space. This is a severe simplification, because most sedimentary materials are also composed of conductive minerals, such as clay.

Impact of Clay Content on Rock Resistivity

Electric resistivity in clay-bearing geologic materials has been often studied (e.g. (Butler and Knight 1988; De Witte 1955; Poupon et al. 1954; Waxman and Thomas 1974) and various methods have been proposed to correct for the effect of clay on the formation resistivity (for an overview in the context of shaley sands see Worthington 1985). Frohlich and Parke (1989) extended the Archie equation to a parallel connection of the pore-space resistivity and the clay-related resistivity ρ_s

$$\frac{1}{\rho} = \frac{\phi^m (1 - S_{CO_2})^n}{A} \frac{1}{\rho_w} + \frac{1}{\rho_s} \tag{8.2.26}$$

In fact, ρ_s is also dependent on the clay content, *cc,* for which Rhoades et al. (1989) presented an empirical calibration (that yields ρ_s in Ohmm)

$$\frac{1}{\rho_s} = \sigma_s = 20.3cc - 00.021 \tag{8.2.27}$$

The Ketzin site can be used as an example of applying the Archie model as well as the Frohlich and Parke model to make first-order resistivity descriptions of the reservoir. Using an average clay content of about 20 % (Norden et al. 2010) within the reservoir units and assuming a porosity of 30 % a surface resistivity of 22.8 Ω is obtained from the Rhoades equation. In order to improve the choices of the remaining parameters, these can be adjusted by results from laboratory data. Based on two core samples from the Ketzin site, Kiessling et al. (2010) reported an average resistivity ρ_0 of about 0.5 Ω at full brine saturation. Still, A and m remain unknowns, but the ratio $\phi_m A^{-1}$, the so-called formation factor, can be considered as a single unknown. Thus, given experimental knowledge about ρ_w, ϕ and the rock's resistivity for full brine saturation ρ_0, any set of A and m can be chosen which satisfies

$$A(m) = \frac{\phi^m}{\rho_w} \left(\frac{1}{\rho_0} - \frac{1}{\rho_s} \right)^{-1} \tag{8.2.28}$$

Selecting the porosity exponent m equal to 2, a value of about 1.24 is obtained for A. The respective models are shown in Fig. 8.6 and generally show a rather moderate increase in resistivity for $S_{CO_2} < 0.7$. For larger saturations a more drastic resistivity increase is observed with the respective maxima at full CO_2 saturation. This is a generic behavior of Archie models which has been well discussed regarding its potential for geoelectric monitoring of CO_2 migration (e.g. (Hoversten and Gasperikova 2005).

For CO_2 saturations up to about 70 %, clay has a rather neglible impact (Fig. 8.6). This can be explained by the (highly salinized) pore fluid which strongly exceeds the clay in terms of conductivity at low and intermediate CO_2 saturation. The difference between models is considerable for high CO_2 saturations. In such a

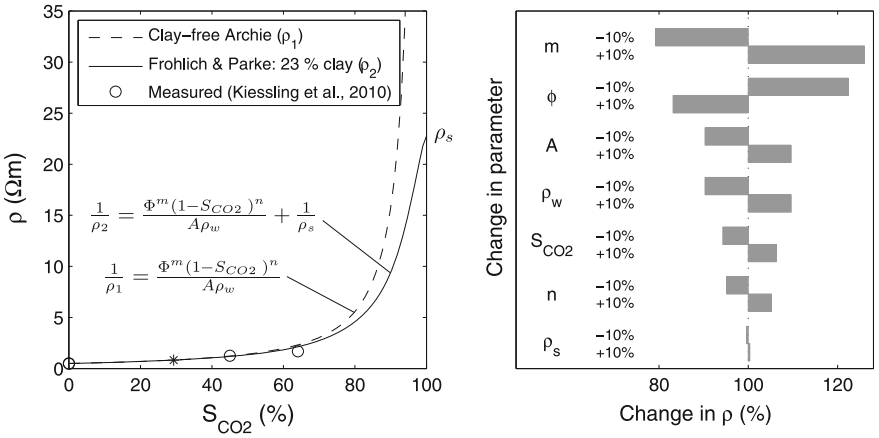

Fig. 8.6 *Left* Electric resistivity models as functions of the CO_2 saturation for the Ketzin reservoir model. A, m, and n were chosen to 1.24, 2 and 1.5, to fit experimental data reported by Kiessling et al. (2010). For further parameters of the reservoir model see text. *Right* Change in model resistivity due to uncertainties in the resistivity model parameters. Analysis had been carried out for the Frohlich and Parke model with a CO_2 saturation of 30 % (see *star symbol* in the *left hand* diagram). Estimation errors in the porosity exponent m and porosity ϕ can be seen to pose the strongest uncertainties on the resistivity predicted by the model

situation, the Archie model does not account for the clay-related conduction, whereas the Frohlich and Parke model allows some conductivity through the clay. Two considerations for geoelectric monitoring of CO_2 storage now arise. Firstly, ERT will be less sensitive at low CO_2 saturations, but will gain sensitivity as the CO_2 saturation increases. Secondly, if quantitative estimation of CO_2 saturations from resistivity measurements is performed in clay-bearing materials at high CO_2 saturations, the utilized resistivity-saturation relations should be based on in situ (laboratory) experiments or adequately calibrated clay models.

Assuming the Archie model to sufficiently describe the resistivity-saturation relation for the Ketzin reservoir within low and intermediate CO_2 saturations, the Archie equation can easily be used in reverse to estimate CO_2 saturations by

$$S_{\mathrm{CO_2}} = 1 - RI^{-(1/n)} 1 - \left(\frac{\rho_0}{\rho}\right)^{1/n} \tag{8.2.29}$$

The use of the resistivity index *RI* (Guéguen and Palciauskas 1994) allows the substitution of ρ_w with ρ_0 by

$$RI = \frac{\rho_0}{\rho} = (1 - S_{\mathrm{CO_2}})^{-n} \tag{8.2.30}$$

Note that the parameters A and ϕ_m become obsolete when using the ratio of two resistivities at different CO_2 saturations. The saturation exponent n is the only rock parameter required in this equation and with rearrangement of it resulting in

$$S_{CO_2} = 1 - RI^{-(1/n)} = 1 - \left(\frac{\rho_0}{\rho}\right)^{-(1/n)} \tag{8.2.31}$$

and allowing estimation of CO_2 saturation from a measured resistivity ρ and its baseline resistivity ρ_0. However, it is important to note that this assumes the porosity related parameters ϕ_m and A to be constant throughout the fluid-substitution process (no dissolution or cementation).

8.3 Tracer Tests for Monitoring CO_2 Plume Migration

Alexandru Tatomir, Iulia Ghergut and Martin Sauter

The success of CO_2 geological storage projects relies on technologies and capability to efficiently monitor the migration and fate of the injected CO_2 plume. Various types of tracers in the liquid and/or gas phases constitute one such monitoring technology. The overall goal of monitoring tracers is the characterization of processes occurring in the reservoir during and after the CO_2 injection. This involves the determination of the residual and dissolution trapping mechanisms and efficiency, the leakage pathways, the CO_2-brine interface area, extent of the CO_2 plume spreading, etc.

A summary of the various uses of the conservative and reactive tracers for monitoring purposes is given in Table 8.6.

The CO_2 can be present in several states depending on the temperature, pressure and chemical composition of the fluids in the reservoir which makes the assessment of the chemical tracers a challenging issue. CO_2 has been used on regular basis in the oil and gas industry to enhance the oil recovery. Among the most frequently used compounds are (see Table 8.6, Noordman et al. 2000): alcohols (Dwarakanath and Pope 1998), phase partitioning non-condensible gases such as O_2, CO_2, CH_4 (Elodie and Philippe 2012), noble gases (e.g. Kr; Vulava et al. 2002), volatile organic chemical compounds, fluorinated hydrocarbons (McCallum et al. 2005; Wells et al. 2007) and naturally occurring isotopes (e.g., 222Rn; Hunkeler et al. 1997), radioactive isotopes tracers (Johnson et al. 2011a, b).

Within the context of CCS projects, tracer methods can provide understanding over the subsurface movement of the CO_2 plume (Boreham et al. 2011; Freifeld et al. 2005; Underschultz et al. 2011; Vandeweijer et al. 2011), characterize geochemical processes (Assayag et al. 2009; Matter et al. 2007), assess the residual

Table 8.6 Use of tracers for monitoring during storage site operation

Target information	Suitable method	Suitable tracer species	Limitations	Application examples
Tracking or anticipating CO_2 breakthrough	Passive real-time monitoring of gas fluxes	Inert gases; optionally complemented by defined isotopic signatures for the injected CO_2 and accompanying tracers	Some gas species may arrive earlier, some later than the injected CO_2	Ketzin: Nitrogen, Krypton Frio: PFCs, SF_6, Kr Otway: SF_6, Kr, CD_4 (perdeuterated methane)
Tracking thermal fronts	Forced-gradient brine sampling	"Thermo-sensitive" tracers	Discussion on thermo-sensitive tracers in Chap. 6	Table 7.6
Estimating CO_2-brine interfaces	Passive monitoring	partitioning tracers	Requires accurate knowledge of partitioning coefficients, considering various in situ influences on them (temperature, salinity, etc.)	Fagerlund et al. (2013a) Tong et al. (2013) Myers et al. (2013a, b)
Dynamic tracking of CO_2-brine interfaces	Passive monitoring forced-gradient fluid sampling	"KIS" (kinetic interface-sensitive) tracers	Discussion on KIS tracers in Chap. 6	Schaffer et al. (2013) Tatomir et al. (2015)
Brine displacement	Passive monitoring forced-gradient brine sampling	Brine-soluble tracers partitioning tracers	Difficult to detect; extremely high dilution for brine-soluble species; forced-gradient brine sampling is not desirable during CCS site operation	Ketzin (attempted with brine-phase tracers like naphthalene-sulfonic and fluoro-benzoic acids); Behrens et al. (2014)
Cap-rock integrity	Passive monitoring	Geochemical and isotopic tracers, cation dissolution	Requires very sensitive detection (low detection limits); source attribution not always unique	Luquot and Gouze (2009)
Wellbore integrity	Passive monitoring	Geochemical and isotopic tracers, trace elements		Crow et al. (2010)

(continued)

Table 8.6 (continued)

Target information	Suitable method	Suitable tracer species	Limitations	Application examples
Residual trapping of CO_2	Forced-gradient push-pull sequence	Pressure signals—as an alternative to using solute tracers	Geological uncertainty	Zhang et al. (2011)
Residual and dissolution trapping	Inter-well dipole, forced-gradient	Partitioning tracers	Geological heterogeneity	Fagerlund et al. (2013a, b) Myers et al. (2013a, b), LaForce et al. (2014), Rasmusson et al. (2014)

trapping capacity (Myers et al. 2012; Rasmusson et al. 2014; Zhang et al. 2011; Fagerlund et al. 2013a, b). LaForce et al. (2014), determine the containment and leakage rates for monitoring and verification programs (Strazisar et al. 2009; Wells et al. 2010, 2007), measure the rate of CO_2 dissolution (Fagerlund et al. 2013a, b) or provide information about individual trapping mechanisms.

A recent literature review of several relevant CCS tracer applications is done by Myers et al. (2013a). They present case studies from West Pearl Queen, a depleted oil formation in southeastern New Mexico, and from Zero Emission Research Technology Center (ZERT) project in Bozeman, Montana (USA) where several cyclic perfluorocarbon tracers were used for monitoring and verification (Strazisar et al. 2009; Wells et al. 2007, 2010). Furthermore the Pembina Cardium project in Alberta (Canada) is presented, where distinct in situ isotopes were used as tracers for understanding breakthrough and plume migration (Johnson et al. 2011b). At the K12-B gas field in the Dutch sector of the North Sea and Frio Brine I pilot project, perfluorocarbons and inert gas tracers were used for understanding breakthrough and plume migration. At Kezin CO_2 injection site (Germany) the observations obtained from two monitoring wells showed that the two tracers, nitrogen and krypton have arrived prior to the CO_2 breakthrough (Elodie and Philippe 2012; Martens et al. 2011; Zimmer et al. 2011).

In general, when designing the tracer tests for the characterization and monitoring stages of a CO_2 storage site several key aspects must be considered (Myers et al. 2013a, b): chemical stability, environmental safety, cost effectiveness, ease of detection, toxicity, injection/sampling protocols and behavior in the reservoir conditions. Additionally, further restrictions have to be considered in the test design considering single-well and inter-well testing (Ghergut et al. 2013):

1. mobile-fluid volumes (e.g. CO_2 plume) can be measured from inter-well conservative-tracer tests, whereas single-well push-pull tests are generally insensitive to mobile-fluid volumes;
2. immobile-fluid volumes, in single-phase systems, are rather difficult to measure, by either kind of test;
3. fluid-phase saturations can be determined from inter-well tests using partitioning tracers at equilibrium exchange between phases; whereas single-well tracer push-pull tests are rather insensitive with respect to tracer exchange processes at equilibrium;
4. mobile and immobile fluid regions, or fluid-fluid interface areas can, in principle, be determined from single-well tracer push-pull tests relying on kinetic exchange processes between compartments or phases (Schaffer et al. 2013; Tatomir et al. 2013, 2015).

An interesting trade-off between the advective- or equilibrium-dominated parameter sensitivity regimes, and the advection- or equilibrium-insensitive

regimes is obtained using in situ tracer creation, or conversion, in a time-dependent manner (from another initially-injected tracer with different phase-partitioning properties), as had originally been proposed by Tomich et al. (1973) for determining residual-oil saturations.

Reactive tracers constitute a promising research area for innovative process characterization, especially the thermo-sensitive tracers for tracking in situ temperature fronts, as proposed by Nottebohm et al. (2012), and the new class of KIS tracers (CO_2-brine interface sensitive), as proposed by Schaffer et al. (2013) and modeled in (Tong et al. 2013) and Tatomir et al. (2015).

Examples of tracer uses in terms of classical site characterization is given in Table 7.5, for characterizing the sites CO_2 trapping properties through CO_2 injection experiments in Sects. 7.4 and 8.6.

8.4 Well Instrumentation

Barry Freifeld

8.4.1 Objective of a Borehole Monitoring Program

The overarching objective of monitoring geologically sequestered CO_2 is to demonstrate the safe and effective long-term storage and integrity in the target reservoir. This is accomplished through a multi-faceted monitoring program by which data is acquired that (1) assures the public and regulators that the reservoir is behaving as intended, (2) validates conceptual models developed for reservoir engineering and storage management, and (3) demonstrates protection of drinking water and the greater environment. Dedicated monitoring wells are expensive and it is most efficient to use them to simultaneously acquire a diverse set of complementary data sets. The concept of integrated well monitoring is to engineer each completion such that tradeoffs necessary to deploy disparate technologies are considered in a holistic way so that the end result is an optimal suite of tools to accomplish monitoring objectives. Examples of integrated monitoring completions for CO_2 storage are available in both demonstration and pre-commercial deployments. These include the Ktzi 200, 201 and 202 boreholes at the Ketzin pilot site, Germany (Prevedel et al. 2008), the CO_2CRC Otway Project Naylor-1 Well (Jenkins et al. 2012), and the Modular Borehole Monitoring system developed at Lawrence Berkeley National Lab for the D9-8 Well (CO_2 Capture Project 2013).

8.4.2 Monitoring Environmental Challenges

The geologic reservoirs targeted for geological storage of CO_2 are normally at pressures and temperatures above CO_2's critical point: 31.1 °C at a pressure of 73.8 bar. These temperatures and pressures are typically found at depths greater than ~750 m, and sequestration pilots have often been at 2–3 km depth where multiple sealing layers provide redundant barriers to migration of CO_2 to the surface. There are many engineering challenges associated with the environmental conditions encountered, which include elevated pressures, temperatures, and aggressive groundwater chemistries to name a few.

The depth of the target reservoir and the corresponding hydrostatic pressure provides a significant challenge to the design and survivability of complex monitoring instruments. A 3000 m deep well will develop around 300 bar static pressure at bottom. This can be even greater depending on the salinity of the fluid.

In addition to pressure, elevated temperatures present additional engineering challenges for MVA (monitoring, verification and accounting) tool design. Downhole electronics experience increasing rates of failure at temperatures above 100 °C, with lifetimes of downhole electronic circuitry decreasing nonlinearly with increased temperatures. A study conducted by Quartzdyne, Inc. a major manufacturer and OEM supplier of quartz crystal and electronic circuit boards for permanent pressure/temperature gauges found that surface mounted electronics could be used reliably at up to 150 °C, with lifetimes of 5 years at 125 °C. Hybrid electric circuitry assemblies can last up to two years at 200 °C or five years at 180 °C (Watts 2003). These durations are frequently much shorter than would be expected during a permanent CO_2 monitoring program, and hence some means for removal and replacement of electronic based sensors would be needed for a "life-of-the-well" solution.

Similarly, fiber-optics also suffer from degradation at elevated temperatures. Standard acrylate coated optical fibers are rated for use up to 85 °C, with high temperature acrylate fibers acceptable for extended usage at 150 °C. Polyimide coatings are used at temperatures up to 300 °C, while difficult to manufacture fibers using metallic coatings are available beyond this temperature. Two of the challenges that metallic coated fibers face is in the reliable fabrication of long lengths and the difficulty in recoating after splicing. Optical fibers in general suffer a condition known as hydrogen darkening at elevated temperatures, where hydrogen diffuses into the fiber and degrades the optical characteristics. In high temperature boreholes (>200 °C) with hydrocarbons present, the diffusion of hydrogen into fibers can be severe and seriously degrade the life of a fiber-optic cable in the timespan of several months (Rassenfoss 2012).

Corrosion and chemical resistance of the materials selected for downhole use in the MBM (modular borehole monitoring) system is an important consideration and is related to the temperature issue because of the exponential dependence of reaction rates on temperature. Deep sedimentary aquifers, often rich in dissolved salts, are considered the largest potential targets of CO_2 sequestration. Monitoring

in wells used for fluid sampling means exposure to CO_2 rich fluids. CO_2 dissolved in formation waters will form carbonic acid, with the resulting acidity determined by the host formations buffering capability. Acidic waters form a hostile environment to most ferritic materials commonly used in well completion. To mitigate potential high corrosion rates carbon steel is often replaced by high chromium alloys, which in turn increases well costs. Fiberglass is an alternative casing material to consider, but the structural integrity needs to be considered in deep well installations, particularly in designing cementing operations that limit compressive forces.

8.4.3 Monitoring Technologies

Many of the technologies that have been employed for monitoring CO_2 sequestration sites are derived from the oil and gas industry. These include permanent pressure and temperature gauges, fiber-optic temperature, acoustic, and strain, as well as numerous wireline logging technologies. For geophysical logging there has not been a broad adoption of permanent sensing in the oil and gas industry, but there have been examples of in well electrical and seismic sensor arrays. Permanent microseismic sensing has frequently been employed for monitoring unconventional hydraulic fracturing operations. Downhole fluid sampling in the oil and gas industry is typically performed using wireline tools to acquire accurate PVT information during the reservoir appraisal process, as wellhead samples are normally used after a well is put into production. For continuous monitoring of brines for CO_2 sequestration alternative methods have been developed such as U-tube fluid sampling (Freifeld et al. 2005) or Schlumberger's Westbay Multilevel sampling system (Picard et al. 2011).

8.4.3.1 Pressure/Temperature

Subsurface pressure and temperature are fundamental parameters used in all reservoir models. Hydrologic testing requires knowledge of the evolution of a pressure transient during fluid injection or withdrawal in order to assess a reservoirs permeability and storativity (see Chaps. 3 and 8 for definitions). In a CO_2 storage reservoir having pressure gauges deployed both at the bottom and top of a perforated interval permits an estimate of the fluid density, and hence the height of a column of CO_2 in brine.

Permanently deployed discrete pressure/temperature gauges are commercially mature products with dozens of vendors that will supply and install the instruments. Pressure gauges operate using a variety of measurement methods, with the deep well environment sensors dominated by piezoresistive and quartz gauge technology. Resonating quartz cells are considered the most stable and accurate. Data from permanent gauges are typically read out at the surface through single conductor

TEC (tubing encapsulated conductor). Alternatively, memory gauges can be installed in side pocket mandrels and retrieved periodically to download data and replace batteries. The benefit of retrievable gauges is that they can be replaced upon a gauge failure, whereas a permanent gauge with surface readout cannot be replaced if it fails. Because of the high value of real-time data early in the life of a project it is possible to install permanent gauges that may fail in five or ten years, but with either side-pockets or landing subs that would allow easy deployment of retrievable gauges in the future.

8.4.3.2 Fluid Sampling

There are numerous methods for obtaining subsurface fluid samples, including wireline samplers, formation testers, gas lift systems, and U-tube samplers (Freifeld et al. 2005). For fluid samples from two-phase reservoirs, such as exist in mixed brine CO_2 systems, methods that preserve the relative ratio of the separate phases are preferred as they provide information deemed important to understanding the state of the reservoir. Electrical pumps and gas lift significantly distort the composition of the fluid, and hence downhole wireline and U-tube samplers are the preferred techniques for monitoring CO_2 sequestration reservoirs. A comparison of all of these sampling methods was conducted at the Citronelle field site by a team led by Yousif Kharaka, USGS Menlo Park. Unpublished results showed that the wireline and U-tube samples provided the least disturbed dissolved gas chemistry, resulting in more representative samples than submersible pumps and gas lifting fluids.

Additional tools have been developed by major oilfield service provides for sampling fluids through casing. This involves creating a hole, extracting fluid, and repairing the hole. As expected these tools are highly specialized and carry significant costs to mobilize and use. They however can provide one of the few methods by which suspected leakage above zone can be investigated.

If it is known in advance that fluid samples are required to be collected above the reservoir, there are a couple of different experimental methods by which a permanent sampling system can be installed outside of the casing. As part of the PTRC (Petroleum Technology Research Centre) Aquistore Project, a cement diverter has been installed with a U-tube sampling port and fluid sampling lines cemented outside of casing. To date, the performance of the system is unknown as it has not been function tested since installation, which occurred shortly before the writing of this report.

An alternative method is to deploy a U-tube as part of a behind casing perforation system. Behind casing perforation systems have been used to couple discrete pressure/temperature gauges to the formation. This works by installing a hollow perforation charge carrier connected through capillary tube to the pressure sensor. The perforations create a fluid pathway between the formation and the pressure gauge. This type of device has been marketed by several companies including Promore, Houston, TX and Sage Rider, Rosharon TX. Alternatively this same deployment method can be used to couple the formation to a U-tube fluid sampler.

8.4.4 Fiber Optic Technologies

8.4.4.1 State-of Sensor Technology

Fiber optic based sensor systems are either distributed, based upon Raman or Brillouin scatter or discrete or multi-point, based upon Fabry-Perot cavities or Fiber Bragg Gratings (FBGs). Distributed temperature sensing is by far the most widely adopted well monitoring technique, having been first developed in the early 1980s at the Southampton University in England. The technique was commercialized initially by York Sensors Ltd and several other companies including Sensortran, Sensornet, LIOS Technology and APSensing (a spin-off from Agilent Systems) have since developed commercial products. Performance specifications for RAMAN based DTS systems are usually a function of the overall cable length and the integration period for each measurement cycle, with spatial resolutions typically 15 cm to 1 m and temperature resolution as high as 0.01 °C.

Brillouin based temperature monitoring systems typically have lower measurement resolution and accuracy than Raman Systems, but because strain induced variations in optical properties can be decoupled from the temperature measurements, the technique is less susceptible to noise induced by strain on the cables. Because the Brillouin technique uses low loss single-mode fiber it can be operated at ranges as long as 100 km. Brillouin measurements use single mode fiber in comparison to the multimode fiber employed for Raman based temperature measurement. Brillouin sensing is also used for monitoring fiber-strain. Typical sensitivity limits for stain are from 2 με to 10 με up to as high as 4 % strain depending on the cable material. One difficulty in monitoring strain is the challenge of transferring environmental strain onto the cable in a way that accurately transfers the strain but does not degrade the environmental integrity of the fiber-optic cable encapsulation, which needs to still resist the elevated pressures of the deep subsurface environment. This is still an area of active research. FBG strain sensors are more commonly deployed to monitor strain at discrete locations because of the difficulty of imparting strain onto a continuous fiber. Baker Hughes and Shell jointly developed an FBG based real-time compaction imaging system to monitor sand screen deformation and casing shape which used FBG strain sensors.

A technology that is more recent than DTS, but has rapidly evolved in only a few years is distributed acoustic sensing (DAS). Discrete fiber-optic based geophone sensors have been marketed for many years based on FBG technology. However, there was little commercial uptake of the technology as the advantage over conventional copper wire based geophone sensors was not significant enough to overcome the price for utilizing the fiber-optic technology. DAS uses commercial grade single-mode telecom fibers to monitor with high spatial resolution (up to 1 m) to provide truly distributed sensing over kilometers of cable.

Fiber-optic DTS monitoring specifically for CO_2 sequestration has been deployed at the CO_2SINK site at Ketzin, Germany (Giese et al. 2009), the CO_2CRC Otway Project and the SECARB Cranfield Site, in Mississippi (Daley et al. 2013)

and at the Quest project in Alberta, Canada. Both the CO_2SINK and Otway Project sites deployed a variant of passive DTS monitoring, referred to as heat-pulse monitoring (Freifeld et al. 2008) which provides for the creation of a thermal pulse to investigate the thermophysical setting of the near wellbore environment.

Many technologies have been developed for borehole deployment as stand-alone measurements. We will consider these to the extent they could possibly be integrated into a modular deployment. A good example is strain. Current fiber optic technology, typically used for distributed temperature sensing, is being applied to strain measurements. Current measurement sensitivity is sufficient for sensing casing damage.

8.4.5 Instrumentation Deployment Strategies

There are several different methods for installing instrumentation in boreholes, but by far the most common method is run-in-hole on tubing, where the instruments sit in the annular space between tubing and casing. The hardware associated with a tubing deployment has a mature supply chain, and the engineering expertise is readily available. Less common but still considered relatively mature is behind casing installation. In a behind casing installation the instruments sit outside of the casing, allowing the full interior space within the well to be available for temporary deployments. The deployments at the Ketzin pilot site were an example of a hybrid installation, where some instruments sat outside of the casing and others were affixed to tubing (Prevedel et al. 2008). Considered as experimental techniques are coiled tubing installations and wireline/umbilical installation of instruments.

8.4.5.1 Tubing

In many ways tubing instrumentation deployments are operationally similar to ESP (Electrical Submersible Pump) deployments, as the specialized equipment to protect and run-in-hole with instrumentation control lines are identical. Specialized vendors are required to oversee the installation and operation of their particular instruments and a spooling operator coordinates with the rig floor workers for the installation of mandrels, clamps, and bands during the installation. The wellhead will need to accommodate control lines feeding through the tubing hanger and out through the tubing head adapter flange. Tubing deployment of instruments is more common than installation outside of casing, and the variety of vendors and service organizations with familiarity with the process is greater. However tubing deployment lacks the benefit of behind casing sampling for sensors that require close contact to the formation, particularly seismic and electrical sensors.

8.4.5.2 Cemented Outside Casing

As part of standard techniques within the oil and gas industry, methods for instrumenting the outside of a well casing with control lines that are cemented in place have been developed. The installation of DTS cables outside of casing provides a real-time and continuous evaluation of cement operations, allowing the concentration of cement to be assessed by its exothermic curing process. Other instrumentation can be deployed on casing as part of an MVA effort. Many MVA tools such as ERT (Electrical Resistivity Tomography), seismic sensors, samplers, etc., have been installed using casing deployment in demonstration programs such as the Ketzin pilot site and SECARB's Cranfield DAS test in Cranfield, Mississippi. There are several significant benefits to deployments of instruments behind casing, which includes leaving the wellbore available for wireline logging and other temporary tool deployments and better coupling to the formation for seismic or electrical sensors. The entire deployment of instrumentation on casing requires the use of specialized subcontractors that have experience in completion operations that are modified to accommodate the physical presence of the instrumentation.

While casing deployment is similar in many ways to tubing deployment, as spooling units and control line protectors are also used, there are numerous complexities that arise that are not encountered with tubing deployment. The cementing operation of the casing has to take into consideration the damage that could occur during casing movement which is used to improve the cement job. Rotation of the casing is not permitted, however reciprocation can usually still be performed. Perforation needs to be performed in such a way as to mitigate the risk of the perforation charges damaging the instruments. One way to do this is to install behind casing charges which are aimed away from the instruments. This method has most frequently been used for the installation of behind casing pressure/temperature sensors. If the perforation will be performed after cementing than some method for oriented perforating as well as "blast shield" or other protective housings placed over critical instruments are usually employed.

8.4.5.3 Coiled Tubing (CT)

A coiled tubing rig is potentially more economical than a standard workover rig used for conventional tubing deployment. Deployment is more rapid because joints don't have to be made up and there are no control line protectors to be positioned on each joint. However the engineering for instrumented deployments using coiled tubing is far less mature than for convention tubing deployment, and the availability of CT rigs and specialized personal considerably lower leading to large variability in the ability to performed instrumented CT deployments. An example of a service provider offering instrumented CT is Precise Downhole Services Ltd., located in Nisku, Alberta, Canada. To date there has not been a CO_2 monitoring well completed with instrumented coil tubing, although a temporary seismic hydrophone cable was deployed at Weyburn with CT.

8.4.5.4 Wireline/Umbilical

An umbilical system as used in subsea applications that runs from platform to wellhead could bridge the gap between flatpack coiled tubing and standard wireline deployment. CJS Production Technologies, Calgary Alberta, Canada, have been commercializing an umbilical style flat-pack. They have modified a conventional CT rig to use rectangular shaped push blocks that can grip and deploy a rectangular umbilical. More significantly, they have worked on methodologies for performing pressure control, which is one of the significant engineering challenges in an umbilical style deployment. The flat-pack at Citronelle dome is really a hybridization of a conventional tubing deployment with a flat-pack encapsulated instrumentation bundle. Problems that CJS Production Technologies have encountered include leakage between the encapsulant material and the instrumentation lines as well as the need to engineer highly customized wellhead components.

8.4.5.5 Deployment Pressure Control Issues

For both casing and tubing deployment pressure control is critical. Pressure control must be maintained at all times in open hole casing deployment and for tubing deployment in a perforated well. For completed wells this means having the previously mentioned zonal isolation at some depth above the perforations (such as a packer or seal bore) or a well head with a gate valve. All such zonal isolation requires more engineering when monitoring control lines need to be passed through seals. While running in well, often only 'kill-fluid' (high density fluid) is primary well control, with secondary control additional devices such as a hydril, blind ram or shear ram as part of a BOP stack.

8.4.6 Example of an Integrated Monitoring Installation: Heletz H18a

8.4.6.1 Project Background

Heletz is a depleted oil field, filled with brine at its edges. The site is instrumented for scientific CO_2 injection experiments (Niemi et al. 2016). The Heletz H18a is one of two wells drilled in the frame of the EU-FP7 funded MUSTANG project on the characterization of deep saline formations for the storage of CO_2. The two wells were installed into the saline aquifer part of the formation with the objective to develop field scale methods for assessing the capacity and safety of a CO_2 storage reservoir using a combination of both single-well and cross-well experimental tests. The H18a well was drilled from January to May of 2012 to a total depth of 1649 m. The well was perforated through two of three sandstone intervals at depths of 1627–1629 m and 1632–1641 m.

8.4.6.2 H18a Integrated Monitoring Well

The technologies chosen for the H18a injection well include U-tube fluid sampling, permanent quartz pressure/temperature gauges and an integrated fiber-optic bundle to facilitate temperature, seismic, and heat-pulse monitoring. In addition, a chemical injection mandrel and gas lift mandrel facilitate both push-pull injection testing and production of fluids by artificial gas lift. Figure 8.7 provides a schematic layout of the borehole completion package. The primary tubing is 2–7/8″ 6.5 ppf L-80 RTS-8 with an internal coating of Tuboscope TK-805 to improve resistance to exposure to carbonic acid from conventional carbon steel. The 2–7/8″ tubing permits conducting periodic logging campaigns using industry standard 1–11/16″ slim-hole tools.

8.4.6.3 Packer and Overshot Design

In considering zonal isolation for the bottom hole assembly (BHA) both inflatable and hydraulic set packers have been used in the past. Inflatable packers are generally considered not as reliable since any slight leak that develops in the gland or seals can lead to deflation, and the multi-year life required of the completion string requires the highest dependable installation possible. Mechanical set packers require twisting of the string which is not permitted at the packer because of the three control lines that pass through the seal location. For Heletz H18a, a hydraulic set packer coupled with an overshot to connect the tailpiece to the packer was selected for coupling the BHA to the support string based upon recommendations by Denbury Resources and experience they have in long-life installations.

The packer selected was a D&L Hydroset II Packer, which is a hydraulic set, mechanically held dual string packer with asymmetric short and long string connections. The 2–7/8″ long string connection was used for the production tubing while the smaller 1.900 EUE facilitates pass-throughs for the fiber-optic, pressure/temperature gauge, and U-tube sampling lines. Figure 8.8 shows the dual-mandrel packer with an inset picture highlighting the pass-throughs that penetrate the short string coupling. An overshot was used to couple the tailpipe to the packer to avoid twisting the lines running through the packer.

8.4.6.4 H18a Installation

The installation was conducted by running a work string into H18a with a casing scrapper and then circulating 30 m^3 of fluid once on bottom. Starting with the reentry guide, the bottom-hole assembly was assembled and the control lines and pressure/temperature gauges installed on special instrumentation mandrels. Pneumatic spooling units are used to tension the control lines as they were led over a multi-line sheave hung off the derrick board (Fig. 8.9). Total time to install the integrated monitoring completion was two and a half days for well and equipment

SAGE RIDER

Company:		Date:	Temp:	Gun Size:	SPF:	Phasing:	Casing Size/Wt:
Class 6 Solutions Heletz Mon		27-Jan-14	130 °F	0"	0	0°	7
Well Name:	Field:		Expl. Type:	Fluid Wt.	Fluid Type		Job Type:
H18 Injection	0		0	8.5#	2% KCL		Horizontal TCP
County/Parish:	State:		Completion Intervals:		Firing Device #1:		Firing Device #2:
0	0		VI		0		0

Item	Description	O. D.	I. D.	Length	Depth Feet	Depth Meters
						-
						-
						-
						-
						-
						-
						-
						-
	Run 162 total joints and 1 perf joint					-
						-
24	Tubing to Surface	3.660	2.441	2,929.55	-	-
23	Chemical Injection Sub	3.660	2.441	4.09	2,929.55	892.93
22	10 Joints 2 7/8" Pipe Joint 63-72	3.660	2.441	325.73	2,933.64	894.17
21	Gas Lift Mandrel	3.660	2.441	4.09	3,259.37	993.46
20	58 Joints 2 7/8" Pipe Joints 4-62	3.660	2.441	1,922.02	3,263.46	994.70
19	Marker Sub	3.660	2.441	6.30	5,185.48	1,580.53
18	1 Joint 2 7/8" Tubing #3	3.660	2.441	32.57	5,191.78	1,582.45
17	X-Nipple	3.660	1.875	0.99	5,224.35	1,592.38
16	1 Joint 2 7/8 Tubing #2	3.660	2.441	32.59	5,225.34	1,592.68
15	7" 23# Dual String Packer	6.062	2.441	7.83	5,257.93	1,602.62
14	1 Joint 2 7/8" Tubing #1	3.660	2.441	32.58	5,265.76	1,605.00
13	On/Off Tool w/ X profile	4.500	1.875	1.85	5,298.34	1,614.93
12	X-O Pup	3.660	2.441	6.09	5,300.19	1,615.50
11	Dual Gauge Carrier	4.850	2.441	5.67	5,306.28	1,617.35
10	Sample Filter Carrier	3.990	2.441	3.00	5,311.95	1,619.08
9	X-O 2 7/8" NU Box X 2 3/8" Pin	3.660	2.100	0.40	5,314.95	1,620.00
8	Pump out plug	3.063	1.875	0.68	5,315.35	1,620.12
7	X-O 2 3/8" Box X 2 7/8" Pin and 2' pup	3.660	1.995	2.67	5,316.03	1,620.33
6	1 Joint 2 7/8" Perforated Pipe	3.660	2.441	32.55	5,318.70	1,621.14
5	X-O Pup	3.660	2.441	6.08	5,351.25	1,631.06
4	Dual Gauge Carrier	4.850	2.441	5.67	5,357.33	1,632.91
3	X-O Pup and Fiber Termination Sub	3.660	2.441	5.62	5,363.00	1,634.64
2	Wireline Re-entry Guide and XN Nipple	3.660	2.441	1.38	5,368.62	1,636.36
1	Bottom of W/L Re-entry Guide				5,370.00	1,636.78
						-

Comments: Perforations:

Total Length of BHA =	2440.45'	743.85'
Total BHA w/o Pipe=	94.96	28.94

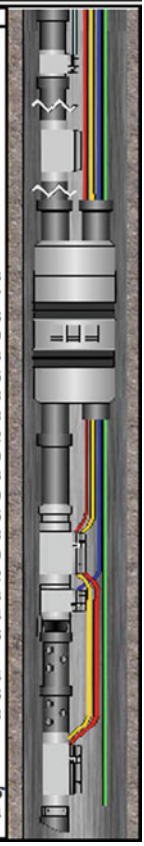

Fig. 8.7 Borehole completion package for the Heletz Site H18a injection well

preparation, one day to assemble the bottom assembly and run-in-hole and a final day to complete the well head and install surface lines and equipment.

8.4.7 Conclusions

A variety of permanent monitoring technologies can be engineered for installation into a single integrated package for comprehensively monitoring a CO_2 storage site. Well designs exist that facilitate simultaneous geophysical monitoring, permanent

Fig. 8.8 D&L dual-mandrel hydraulic set packer with short string fitted with adapter to seal around control lines using compression fittings

discrete instrument gauges, and repeat wireline logging. While some technologies such as permanent pressure/temperature gauges have been available for decades, new and emerging technologies such as distributed fiber-optic acoustic sensing are making rapid strides in becoming accepted technology and have been demonstrated in carbon sequestration pilot tests. Given the requisite long duration for a CO_2 monitoring program only the most robust technologies and carefully selected materials and installation methods will provide life-of-the-field solutions.

Fig. 8.9 Workover operation in progress at H18a showing rig with double stands of tubing and pneumatic spooling units used to tension control lines as they are fastened to the tubing

8.5 Monitoring Results from Selected Large Scale Field Projects

Larry Myer

The following sections summarize the findings from monitoring programs at selected, major, large scale CO_2 storage projects, worldwide, which have made significant technical contributions toward enabling broad, global, geologic storage of CO_2. The projects discussed are: Sleipner, offshore saline formation storage, Europe; In Salah, onshore saline formation storage, Africa; and Weyburn-Midale, onshore EOR/storage, North America.

8.5.1 Sleipner

8.5.1.1 Project Overview

The Sleipner CO_2 storage project is the world's longest running geologic storage project. Since 1996, approximately 1 M tons of CO_2 per year have been injected from a single well drilled into the saline water-saturated Utsira Formation (Alnes et al. 2011). The Sleipner storage project is being carried out in conjunction with a commercial natural gas production project operated by Statoil. Located about 240 km off the coast of Norway in the North Sea, natural gas is produced from the Sleipner West field from a reservoir below the Utsira. In order for the natural gas to meet the sales gas specification, its CO_2 content is reduced from about 9 % down to 2.5 % (Nooner et al. 2007).

The regional geometry of the Utsira and overlying units was well defined from interpretation of nearly 14,000 line kilometres of 2D seismic data and over 300 wells (Chadwick et al. 2000). The Utsira sand is a tabular, basin-restricted unit stretching about 450 km from north to south and 40–90 km west to east. It lies at depths of about 800–1100 m below the sea floor with a thickness of about 250 m around the injection site (Arts et al. 2008). Overlying the Utsira sand is the Nordland shale, which, in the Sleipner area is between 200 and 300 m think (Arts et al. 2008). Immediately overlying the sand is a shale drape, which is a tabular, basin-restricted, seal (Chadwick et al. 2000). The Utsira sand is poorly consolidated, highly porous (30–40 %) and very permeable (1–3 Darcy) (Arts et al. 2008). The very high permeability, high porosity, and large reservoir volume has resulted in negligible pressure increases in the reservoir.

8.5.1.2 Seismic Monitoring

At Sleipner, the primary monitoring method has been time-lapse 3-D seismic. It is a very important case history because Sleipner was the first project to clearly demonstrate the potential of seismic surveys for monitoring CO_2 storage. By 2010, nine 3-D surveys had been carried out, with the first, in 1994 providing the pre-injection baseline. The time-lapse seismic results clearly show the steady expansion of the plume over time. The results also show that the expansion is affected by mudstone layers in the reservoir, leading to new understanding of the effects of internal reservoir structure and heterogeneity on plume movement (Fig. 8.10). Well logs revealed the presence of the thin (on the order of one meter thickness), laterally discontinuous mudstone layers, but they were not visible in the pre-injection seismic data (collected in 1994) and their significance not recognized until the first repeat 3D seismic survey carried out in 1999. That survey showed reflections from CO_2 in a stack of layers, which were then correlated with the mudstone layers observed in the well logs. A seismic reflection would be expected from increases in the acoustic impedance contrast between sandstone and a

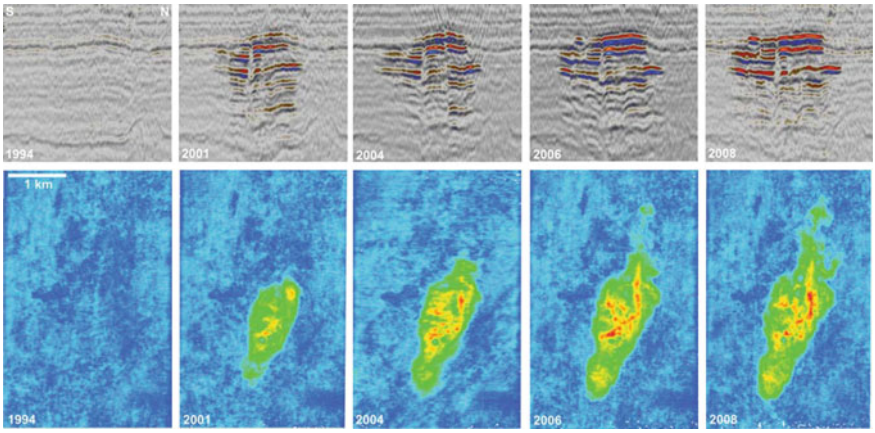

Fig. 8.10 Time-lapse seismic images of the Sleipner CO_2 plume—NS inline through the plume (*top*); plan view of total reflection amplitude in the plume (*bottom*) (Chadwick et al. 2010)

mudstone layer, resulting from high saturations of CO_2 accumulating at the top of the sandstone layer. The mudstone layers baffle the upward migration of the CO_2 within the reservoir, having a significant effect on the storage efficiency of the reservoir.

In addition to the effects of mudstone baffles, seismic data from Sleipner also show that the expansion of the plume is significantly influenced by the topography of the interface between the sand reservoir and the caprock. This interface undulates, creating topographic highs. Under buoyancy drive, the CO_2 fills one high spot before spilling laterally to fill the next. Seismic reflection amplitude maps of the topmost layer show that CO_2 first reached the reservoir top in 1999, as two small separate accumulations within a local topographic dome. It then spilled northwards along a prominent north-trending linear ridge before entering a more vaguely defined northerly topographic high. Lateral migration was particularly rapid along the linear ridge where the CO_2 front advanced northwards at about 1 m per day between 2001 and 2004 (Chadwick and Noy 2010).

Boait et al. (2012) extended previous analyses by detailed mapping of the seismic data acquired between 1999 and 2008. The mapping revealed nine distinct reflective horizons. In each horizon, the area of reflectivity, interpreted as the CO_2 plume, is roughly elliptical with eccentricities ranging between two and four. In the top half of the reservoir, the interpreted plume grows linearly with time. In the bottom half, the interpreted plume initially grows linearly for about eight years and then progressively shrinks. The detailed analysis of Boait et al. (2012) also found a decrease in reflectivity over time in the central portion of several of the horizons. This was interpreted as being caused by flow of CO_2 between layers.

The Sleipner seismic dataset has also been valuable for testing of methods for quantitative interpretation/analysis of plume characteristics. Eiken et al. (2011) reported that the sum of the seismic amplitudes was observed to track linearly with

the volume of CO_2 injected. Chadwick et al. (2010) performed prestack and poststack inversion and found that prestack inversion provided improved characterization of the sand unit between the reservoir top and the uppermost intra-reservoir mudstone. They used specialized spectral decomposition algorithms to identify frequency tuning, from which CO_2 layer thicknesses could be derived. They found that AVO analysis to estimate CO_2 layer thickness proved challenging, in part because the CO_2 layers are thin. They also used a technology called extrema classification (Borgos et al. 2003) in order to better detect and map the intra-reservoir mudstones.

Finally, the plume migration shown by the seismic data has also been used as a basis for validation and refinement of numerical reservoir simulators (Bickle et al. 2007; Cavanagh 2013; Chadwick and Noy 2010; Estublier et al. 2013; Fornel and Estublier 2013; Nilsen et al. 2011; Singh et al. 2010). These studies involved conventional simulators based on Darcy flow, as well as invasion percolation simulation, which assumes that gravity and capillary forces dominate flow. Results show that available simulators are able to reproduce the Sleipner plume migration reasonably well, but the layering, which produce thin plumes with large differences in horizontal and vertical dimensions, and the complex topology of the flow paths, create challenges.

8.5.1.3 Other Monitoring at Sleipner

Sleipner is also the first project to employ gravity methods as part of the monitoring program. Gravity measurements have much lower spatial resolution than seismic measurements. However, gravity can provide information in situations where seismic methods do not work as well, and gravity measurements can be used to assess the amount of dissolved CO_2, to which seismic measurements are insensitive.

At Sleipner, precision gravity measurements were carried out using a ROVDOG (Remotely Operated Vehicle deployable Deep Ocean Gravimeter) at 30 seafloor stations above the CO_2 plume in the years 2002, 2005, and 2009 (Alnes et al. 2011; Nooner et al. 2007). About 5.88 million tons of CO_2 had been injected over this time period. Inversion for average density using geometry constraints from seismic gave 675–715 kg/m^3 for the density of the separate phase CO_2 in the reservoir. Combining this with temperature measurements, Alnes et al. (2011) concluded that the rate of dissolution of the CO_2 into the water did not exceed 1.8 % per year.

A Controlled Source Electromagnetic (CSEM) survey was carried out in 2008 (Eiken et al. 2011) using conventional surface-to-surface techniques. Modeling by Park et al. (2013) showed that the expected resistivity anomaly is around 5 % and probably close to the noise level of surface-to-surface CSEM data. Their modeling results also suggest, however, that the surface-to-borehole CSEM survey could provide high sensitivity data, opening a new possibility of applying CSEM to CO_2 reservoir monitoring in the future.

8.5.2 In Salah

8.5.2.1 Project Overview

The In Salah project, located at the Krechba Central Processing Facility in the central Algeria Sahara, is a joint venture of BP, Statoil, and Sonatrach. It is a commercial natural gas production project in which CO_2 is removed from the natural gas in order to meet the gas export specification of 0.3 % CO_2. The CO_2 content of the natural gas is 5–10 % (Ringrose et al. 2009). From 2004 to 2010 more than 3 million tons were stored. An extensive monitoring program was undertaken, both to meet the commercial needs of the project, and to support development of monitoring technologies. Monitoring was provided by the Joint Industry Project (JIP). This project is an interesting case history because of the unique monitoring technologies applied.

The Krechba Carboniferous reservoir is a sandstone rock which on average is 20 m thick with a porosity of about 13 % and a permeability of 10 mD (Ringrose et al. 2009). Structurally, it is a four-way dip (dome-like) closure, in which the hydrocarbons have accumulated at the high part of the dome. Down-dip from the natural gas, the rock was saturated with saline water, and the CO_2 was injected in this portion of the reservoir at a depth of about 1950 m. There were three CO_2 injection wells at Krechba, injecting up to about 2800 metric tons per day of CO_2. The reservoir is overlain by about 900 m of mudstone rock which acts as a seal against vertical migration of both the natural gas and the CO_2.

8.5.2.2 Monitoring at In Salah

The JIP mentioned above was set up in 2005 to monitor the CO_2 storage process using a variety of geochemical, geophysical, and production techniques (see Table 8.7) over a 5-year period. To help select monitoring technologies, the JIP also used a "Boston Square," which allows a comparison of techniques based on two criteria—cost and benefit to the project (Ringrose et al. 2013). Of the 29 monitoring technology options assessed, repeat 3D surface seismic technology had the highest benefit but also the highest cost. The use of surface seismic technology is challenging at Krechba. The Krechba sandstone storage domain is onshore, deep, thin, and has low porosity and permeability compared to other sites, such as Sleipner.

An extensive 3D seismic survey was carried out at Krechba in 1997. This survey defined the overall structure of the reservoir and provided information about its internal architecture and distribution of the sandy portions with the best porosity and permeability, but no significant faults were identified in this survey (Iding and Ringrose 2009). In 2002, when drilling began in the development phase of the project, it became evident that fractures and faults could play a role in production and injection operations. Data from the wells suggested that the injection horizon

Table 8.7 In Salah monitoring and verification technologies (adapted from Mathieson et al. 2011)

Monitoring technology	Application	Comment
Repeat 3D seismic	Plume migration	Initial survey in 1997
	Subsurface characterization	High resolution repeat 3D survey acquired in 2009
Microseismic	Caprock integrity	500 m test well drilled and recording information above KB502
InSAR monitoring	Plume migration	Images captured using X-band (8 days) and C-band (32 days)
	Caprock integrity	
	Pressure development	Used to develop time lapse deformation images
Tiltmeters/GPS	Plume migration	Used to calibrate satellite data
	Caprock integrity	
	Pressure development	
Shallow aquifer wells	Caprock integrity	5 wells drilled to 350 m—one beside each injector, one remote and one between KB5 and KB502
	Potable aquifer contamination	
Wellhead/annulus samples	Wellbore integrity	2 monthly sampling beginning 2005
	Plume migration	
Tracers	Plume migration	Different perflourocarbon tracers into each injector
Surface flux/soil gas	Surface seepage	Initial survey pre-injection
		Two surveys in 2009
Microbiology	Surface seepage	First samples collected in late. 2009/early 2010
Wireline logging/sampling	Sub-surface characterization	Overburden samples and logs in new wells
	Geomechanical and geochemical modeling	

and the immediate overburden are naturally fractured with a preferred NW-SE orientation (Iding and Ringrose 2009). A repeat 3D seismic survey was acquired in 2009 with improved shot spacing and fold to gain better imaging of the storage interval and caprock sequence. Two NW-SE trending linear features in the vicinity of the KB502 and KB503 CO_2 injectors were observed as slight depressions (velocity/amplitude pull-downs) on the 2009 3D seismic. These features are aligned with the dominant fracture orientation as identified in the well data.

When seismic is challenging, other methods take on additional importance in a monitoring program to provide information on the behavior of the plume. At In Salah, these methods included ground surface displacement measurement, annulus and wellhead monitoring, including tracer analysis and pressure monitoring, combined with history matching.

The tracer monitoring approach involved injection of small amounts of perfluorocarbons along with the CO_2, and sampling of well bore fluids in observation wells. Different perfluorocarbons were used to 'tag' the CO_2 injected at each

injection well, so that any CO_2 detected can be differentiated from the natural CO_2 in the subsurface and traced back to an individual injection well. The results of the perfluorocarbon tracer measurements confirmed that the CO_2 migrated from the injection well KB502 to well KB5, further demonstrating the impact of the NW-SE preferred fracture direction on plume migration.

Surface displacement measurements are a unique and significant aspect of the monitoring program at In Salah, which is the first application of satellite InSAR technology for monitoring of geologic storage. InSAR, which stands for satellite airborne radar interferometry, detects changes in elevation at the earth's surface. Injection of the CO_2 causes an increase in the pore pressure in the reservoir, and that pressure increase results in small displacements at the ground surface above the reservoir. The amount of surface displacement depends on the magnitude of the pressure, as well as geometry of the pressurized region, depth, and rock properties.

One advantage of InSAR data is the relative low cost and ease of acquisition compared to seismic data. The satellite is collecting data all the time, so the frequency with which data is available for a specific site is related to the orbit of the satellite and how often it passes over the site of interest.

A major challenge in application of this technology is to be able to resolve the very small surface displacements associated with CO_2 injection. At In Salah, the surface uplift due to CO_2 injection was about 3–5 mm/year, compared to approximately 200 mm per day due to earth tides. Methodologies for processing the satellite data to obtain higher resolution displacement measurements continue to evolve. PSInSAR (Permanent Scatterer InSAR), which has been applied at In Salah, gives an accuracy of around 5 mm/year and up to 1 mm/year for a longer term average (Ringrose et al. 2009).

Integration of InSAR data with geomechanical models, along with seismic and fracture data, provided important additional understanding of the impact of fractures/faults on plume migration at In Salah. InSAR data collected in 2006 and 2007 showed that, above the active injection wells, there was surface uplift, which was elongated and extended several km in the direction of the well KB5. The location and orientation of the uplift was found to be well aligned with the NW-SE trending linear features in the 2009 3D seismic data (Fig. 8.11). The uplift above injector KB-502 was in the shape of a double lobe, which Vasco et al. (2010) showed could be caused by opening of a vertical fracture extending above and below the injection zone. Evaluation of the rate and pattern of surface uplift at In Salah and its relationship to fluid pressure changes and fractures in the subsurface, has been the subject of several geomechancial modeling studies including Vasco et al. (2008), Rutqvist et al. (2010), and Gemmer et al. (2012).

Limited microseismic monitoring was also carried out at In Salah. A set of vertical 3-component geophones was deployed in a microseismic pilot well drilled to a depth of 500 m directly above the trajectory path of the KB-502 injection well. P-S arrival times, shear wave polarisation and time series analyses indicated that most of the observed events (over 1000 microseismic events) were related to CO_2 injection (Oye et al. 2013). Event location was very limited because the array was limited to a single pilot well, but analysis of the microseismic waveform data using

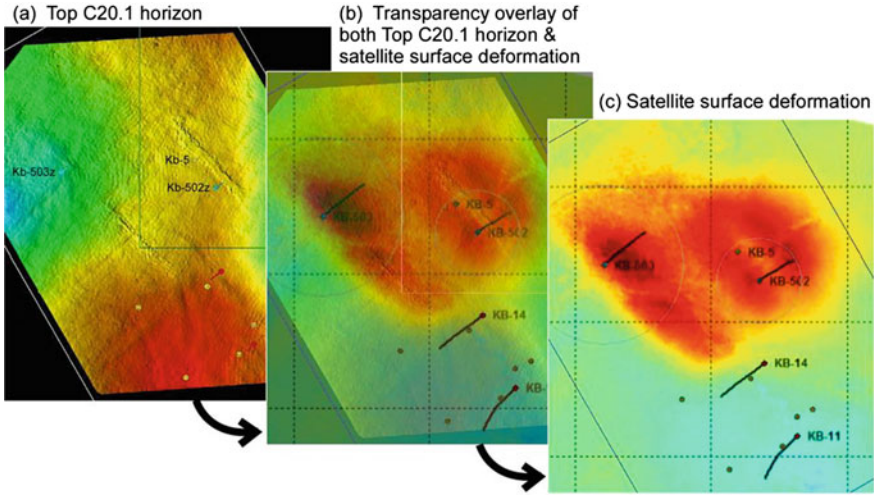

Fig. 8.11 NW-SE linear features seen on 2009 3D seismic data compared with InSAR surface deformation data (Ringrose et al. 2013)

cross-correlation techniques indicated that most events occurred within distinct spatial clusters (Oye et al. 2013).

Assessment of the microseismic data in combination with the other monitoring data discussed above has led to the conclusion (Ringrose et al. 2013), that CO_2 injection at In Salah stimulated natural fractures, and may have introduced new hydraulic fractures, in the vicinity of injection well KB-502. While analyses indicate that these fractures did propagate upwards into the lower caprock, it is considered unlikely that they propagated further through the upper caprock (Ringrose et al. 2013).

8.5.2.3 Other In Salah Monitoring Results

In addition to 3D seismic and InSAR measurements, data acquisition prior to injection included extensive sampling and logging programs (including image logs) in the new development wells, saline aquifer sampling and headspace gas sampling through the overburden, soil gas surveys around each of the new wells, and soil gas sampling from the shallow aquifer water wells.

Shallow soil gas and flux measurements were difficult because of the hard ground, but not impossible. Loose sand and gravel was found where the ground was not hard and these loose materials also presented difficulties because of the potential for contamination of samples due to movement of atmospheric gases through the highly permeable materials. Despite these difficulties, elevated CO_2 soil gas and flux measurements were observed near the KB-5 well, as would be expected given the breakthrough of CO_2 at the well (Jones et al. 2011).

Soil gas and flux measurements also provided some data on background CO_2 levels in a harsh desert environment. In comparison with more vegetated sites from temperate regions, the soil gas values were found to be lower by at least an order of magnitude compared with vegetated sites from temperate regions.

Changes which occur in plants in response to elevated levels of CO_2 in the soil, though not a direct measure of CO_2, are considered to be another indicator of leaking CO_2. Finally, it has been proposed that elevated levels of CO_2 in the soil might also affect microbial communities. At In Salah, vegetative cover is very low, commonly 10 % or less, though somewhat higher in topographic lows, reflecting the desert environment. Some of the plants represented species which might be affected by CO_2, if exposed to elevated soil gas concentrations. Microbial populations were also low, but were present (Jones et al. 2011).

8.5.3 Weyburn-Midale

8.5.3.1 Project Overview

The IEA GHG Weyburn-Midale CO_2 Monitoring and Storage Project began in 2000 in close collaboration with EnCana, which is the operator of the CO_2 EOR project in the Weyburn Field in Saskatchewan, Canada. While CO_2 EOR is considered a commercial technology, this project is unique because of its research focus on storage in conjunction with EOR. The Weyburn CO_2 EOR flood is likely the most intensely studied operation of its kind in the world.

The CO_2 EOR reservoir is the Midale beds of the Charles Formation. The Midale consists of a layer <30 m thick of fractured carbonate rock at a depth of about 1500 m. The reservoir is comprised of vuggy limestone ("Vuggy") and overlying marly dolostone ("Marly"). The reservoir is overlain by a seal of evaporate rocks (anhydritic dolostones and anhydrites). Above these are a series of additional sealing formations, including the Lower Watrous Member, which forms the most extensive primary seal to the Weyburn system (Whittaker 2004).

The Midale reservoir has been under oil production for decades. At the end of primary production in 1964, water flooding was begun to enhance production. Further field development, including application of horizontal wells, began in 1991 (Preston et al. 2005), and CO_2 injection began in 2000. By the end of 2011, a total of 21 M tons of CO_2 had been stored in the Weyburn-Midale field with total field injection rates of approximately 13 k tons per day (White 2013a). The CO_2 (a byproduct of gasification of lignite) is purchased from the Dakota Gasification synthetic fuel plant in Beulah, North Dakota, and transported through a 320 km pipeline to Weyburn.

8.5.3.2 Monitoring Activities in the Weyburn-Midale Project

Monitoring methodologies investigated as part of the project included:

- geochemical fluid sampling,
- surface seismic, augmented by VSP,
- passive seismic,
- shallow well monitoring and sampling,
- soil gas surveys, and
- tracers.

A comprehensive set of papers presenting results of Weyburn-Midale Project monitoring efforts has been published elsewhere (Wildgust et al. 2013). Some of the key findings are discussed below.

Unique among the global storage demonstrations is the geochemical fluid sampling campaign at Weyburn. A baseline geochemical sampling survey was followed by sampling on 16 occasions over the course of two time periods—from 2000 to 2004, and from 2008 to 2010. Wellhead fluid and gas samples from about 50 wells were analyzed for over 40 compositional and isotopic parameters, generating a unique, comprehensive database. The spatial and temporal changes in pH, alkalinity, concentrations of Ca and Mg, and carbon isotopes were found useful in monitoring the movement and fate of the CO_2 in the subsurface and providing indication of incipient CO_2 breakthrough at wells (Emberley et al. 2005; Gunter and Perkins 2004). The results show that geochemical monitoring provides valuable information for identifying the time scales required for solubility and ionic trapping of injected CO_2. Solubility trapping, i.e. the formation of H_2CO_3, was observed within six months of the onset of CO_2 injection and ionic trapping, i.e. the reaction of CO_2 with carbonate minerals, commenced within one year of injection (Shevalier et al. 2013). Results also showed that brine resistivity can be used to indirectly track the movement of injected CO_2 within the reservoir (Shevalier et al. 2013).

Advances in the application of surface seismic technology for monitoring were also made in the Weyburn-Midale project. The Midale reservoir was a challenging surface seismic because of its thinness and rock properties, but, through application of advanced acquisition and processing methods, it proved successful. 3D, three-component, time-lapse seismic data were acquired over a portion of the project area in 1999 (baseline survey), 2001, 2002, 2004, and 2007. Waveform correlation techniques were used during post-stack normalization of the time-lapse seismic data and then subsequently in determining the amplitude and travel time variations (White 2013a, b). The effects of CO_2 injection and oil production were observed in the 3D difference seismic volumes in both the amplitude changes for reflections from the reservoir, and in travel time changes for travel paths through the reservoir. Figure 8.12 is a plan map of the seismic amplitude changes which shows the spatial correlation between the amplitude changes and CO_2 injectors, and the temporal increase in area of these changes as injection increased. Comparison of the time-lapse seismic results to reservoir flow simulations demonstrated a clear

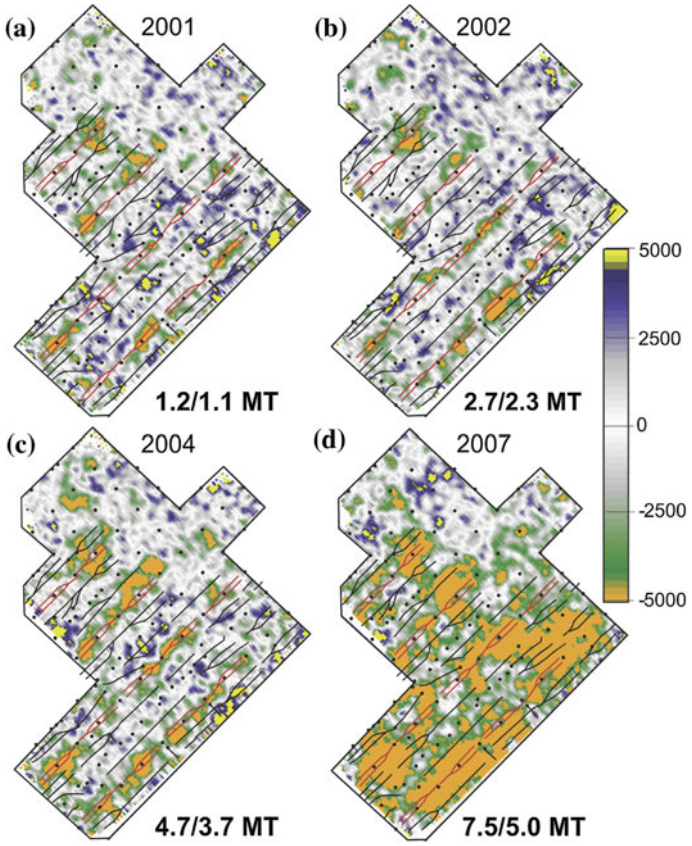

Fig. 8.12 Seismic amplitude difference maps at the Marly reservoir level for time-lapse surveys from 2001 to 2007. Estimates of the quantities of CO_2 injected and CO_2 stored (injected amount minus produced amount) are shown for each time. The amplitudes in each panel are scaled the same and are unitless. Horizontal CO_2 injection wells are shown in *red* whereas horizontal production wells are shown in *black* (White 2013a, b)

correlation between the injection-related reservoir changes and the resultant seismic response (White 2013a, b).

Additional processing (Meadows and Cole 2013), combined with extensive laboratory testing and rock physics modeling (Meadows 2013; Njiekak et al. 2013) was carried out to more quantitatively interpret the time-lapse seismic data at Weyburn. Prestack seismic data was migrated and used in an impedance inversion to obtain P- and S-wave impedance volumes. The resulting time-lapse impedance changes were input, along with the rock physics model, into a direct inversion algorithm to generate volumes of pore pressure and CO_2 saturation changes over time (Meadows and Cole 2013).

The 3D time-lapse seismic data was also analyzed to evaluate caprock integrity and to look for CO_2 which might have migrated vertically from the reservoir (White

2011, 2013a). White (2013a) used log-based fluid substitution modeling for calculating the seismic sensitivity to the presence of CO_2 within the various intervals, accounting for the effects of rock lithology, porosity, pore pressure and temperature. His analyses indicated that the maximum estimated proportion of CO_2 residing in either interval above the regional seal was ≤ 1 %, and the maximum amount of CO_2 potentially residing above the regional seal by 2007 was <56,000 tons.

Though limited in array size, the Weyburn Project was the first large-scale CCS pilot project to include downhole microseismic recording as a monitoring tool. The microseismicity was low in rate and intensity. During the monitoring period of 2003–2011, approximately 200 microseismic events were located (Verdon et al. 2013). The microseismicity predominantly occurred in episodic temporal clusters that were linked to specific operational field activities. Verdon et al. (2011) carried out coupled fluid flow-geomechanical simulations and found that stress changes induced by deformation of the reservoir were transferred into the overburden, leading to an increase in shear stress above the production wells. This stress transfer into the overburden has been interpreted (Verdon et al. 2013) as the likely cause of the events located in the overburden above the producing wells.

8.5.4 Discussion of Field Study Results

The results of these field projects have clearly yielded many advances in geologic storage through validation and demonstration of monitoring technologies. A diverse set of technologies for measurements at the surface and in the subsurface have been field tested. Technologies conventionally used by the oil and gas industry have been validated for application to monitoring of CO_2, and some unique new technologies have been demonstrated. The successful application of seismic techniques for monitoring the movement of CO_2 in the reservoir was clearly demonstrated. Positive results were obtained not only under "ideal" conditions like those at Sleipner, but elsewhere, under more challenging conditions associated with thin, deep, reservoirs. Studies also used seismic measurements to demonstrate that CO_2 has not migrated above confining zones. Though more work is needed, these studies have also provided some insight on the leakage volume detection threshold of surface seismic methods.

Though seismic methods have the highest resolution of the geophysical monitoring methods, it is clear that there are some circumstances where their applicability is limited, and the field studies also showed that other methods can provide complimentary information to improve understanding of plume behavior. Field projects (those discussed above and others) have now demonstrated successful use of satellite-based surface deformation, gravimetry, and electrical techniques, though more work is needed to better determine how broadly applicable they will be. Based on field performance in major pilots and some modeling, Fabriol et al. (2011) have offered the following comparative assessment of seismic, electrical, and gravimetric techniques (Table 8.8).

In addition to geophysical monitoring, the field tests have also demonstrated the value of other types of monitoring measurements, including pressure and temperature, tracers, fluid sampling for geochemical analyses, and well logs of many kinds. Geophysical monitoring is generally considered to be the most expensive type of monitoring, and it is noted that cost effective technologies such as wellhead and annulus monitoring were also proven to be useful.

While the field tests indicate that a portfolio of monitoring technologies is available, they do not yield a single prescriptive list of technologies which are applicable, or necessarily sufficient, for all situations. In fact, the experience to date suggests that monitoring programs will need to be developed to accommodate the unique geology, and risks, associated with each site.

Another observation, not only related to monitoring, but more generally to overall technical management of storage operations, is that injection strategies and monitoring plans need to be adaptable, and should be expected to evolve as experience and monitoring data become available during operation of the project. In none of the reviewed projects was the behavior of the CO_2 in the reservoir exactly as predicted before injection began.

The overall experience represented by the reviewed projects shows that monitoring of geologic storage of CO_2 is technologically feasible in a diverse set of geologic environments. Given the geology-specific nature of the technology, this experience is not sufficient, however, to draw conclusions about all geologic environments. Further work is needed to assess the technical feasibility across the spectrum of depositional environments that might be considered. In addition, very

Table 8.8 Comparison of performance of geophysical monitoring methods (adapted from (Fabriol et al. 2011)

Method	Minimum quantity for verification at reservoir depth (>800 m)	Minimum quantity for leakage detection at reservoir depth	Secondary reservoir detection (at depth ca. 200–300 m)	Minimum quantity in theory detectable in secondary reservoir	Geological limitations specific to CO_2 storage
4D seismic	Hundreds of km	Few km	Yes	Few hundreds of tons	Reservoir: low porosity, thin layers (tuning effect)
Electrical CSEM	1 Mt Few tens of ktons (at Ketzin at 600–700 m deep)	Not yet proved	Yes	Few tens of ktons	Low resistivity, thin layers (either resistive or conductive)
Gravimetry	1 Mt	Not yet proved	Yes	Few tens of ktons	Seasonal surface variations

little data has been developed about the post-injection behavior of CO_2 in the reservoir. The same monitoring tools used during the operational phase of storage are applicable to post-injection phase, but field demonstrations of the processes that lead to plume stabilization and long-term trapping are needed.

8.6 Pilot Scale CO_2 Injection and Monitoring: Frio Site

Christine Doughty

The Frio brine pilot, a research project conducted at the South Liberty oil field operated by Texas American Resources in Dayton, Texas, USA, injected 1600 metric tons of CO_2 over a period of 10 days into a steeply dipping brine-saturated sand layer at a depth of 1500 m (Hovorka et al. 2006). The pilot employed one injection well and one observation well. Pre-injection activities (see Chap. 7) included review of the regional geological setting, development of a detailed local geological model, analysis of wireline logs, laboratory analysis of core samples, collection and chemical analysis of brine samples, pressure-transient analysis of an interference well test, and breakthrough curve analysis for a two-well recirculation tracer test. During CO_2 injection, pressure transients were monitored at both wells and downhole fluid samples were collected frequently at the observation well. Geophysical monitoring of CO_2 movement in the subsurface during and after the injection period provided information on the spatial distribution of CO_2 at several different scales. Frio brine pilot activities are outlined in Table 8.9, and are described in the following sections. Table 8.10 summarizes the material properties and formation conditions inferred from traditional site characterization. This Chapter highlights results from the Frio Brine Pilot monitoring campaign and associated modeling, with an emphasis on lessons learned for future GCS activities. More details on monitoring and modeling of the Frio Brine Pilot may be found in Hovorka et al. (2006), Kharaka et al. (2006), Doughty et al. (2008), Daley et al. (2008, 2011) and Xu et al. (2010).

8.6.1 Geologic Setting and Development of Geologic Model

The Oligocene Frio Formation is an extensive sedimentary formation in the Gulf Coast of the USA, with ample capacity for GCS in thick sandstone layers separated by shale seals, underlying an abundance of CO_2 point sources. The Frio Formation extends over much of the Texas Gulf Coast ($\sim$500 km), at depths ranging from 0 to 3000 m. For depths greater than 800 m (below which CO_2 is supercritical at Frio), porosity ranges from 0.25 to 0.30, net sand thickness is 100–500 m, and permeability is 100 md to 5 d. This setting makes the Frio Formation a logical choice for an early pilot of GCS.

Table 8.9 Activities at the Frio brine pilot

Activity	Monitoring	Information obtained
Review existing data related to historical oil production	3D seismic	Structure of sand and shale layers surrounding salt dome
	Wireline logs in regionally distributed wells	Compartmentalization into fault blocks
Well log analysis	Wireline logs in injection and observation wells	Target sand layer and overlying shale caprock
		Extent, continuity, and variability of layers
		Permeability, porosity, relative permeability parameters (estimated using literature correlations)
Core analysis from newly drilled injection well	Porosity	Calibration for well-log estimates of porosity and permeability
	Permeability	
	Mercury injection	Capillary pressure/saturation relationship
Interference well test	Pressure transients	Inter-well connectivity
		Flow properties of lateral boundaries
		Field-scale permeability
		Estimates of pressure increase during CO_2 injection
Aqueous-phase tracer test	Fluorescein breakthrough curve (BTC)	Single-phase dispersivity
		Porosity-thickness product of sand layer
CO_2 injection and post-injection rest period	CO_2 arrival at observation well	Average CO_2 saturation between wells
	Pressure transients	Two-phase flow properties
	RST (reservoir saturation tool)	CO_2 saturation profiles at injection and observation wells
	Crosswell seismic	CO_2 distribution between injection and observation wells
	VSP (vertical seismic profile)	CO_2 distribution updip of observation well
Two-phase tracer test (concurrent with CO_2 injection)	Two-phase tracer BTC	Two-phase dispersivity
		Evolution of CO_2 saturation distribution with time

In the vicinity of the South Liberty field, the fluvial-deltaic Frio Formation is overlain by the regionally extensive, low permeability Anahuac shale, which acts as a regional upper seal for the Frio Formation sands. Individual sand layers, identified as A, B, C, etc., are separated by more localized shale layers that also serve as barriers to flow. At the South Liberty field, numerous wells drilled for historical oil production at depths around 2400 m provide structural information about the site (Hovorka et al. 2006). The brine-saturated sand layer targeted for CO_2 storage, the C sand, is near the top of the Frio Formation at a depth of 1500 m and is on the flank of a salt dome (Fig. 8.13), where the Frio Formation is laterally compartmentalized by faults (Fig. 8.14). A new injection well was drilled for the Frio brine pilot, sited 32-m down dip from an existing well that served as the observation well. The fault block in which the wells lie is about 800 m across and at least 2500 m

Table 8.10 Material properties and formation conditions obtained from traditional site-characterization

Property	Method	Value	Comments
Injection interval (thickness of high-permeability clean sand), h	Wireline logs	5.5 m	Figure 8.15b
	Match tracer test BTC	8 m	Figure 8.17
			Thickness varied, porosity held fixed at 0.34
Porosity, ϕ	Wireline logs calibrated to core analysis	0.34 average over 5.5-m injection interval	Figure 8.15a
		0.28 average over 23-m thick C sand	
Permeability, k	Wireline logs calibrated to core analysis	2264 md average over 5.5-m injection interval	Figure 8.15b
		1001 md average over 23-m thick C sand	
	Interference well test	Around wells: kh product consistent with wireline logs, low vertical permeability below clean sand creates leaky aquifer	Figure 8.16
			Average k = 1556 md for an 8-m thick layer
Hydrologic properties of small fault	Interference well test	No hydrologic effect	Figure 8.16
Formation compressibility, C	Interference well test	1.28×10^{-9} Pa^{-1}	Figure 8.16
			Defined as $C = (1/\phi)\partial\phi/\partial P\|_T$
Capillary pressure parameters	Mercury injection on core samples	van Genuchten (1980) parameters: P_{c0} = 6500 Pa, n = 1.7, S_{lmin} = 0.03 for a sample with k = 837 md	Curve-fit to drainage curves, also used for imbibition curves $P_{c0} \sim k^{-1/2}$
Dispersivity, α	Match tracer-test BTC	0.1 m	Figure 8.17
Pressure, P	Downhole sensor	152 bars	
Temperature, T	Wireline logs, fluid sampling	59 °C	Average of 56–65 °C range obtained for different measurements
Salinity	Fluid sampling	0.093 mg/L	

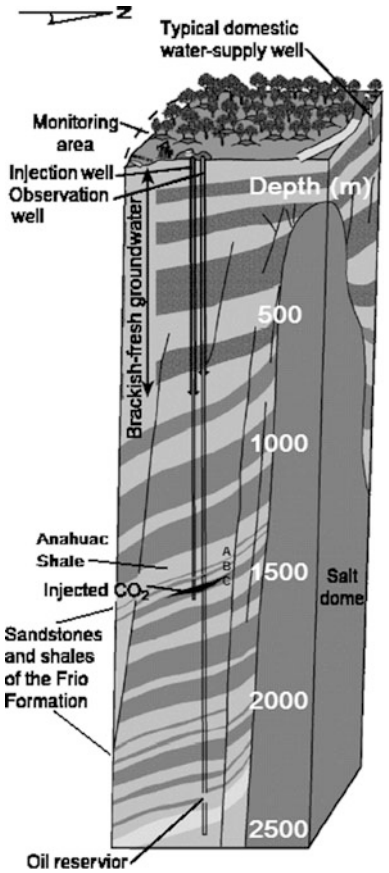

Fig. 8.13 Schematic of the Frio brine pilot site (after Hovorka et al. 2006)

long, and is bounded by mapped faults to the northwest and southeast. Several smaller intra-block faults also exist.

Figure 8.15 shows the porosity and horizontal permeability profiles for the C sand inferred from injection-well logs, with calibration to porosity and permeability measurements made on core samples (Sakurai et al. 2006). Observation-well logs (not shown) contain similar features, suggesting good layer continuity between the two wells. The ratio of vertical to horizontal permeability is assumed to be an increasing function of porosity, and ranges from 0.1 to 1.0. Each well was perforated over approximately 6 m in the upper portion of the 23-m thick C sand, which Fig. 8.15 identifies as a thick interval of clean sand. The lower limit of the injection interval is delineated by a thin marker bed, which is interpreted as low-permeability shale. Capillary pressure as a function of saturation was measured for two core samples, one sandstone and one shale, using mercury injection (Sakurai et al. 2006).

Frio Formation brine samples were collected from both wells at a series of times

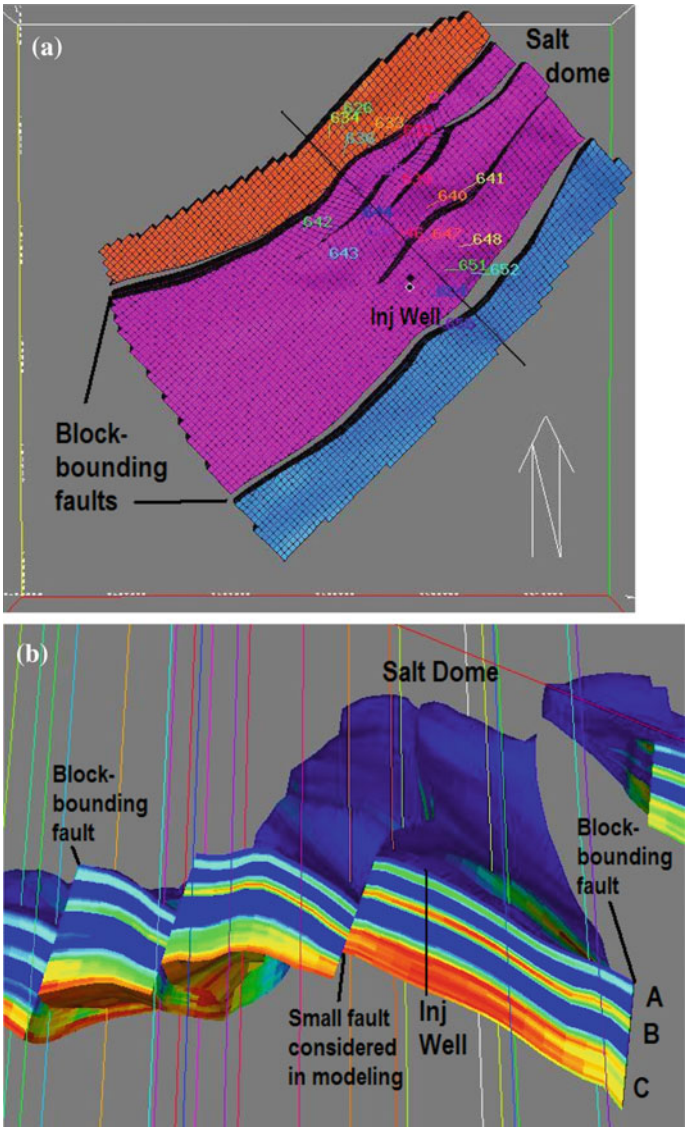

Fig. 8.14 Geological model of the upper Frio Formation at the South Liberty field (courtesy of Joseph Yeh, TBEG). **a** Plan view of the modeled fault block (*pink*) and two adjacent fault blocks. The new injection well is shown as a *black dot with a white border*. The existing observation well is the *black dot* just to the north. **b** Vertical cut through the model along the *black line* shown in the plan view. Vertical exaggeration is approximately a factor of two. *Colored lines* and *numbers* identify wells used to create the geological model

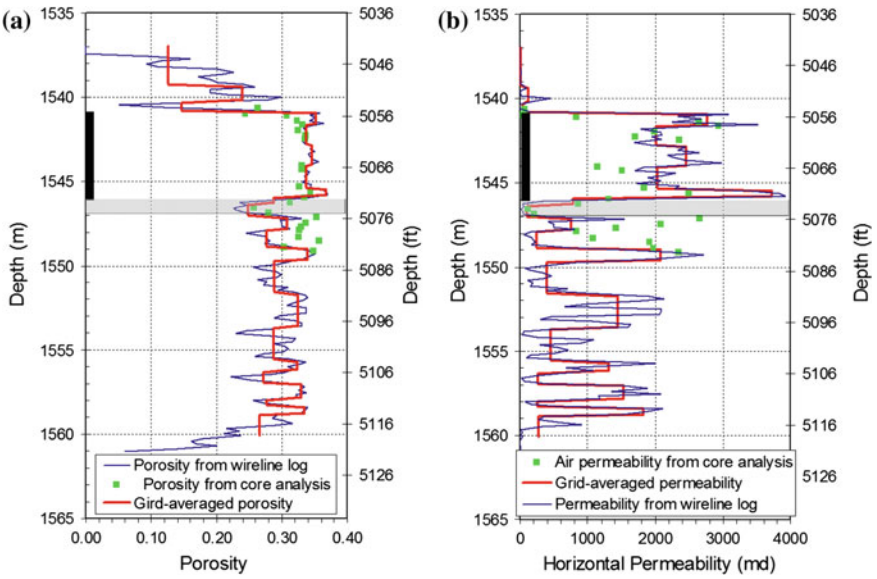

Fig. 8.15 Injection-well property profiles for the C sand (courtesy of Shinichi Sakurai, TBEG), and the grid-averaged values used for the original 3D numerical model: **a** porosity and **b** horizontal permeability

before CO_2 injection. Chemical analysis identified a Na-Ca-Cl-type brine with 93,000 mg/L total dissolved solids (TDS), nearly saturated with methane (CH_4) at formation conditions of about 150 bars and 60 °C (Kharaka et al. 2006). These dissolved salt and methane contents are typical of brine formations found in the vicinity of petroleum resources in the northern Gulf of Mexico basin (Kharaka and Hanor 2003).

8.6.2 Site Characterization

8.6.2.1 Numerical Model for Flow and Transport

Based on the geological model shown in Fig. 8.14, a three-dimensional numerical model employing the TOUGH2 simulator (Pruess et al. 1999) was developed to simulate flow and transport for the Frio brine pilot, and is described in more detail in Doughty et al. (2008). The model represents the C sand and extends over the entire fault block in which the injection and observation wells lie.

8.6.2.2 Interference Test

A 24-h interference well test was conducted by pumping from the observation well and observing pressure changes in both wells. Figure 8.16 shows the pressure transient at the injection well and several modeled pressure transients obtained with different analysis methods. The simplest method is to match the pressure transient to an analytical solution (Theis 1935), which assumes a uniformly thick, homogeneous, flat layer of infinite radial extent that is perfectly sealed above and below. For the early-times behavior a good match to the pressure-transient data could be obtained with the Theis solution (Fig. 8.16), but the linear Theis curve begins to deviate from the field data after about one-half hour of pumping, predicting too large a pressure drawdown.

The pressure drawdown obtained by simulating the interference test with the 3D model becomes too small after only about 100 s ("Original Model" in Fig. 8.16), but has the linear shape of the Theis solution. Figure 8.16 shows that the data do not have the linear character of the Theis solution, but rather show a marked flattening. Such a response is characteristic of a leaky aquifer, in which fluid flows to the pumped well from both the pumped interval and to a lesser extent from above and/or below (Hantush and Jacob 1955), see also Chap. 7. From Fig. 8.15b it can be seen that the permeability just above the pumped interval is very low, but that the permeability of the marker bed below the pumped interval is moderate. By decreasing the vertical permeability of the marker bed from 3 md to 0.25 md, the pressure drawdown labeled "Leaky 5.5-m sand, no small fault" in Fig. 8.16 is obtained, in which the observed flattening beginning at 0.5 h is much better represented.

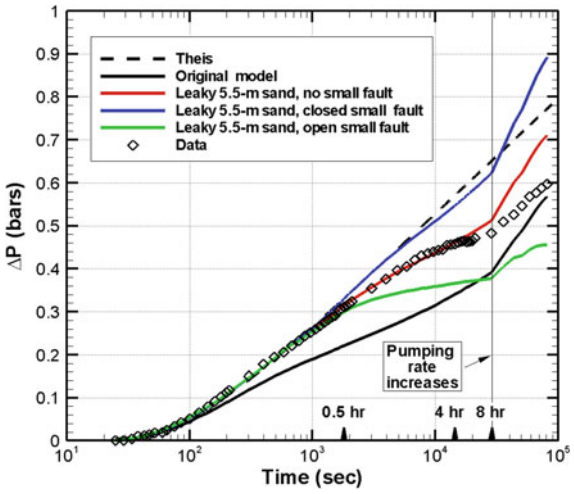

Fig. 8.16 Interference-well-test pressure transient (Doughty et al. 2008) and various model results

To investigate the hydrologic nature of the intersection of the small fault northwest of the observation well and the C sand, three distinct fault conditions are considered with the 3D model: (1) the fault is absent, (2) the fault is a closed boundary, and (3) the fault is a constant-pressure boundary (open small fault). The effect of the small fault is felt about 0.5 h after pumping begins. Both the closed-fault case and the constant-pressure-fault case diverge sharply from the field data, suggesting that the fault does not act as either of these types of boundaries.

There is independent evidence from the tracer test that the thickness of the high-permeability clean sand in which the injection well is perforated is about 8 m, significantly larger than the 5.5 m inferred from the well logs. Because the pressure drawdown response to pumping is primarily sensitive to the permeability-thickness product of a formation, the interference-test data shown in Fig. 8.16 can be equally well matched by a model with a thickness of 8 m, if permeability is decreased correspondingly. The modified model is referred to as the "8-m sand model" and the previous model is referred to as the "5.5-m sand model".

In summary, matching the injection-well (non-pumped well) pressure transient during the interference well test does not provide a single, uniquely-determined hydrologic model of the C sand, but rather two models that bound a range of reasonable models. The clean sand acts as a leaky aquifer, and sensitivity-study results indicate that the small fault within the main fault block should not be considered either a closed or constant-pressure boundary, therefore it was not included in further modeling studies.

8.6.2.3 Tracer Test

After the interference well test had run for 24 h, pumped fluid was reinjected into the injection well, to create a balanced doublet flow field. After another 24 h, when the flow field was steady, a 78-min pulse of fluorescein dye was added at the injection well. The steady flows were maintained for 15 days. Fluorescein arrived at the observation well after 9 days and concentration peaked at 12 days, as shown in Fig. 8.17. The primary parameters to be inferred from the tracer breakthrough curve (BTC) are the porosity-thickness product of the sand layer through which fluid flows and the aqueous-phase dispersion coefficient for the sand, a measure of its heterogeneity. Preliminary attempts to model the tracer test using the 3D numerical model described in the previous section were unsatisfactory, because numerical dispersion smeared out the tracer peak too much for a physical dispersion coefficient to be determined. Therefore, a streamline model (Javandel et al. 1984) is used, with a random walk added to represent dispersion. Figure 8.17 presents modeled breakthrough curves for two different sand-layer thicknesses: the 5.5-m value inferred from the injection well logs (Fig. 8.15), which results in a far too early peak, and an 8-m value, determined by trial and error to best match the observed fluorescein peak time of 12 days. In both cases, porosity is held fixed at 0.34, the average value obtained from wireline logs and core analysis. Matching the width and height of the observed fluorescein peak requires a small single-phase

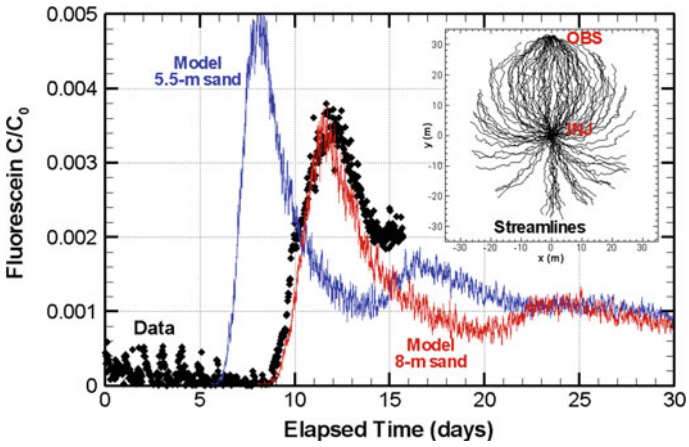

Fig. 8.17 Tracer test data (Doughty et al. 2008) and results of a streamline model

dispersivity (0.1 m), implying that the sand is highly homogeneous, which is considered reasonable for a clean sand. Note that the model breakthrough curves show two peaks, the main peak (8 or 12 days) and a smaller, later recirculation peak (16 or 24 days), which identifies tracer that has arrived at the observation well, been reinjected into the injection well, and traveled to the observation well again. In the field, it does not appear that tracer monitoring continued long enough for a recirculation peak to arrive. The increase in fluorescein concentration observed at 15 days (Fig. 8.17) is considered unlikely to be a recirculation peak, as it would imply a 3-day second trip through the formation, which is too fast.

The 8-m sand thickness inferred from tracer arrival time is certainly possible in terms of the expected variability in sand layer thickness for this geologic setting, and, as described in the previous section, interference test results can be equally well matched assuming either a thickness of 5.5 m or 8 m for the high-permeability zone in which the injection well is perforated. Therefore, the 8-m sand is retained for further modeling studies.

8.6.3 CO_2 Injection and Monitoring

8.6.3.1 Numerical Model for Multi-phase Flow

The well-test and tracer-test described above involve single-phase flow in which gravity does not play a significant role, enabling analysis with an analytical solution or simple single-phase numerical models. However, when CO_2 and brine are both present, multi-phase and gravity effects are significant, requiring a 3D numerical model with two-phase flow capabilities such as TOUGH2 (Pruess et al. 1999).

The simulation results shown here use the capillary pressure curve obtained by fitting to mercury injection data from a C-sand core sample (Sakurai et al. 2006), and hysteretic relative permeability functional forms (Doughty 2007), which are derived from the van Genuchten (1980) formulation (see also Chap. 3). The key parameters of the characteristic curves that need to be identified are the maximum residual gas saturation S_{grmax} and irreducible liquid saturation S_{lr}, below which each phase is immobile, and a parameter describing the interference between the two phases when both are mobile, m, which can range from about 0.4 to 0.9, with lower values of m corresponding to more mobile gas and less mobile liquid, and higher values of m corresponding to less mobile gas and more mobile liquid. During a CO_2 injection period, drainage is the dominant process because the CO_2 plume is growing in all directions. For drainage, the residual gas saturation, S_{gr}^{Δ} , is zero and the parameters controlling plume behavior are S_{lr} and m. After injection ends, the leading edge of the CO_2 plume may still undergo drainage as the plume moves upward and updip by buoyancy forces, but at the trailing edge of the plume imbibition occurs, with S_{gr}^{Δ} depending on saturation history and ranging from zero to S_{grmax}.

Characteristic curves for the base-case simulations of the Frio brine pilot used values of S_{grmax} and S_{lr} taken from the literature: S_{grmax} varies inversely with porosity and averages 0.2 for the C sand (Holtz 2002, 2005); $S_{lr} = 0.15$ (Bachu and Bennion 2007). The parameter m was chosen to produce a liquid relative permeability curve similar to a Corey (1954) liquid relative permeability curve (m = 0.9). Simulations were also run with values of S_{grmax} that are half the literature values and taking $S_{grmax} = 0$; with S_{lr} values of 0, 0.30, and 0.45; and with m values of 0.7 and 0.5.

Figure 8.18 shows a time-series of snapshots of the modeled free-phase CO_2 plume during and after the 10-day injection period, using the base-case parameters and the properties shown in Table 8.10. It is clear that buoyancy forces have a large effect on plume evolution. Figure 8.18 also shows that CO_2 distributions for times later than 29 days are very similar to one another, indicating that by that time most gas saturations have decreased to residual values and the CO_2 plume is largely trapped.

8.6.3.2 Downhole Fluid Sampling with U-Tube

Sampling of representative fluids in deep boreholes is challenging because of the need to minimize external contamination and maintain sample integrity during recovery. The U-tube sampling methodology (Freifeld et al. 2005; Freifeld and Trautz 2006) (Sect. 8.4) was developed to collect large volume, multi-phase samples at in situ pressures. At the Frio brine pilot, a U-tube was used to collect a 52-l sample from the observation well every two hours, which was weighed at the surface while being maintained at downhole pressure conditions ($\sim$150 bars). A decrease in sample density from that of formation brine ($\sim$1070 kg/m^3) to that of

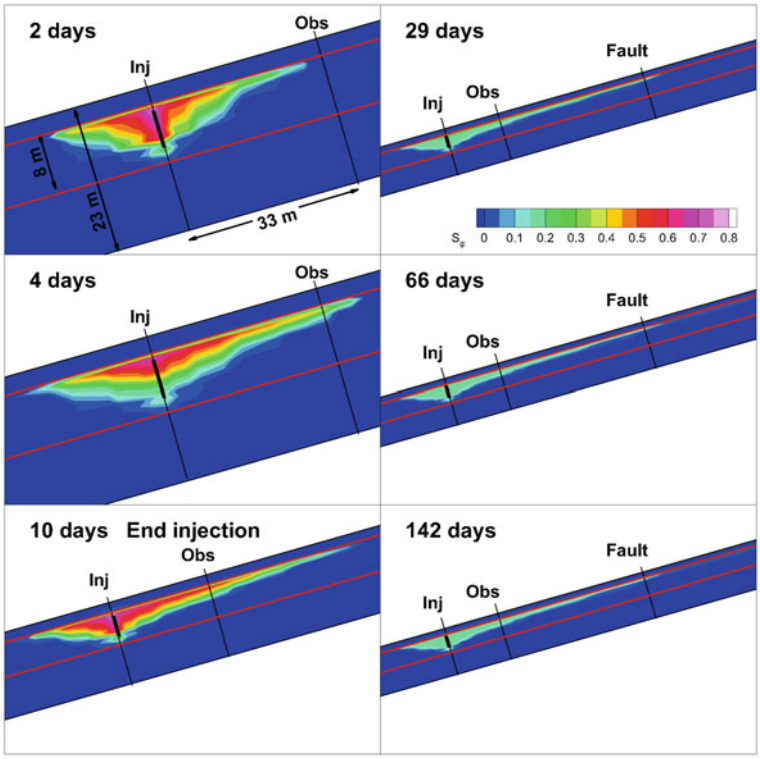

Fig. 8.18 Base-case simulation results showing the evolution of the free-phase CO_2 plume in the vertical cross-section containing the two wells

supercritical CO_2 ($\sim$830 kg/m^3) revealed the transition from single-phase brine to single-phase CO_2 in the wellbore 2.1 days after injection began (Fig. 8.19). Analysis of sample gases (dissolved or separate phase) was performed in the field using a quadrupole mass spectrometer, which also provided unequivocal evidence of the arrival of the CO_2 plume. Additionally, pulses of gas-phase tracers were added to the injection stream at several times during the CO_2 injection period, and their arrival at the observation well provided an indication of changes in CO_2 saturation as injection proceeded.

During the 10-day injection period the CO_2 plume is continually growing, so the formation is undergoing drainage. Therefore, fluid flow (and hence observation-well arrival time) is sensitive to S_{lr} and m, but is not sensitive to S_{grmax}. The CO_2 injection period was modeled using several values of S_{lr} and m, as shown in Fig. 8.19. Note that the U-tube sample density decreases much more than any of the model densities do, because model density represents fluid density in the near-well region, not the density of the wellbore fluid itself, which is what the U-tube samples.

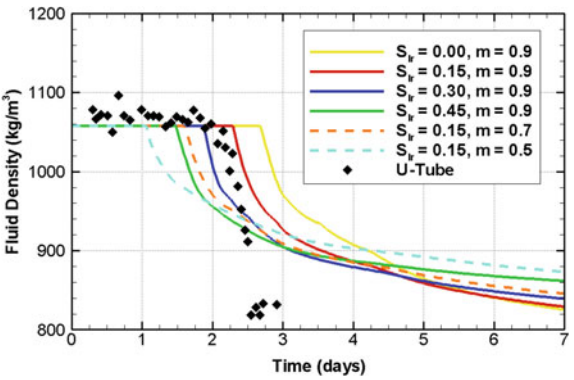

Fig. 8.19 CO_2 arrival at observation well as monitored with U-tube sampling (Doughty et al. 2008) and model results considering different two-phase flow parameters

Figure 8.19 shows that models using S_{lr} = 0.15 or 0.30 and m = 0.9 give the best match to the field data, and that CO_2 arrival time decreases as S_{lr} increases and as m decreases. Larger values of S_{lr} cause a decrease in CO_2 arrival time two ways. First, with a larger S_{lr}, CO_2 bypasses more immobile brine, so it moves faster through the formation. Second, increasing S_{lr} increases total mobility (the sum of liquid- and gas-phase mobilities), hence it enables more buoyancy flow to occur, resulting in an early arrival of a thin finger of CO_2 shallow in the observation well. Decreasing m also increases total mobility and therefore enhances buoyancy flow.

It is worthwhile to note that the travel time between the two wells is much longer for the aqueous-phase fluorescein tracer (~9 days, Fig. 8.17) than for the two-phase CO_2 plume (~2 days, Fig. 8.19). Various factors contributing to this difference are presented in Table 8.11. Differences in the flow fields imposed by injection and pumping conditions (doublet for the tracer test, single-well for the CO_2 injection, lower injection rate for CO_2) tend to delay the CO_2 arrival, but the delay is more than balanced by the speedup arising from the buoyant, two-phase nature of the CO_2 plume. The modeled distribution of CO_2 (Fig. 8.18) indicates that buoyancy flow and the bypassing of brine within the plume both strongly contribute to the early arrival of CO_2. This finding reiterates the value of a numerical model for interpreting field data. It also illustrates the difficulty of trying to define a simple performance measure such as average CO_2 saturation, which is needed for making capacity assessments of potential CO_2 geologic storage sites (Doughty et al. 2001; Hesse et al. 2006). The average CO_2 saturation within the plume primarily reflects two-phase flow behavior, and indicates the fraction of individual pores that are filled with CO_2. Theoretically it should be consistent with values inferred from laboratory studies. However the average CO_2 saturation over the entire formation is more relevant for capacity assessment, and if buoyancy flow (or heterogeneity) causes the CO_2 plume to avoid large fractions of the formation entirely, the formation-average saturation and the plume-average saturation will be quite different. Neither way of averaging is wrong per se, but care must be taken to use each average in the proper context.

Table 8.11 Comparison between aqueous-phase tracer test and co_2 arrival times

	Tracer test	CO_2 injection	Expected impact on CO_2 arrival time
Arrival at observation well	9 days	2 days	
Flow field	Doublet	Single well	3 times slower
Injection rate	50 gpm	40 gpm	20 % slower
Phase conditions	Single-phase	Two-phase	Faster, bypass pore space containing other phase
Density contrast	None	1.5	Faster, buoyancy flow
Viscosity contrast	None	12	Faster, enhanced buoyancy flow
Density in situ	1060 kg/m^3	~800 kg/m^3	20 % faster

8.6.3.3 Pressure-Transient Analysis

Downhole pressure was measured in both wells throughout the ten-day CO_2 injection period and for about two weeks thereafter (Benson and Doughty 2006; Hovorka et al. 2006). Compared to the 24-h interference test, this longer monitoring period enables the hydrologic properties of more distant features of the fault block to be examined. For example, if the two fault-block boundaries nearest the wells (~600 m to the northwest and ~250 m to the southeast) are considered constant-pressure boundaries, which works for the interference test, modeled pressure increases accompanying CO_2 injection are too small. In contrast, if the more distant salt-dome boundary (~1200 m to the northeast) is considered a constant-pressure boundary, model pressure increases during CO_2 injection are about right, whereas a closed boundary there produces model pressure increases that are too large. Whether this boundary is closed or constant-pressure has no effect on the shorter interference test.

Several stoppages were planned for the injection period, so that pressure-transient analysis could be conducted under two-phase flow conditions. Additional short-term breaks in injection occurred due to operational problems. Pressure-transient responses under two-phase conditions are sensitive to relative permeability parameters, in addition to the intrinsic permeability and formation compressibility, which were inferred from the interference well test. Because only short breaks occur in the injection schedule, drainage is the dominant process occurring throughout the injection period, hence S_{lr} and m are the main parameters to infer. Generally, ΔP decreases as S_{lr} increases and m decreases, consistent with the increase in total mobility that accompanies these parameter changes. The best match to observation-well ΔP is obtained for S_{lr} between 0.15 and 0.30, and m between 0.7 and 0.9, but the sensitivity of the observation-well pressure transient data to S_{lr} and m is rather small, implying that other values of these parameters are also possible.

8.6.3.4 Reservoir Saturation Tool

The wireline reservoir saturation tool (RST), developed by Schlumberger, uses pulsed neutron capture to determine changes in brine saturation as CO_2 displaces brine or vice versa (Hovorka et al. 2006; Sakurai et al. 2006). RST logging was deployed prior to CO_2 injection to determine a baseline and 3 times in the injection well (days 10, 66, 142) and 5 times in the observation well (days 4, 10, 29, 66, 142). Comparing depths at which CO_2 appears in the model to those from the RST logs provides valuable insights into geology, whereas comparing the magnitude of CO_2 saturation S_g provides constraints on two-phase flow properties.

At the injection well, RST logs show that CO_2 extends significantly below the perforated interval. This distribution is best reproduced by the 8-m sand model. This finding supports the hypothesis underlying the 8-m sand model that the thin marker bed located just below the perforations does not have nearly as low a permeability as was inferred from well logs (Fig. 8.15b). At both wells, CO_2 extends almost 1 m shallower than predicted by the model, suggesting that a low-permeability layer identified just above the perforations in both wells may not be continuous, allowing CO_2 to move upward into an overlying sand layer. These findings are consistent with the large sand-layer thickness inferred from the single-phase tracer test, but only the CO_2 injection provides specific information about how this greater thickness may arise.

RST logs collected during the injection reflect a growing CO_2 plume, with drainage occurring throughout the plume, while those obtained during the subsequent rest period reflect the trailing edge of a migrating CO_2 plume, where imbibition occurs. Simulations results for values of S_{lr} from 0 to 0.45, m from 0.5 to 0.9, and S_{grmax} from 0 to 0.2 show the expected dependence on S_{lr}, m, and S_{grmax}. During injection, as S_{lr} increases or m decreases, S_g decreases, as more brine is bypassed rather than being displaced by the invading CO_2, whereas during the subsequent rest period, different values of S_{lr} and m have no impact on the S_g profiles. In contrast, during injection S_{grmax} has no impact on the S_g profiles, whereas during the rest period the amount of CO_2 remaining in the region around the wells decreases dramatically as S_{grmax} is decreased.

The model trends support the use of a small value of S_{lr}, a large value of m, and a large value of S_{grmax} for modeling. However, all model S_g values are significantly smaller than the S_g values obtained from the RST logs. The model results represent the average S_g over a 2-m wide grid block. An RST radius of influence smaller than 1 m could therefore account for some of the discrepancy, especially for the injection well, where conditions can change sharply close to the well.

8.6.3.5 Crosswell Seismic

Crosswell seismic data obtained using source and receiver strings in the observation well and injection well, respectively, were collected shortly before injection of CO_2 and again about six weeks after CO_2 injection ended (Daley et al. 2008). P-wave

velocity depends on gas saturation S_g, so a difference tomogram of the seismic velocity before and after CO_2 injection provides an image of the free-phase CO_2 distribution in a vertical plane between the wells, as shown in Fig. 8.20a. A rock physics model for seismic velocity is needed to provide a quantitative relationship between velocity change and S_g. Ideally such a model would be site-specific, derived from core analysis and the relationship between well-log measurements of seismic velocity and well-log measurements of S_g, such as those obtained from the RST. Unfortunately, not all the requisite components for a rock physics model are available for the Frio Formation C sand and a rock physics model calibrated to the Utsira Sand being used for the Sleipner CO_2 storage operation in the North Sea (Carcione et al. 2006; Hoversten et al. 2003) was applied. This modeling suggests that six weeks after CO_2 injection ended, S_g in the vicinity of the injection well was approximately 20 % and S_g near the observation well was approximately 10 % (Daley et al. 2008). RST profiles collected during the CO_2 injection period are shown along the sides of the tomogram, providing a consistency check on the seismic inversion. The crosswell seismic tomogram shows clearly that the inter-well region is heterogeneous, although the resolution of the tomogram (1-5 m) precludes detailed interpretation of specific features.

Plots of the spatial distribution of CO_2 in the vertical plane between the injection and observation wells are shown in Fig. 8.20b for simulations using three values of S_{grmax}. The model plume using the literature values of S_{grmax} ($\sim$0.2) matches the crosswell seismic tomogram best, with $S_g \sim 0.2$ near the injection well, and S_g decreasing and the plume becoming thinner as distance from the well increases. For the case with half S_{grmax}, the shape of the CO_2 plume is similar, but the modeled S_g is too low everywhere, and close examination shows that the maximum S_g does not occur at the injection well, but has migrated away from it. For the case with zero S_{grmax}, the plume migration is extreme and clearly not consistent with the field data. Hence, we infer that the original values of $S_{grmax} \sim 0.2$, which enable significant CO_2 mobility trapping, are optimal.

8.6.3.6 Vertical Seismic Profile

Vertical seismic profile (VSP) data were obtained by creating lines of explosions along the ground surface at three azimuthal directions around the injection well (NW, N, NE), and monitoring P-wave amplitude at the receiver string deployed in the injection well (Daley et al. 2008). VSP data were collected twice: once shortly before CO_2 injection, then again about six weeks after CO_2 injection ended. Figure 8.21 shows the change in P-wave amplitude before and after CO_2 injection, plotted as a function of offset from the injection well, for each direction, along with the corresponding model results for three values of S_{grmax}. The resolution of the VSP data is about 10–30 m, whereas the model resolution varies from 5 m close to the wells to more than 100 m for the largest offsets shown. A quantitative relationship between VSP change in amplitude and CO_2 saturation is not known, so the vertical axes of the plot are adjusted to align these two quantities close to the

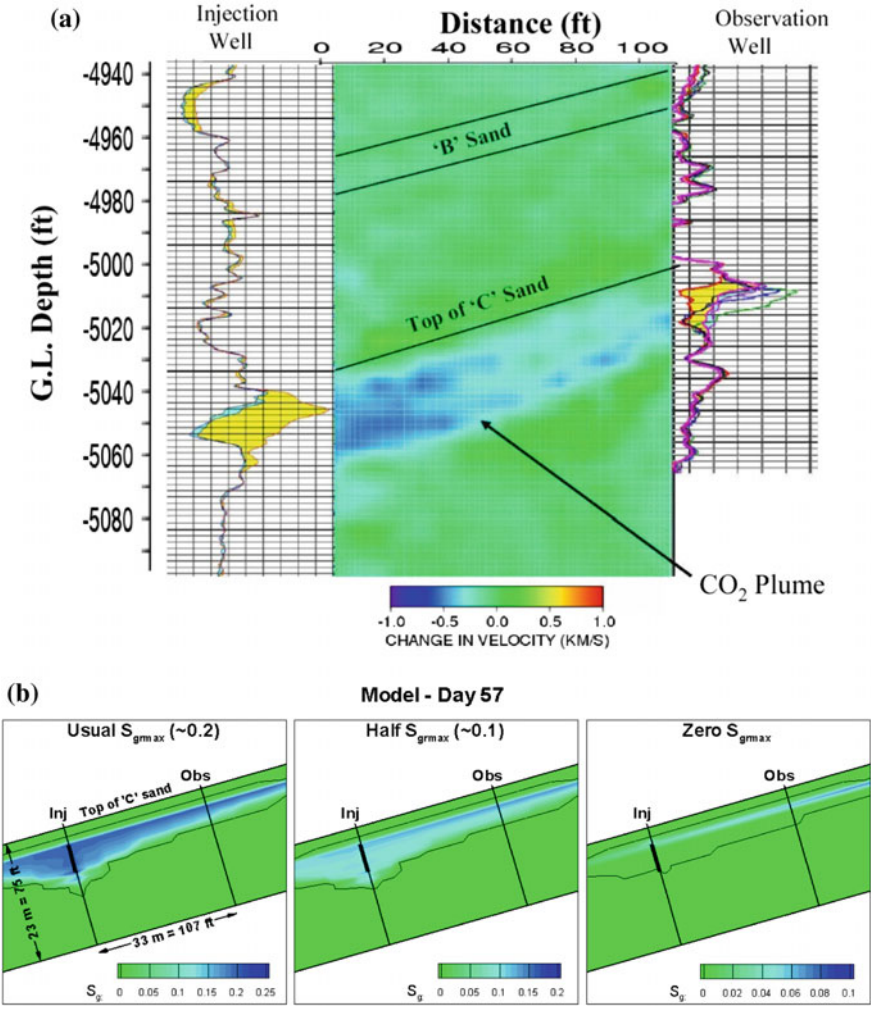

Fig. 8.20 **a** Crosswell seismic tomogram of the difference in P-wave velocity before and after CO_2 injection (Daley et al. 2008). **b** Modeled CO_2 distributions in the plane between the wells considering different values of S_{grmax}. The single black contour line shows $S_g = 0$, an indication of the historical maximum extent of the CO_2 plume

injection well. For the usual S_{grmax} case, Fig. 8.21a shows good agreement between model and VSP in the updip direction (N), but the VSP indicates that the plume has moved farther than the model has predicted to the NE and NW. In fact, the plume has moved as far to the NW as it has to the N, suggesting that either local updip direction is not true north, or there is significant heterogeneity in the permeability distribution beyond the immediate vicinity of the wells, or the planar representation of a warped sand body becomes inaccurate away from the wells. The non-smooth

nature of the model profiles far from the injection well indicates the need for a more refined grid.

For the half-S_{grmax} case, the model shows a little too much plume movement in the updip direction (N), while for the zero-S_{grmax} case, there is far too much plume movement updip, so we infer that the original values of $S_{grmax} \sim 0.2$, which allow less CO_2 to move updip, are optimal. Note that the modeled extent of the plume to the NE and NW is independent of S_{grmax}.

Unlike other post-injection monitoring methods, VSP covers such a large spatial extent that it encompasses the entire CO_2 plume, both the trailing edge around the wells, where imbibition is occurring, and the leading edge farther updip, where drainage is still occurring long after injection ceases. Hence, large-offset VSP results are also sensitive to drainage-controlling parameters S_{lr} and m. For the simulation results shown in Fig. 8.21, $S_{lr} = 0.15$ and $m = 0.9$. For a case with $S_{lr} = 0.3$ and $m = 0.9$, the leading edge of the CO_2 plume is about 10 m farther updip than is shown for the N profile in Fig. 8.21a.

8.6.4 Discussion

The fluorescein tracer test indicated that the high-permeability sand through which most fluid travels from the injection well to the observation well is 2.5-m thicker than that inferred from well logs, but did not provide any specific information on how the thickening occurs. The RST profiles for the injection well suggest that the CO_2 plume extends almost 1 m above and several meters below the perforated interval, which was chosen to match the high-permeability zone identified in the well log (Fig. 8.15b). The RST profile for the observation well confirms CO_2 arrival about 1 m shallower than predicted by the well logs, but because of buoyancy, no CO_2 arrives very far below the top of the high-permeability layer. The crosswell seismic tomogram (Fig. 8.20a) shows a CO_2 plume that is about 7.5 m thick at the injection well and thins toward the observation well. Thus, tracer test, RST, and crosswell seismic results all support the choice of the 8-m sand model over the 5.5-m sand model inferred from the well logs. Some evidence for local variability is provided by the crosswell seismic tomogram (Fig. 8.20a), which shows a change in the character of the CO_2 distribution about half-way between the two wells.

The VSP data (Fig. 8.21) allows examining the evolution of the CO_2 plume beyond the immediate vicinity of the wells. Despite matching the updip migration adequately, the model fails to reproduce two other features of the VSP data. First, the CO_2 plume should extend just as far to the NW as it does to the N, suggesting a different local dip direction than currently employed by the model. Second, the lateral extent of the modeled plume is too small, suggesting a short-coming in the conceptualization of geological structure (e.g., the local dip magnitude may be smaller, lateral permeability anisotropy could exist, or the planar representation of a warped sand body becomes inaccurate). Because plume migration is largely a

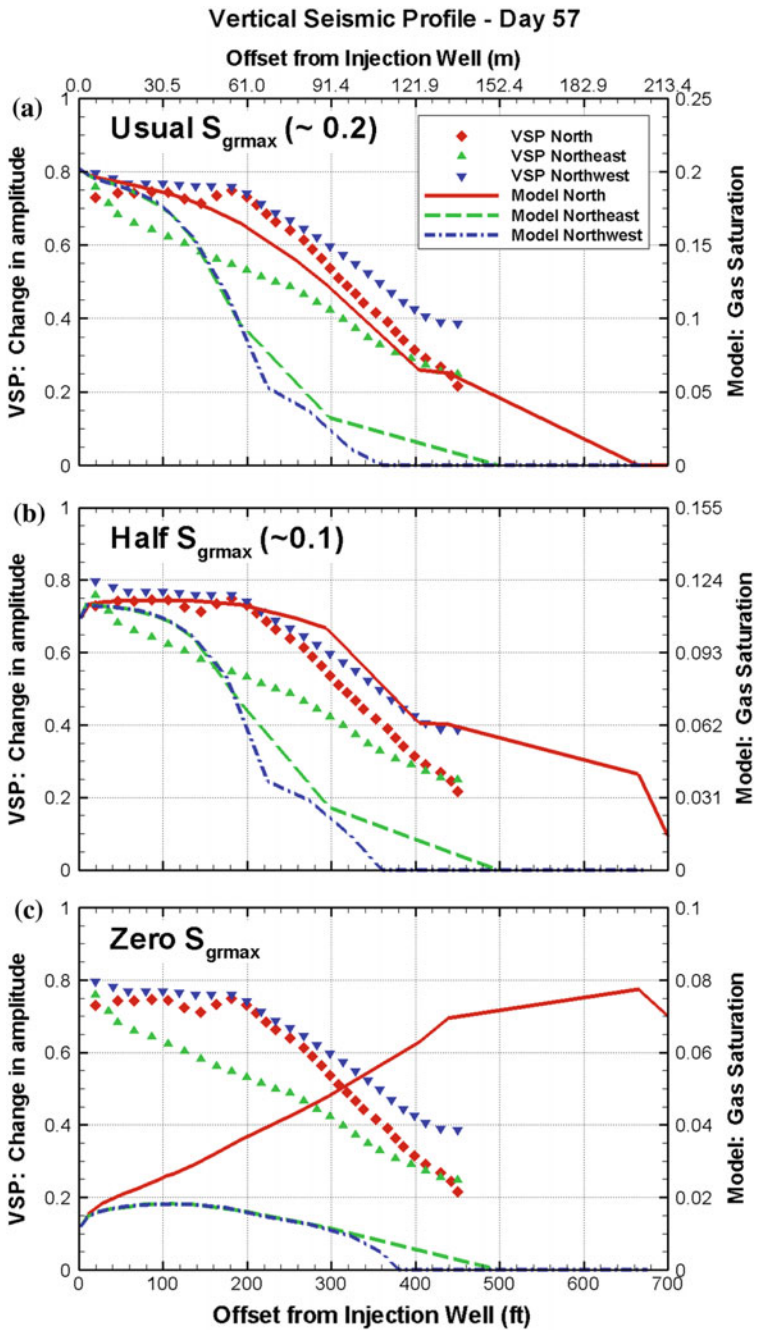

Fig. 8.21 VSP change in P-wave amplitude before and after CO_2 injection (Daley et al. 2008) and model results for far-field CO_2 distribution considering different values of S_{grmax}

consequence of the buoyant flow of CO_2, these features would be difficult to ascertain from traditional site characterization methods.

During CO_2 injection periods, the entire CO_2 plume is undergoing drainage. After injection ends, the leading edge of a migrating CO_2 plume continues to drain, whereas the trailing edge of the plume is undergoing imbibition. Ideally, monitoring should be designed to cover both drainage and imbibition. The drainage process, monitored at the Frio brine pilot via U-tube, early-time pressure transients and RST profiles, and large-offset VSP data, depends on S_{lr} and m, but is not sensitive to S_{grmax}. In contrast, the imbibition process is not very sensitive to S_{lr} and m but depends strongly on S_{grmax}, thus late-time pressure transients and RST profiles, the crosswell seismic tomogram, and small-offset portions of the VSP data provide information on S_{grmax}.

The parameter S_{grmax} is often conceptualized as decreasing with increasing permeability (e.g., Holtz 2002), but these studies strongly support the notion that even for the very high-permeability Frio Formation C sand (>2000 md), S_{grmax} is well above zero, and even provides evidence that the original $S_{grmax} \sim 0.2$ is a better choice than the halved value of $S_{grmax} \sim 0.1$. The late-time RST profiles, the crosswell seismic tomogram, and the VSP data all show consistent results in this regard. Given the importance of a large value of S_{grmax} for trapping free-phase CO_2, this is an important finding for the overall potential for success of CO_2 geologic storage. The results also suggest that S_{lr} is small, consistent with petroleum-literature values (Holtz 2002). The U-tube results for CO_2 arrival at the observation well and pressure-transient analysis supports $S_{lr} = 0.15$, whereas the early-time observation-well RST suggests that S_{lr} is even smaller. A small value of S_{lr} means the CO_2 plume need not bypass so much liquid phase and can form a more compact plume in the subsurface. As one extrapolates from the very high permeabilities of the C sand to moderate permeabilities that may be more typical for CO_2 storage, S_{lr} is expected to increase.

Early in the CO_2 injection period, the simultaneous pressure observations in the injection well, which is surrounded by a two-phase mixture of CO_2 and brine, and the observation well, which is still surrounded by brine, potentially enable deconvolution of multi-phase flow effects, and improved determination of characteristic-curve parameters S_{lr} and m. Unfortunately, the present 3D numerical model is far too coarse (2-m resolution) to adequately resolve near-well effects at the injection well, making such analysis problematic. Studies with a high-resolution model are necessary. For short-time studies, one may be able to increase efficiency by using a 2D axisymmetric model, but for longer times, a 3D model is needed to represent the interplay of heterogeneity, buoyancy, and multi-phase effects.

8.6.5 Concluding Remarks

Well thought-out site characterization is essential for successful geologic storage of CO_2 because of the many physical processes impacting CO_2 plume evolution in the

subsurface. At the Frio brine pilot, site characterization techniques such as geological mapping, geophysical imaging, well logging, core analyses, hydraulic well testing, and tracer testing were all valuable and formed the basis of initial site assessment. However, only through the injection and monitoring of CO_2 could the impact of the coupling between buoyancy flow, geologic heterogeneity, and history-dependent multi-phase flow effects truly be appreciated. Thus, the site-characterization process greatly benefited from the addition of CO_2 injection and monitoring. Moreover, development of a numerical model aided in the synthesis of geological, hydrological, and geophysical observations and provided a framework for understanding the coupled flow and transport processes occurring in the CO_2/brine system.

The advantages of using data collected during CO_2 injection to refine reservoir models are numerous. The obvious benefit of CO_2 injection is to provide information on multi-phase flow properties (in particular, the residual gas saturation, below which CO_2 is trapped), which cannot be obtained from traditional site-characterization techniques that examine single-phase conditions. Additionally, the low density and viscosity of CO_2 compared to brine causes the two components to flow through the subsurface differently, potentially revealing distinct features of the geology. Ultimately, to understand stored CO_2 behavior in the subsurface, there is no substitute for studying the movement of CO_2 directly.

It is humbling that even for the small-scale, very well studied, intensively monitored conditions of the research-oriented Frio brine pilot, there are still uncertainties in data interpretation. Even greater uncertainties are projected for full-scale CO_2 geologic storage projects, where economic constraints will limit the availability of data generated through expensive procedures such as tracer tests, fluid sampling, and crosswell seismic. With only one or two monitoring techniques it is generally not difficult to create a model that can reproduce field observations, making it easy to claim a full understanding of the geologic storage system. As different types of observations are added, matching them all becomes much more challenging, which may produce the feeling that understanding of the system has actually decreased. In reality, an appreciation of ones level of ignorance has increased, which is generally a good first step for improving understanding. Despite the commercial pressures attendant to full-scale CO_2 geologic storage, it should be recognized that the coupled flow and transport processes that take place during CO_2 geologic storage can produce subtle and unintuitive effects that will affect the storage efficiency of a reservoir. It is valuable to investigate as many aspects of the system as possible with a range of monitoring techniques to minimize uncertainty.

8.7 Pilot Scale CO_2 Injection at the Ketzin Site: Experiences from the First European On-Shore Storage Site

Axel Liebscher, Stefan Lüth, Sonja Martens, Fabian Möller, Cornelia Schmidt-Hattenberger and Martin Streibel

8.7.1 Introduction

Although the implementation of Carbon Capture and Storage (CCS) at industrial scale particularly requires successful demonstration of geological CO_2 storage at scales of >1 Mt CO_2 per year, smaller scale pilot sites on geological storage still play an essential role in progressing the CCS technology. While demonstration projects primarily focus on demonstrating and proving the integration and application of mature technologies, pilot sites are needed to develop, test and progress new storage technologies and to perform field-scale experiments on specific technical and operational aspects that may not be executable at demonstration or industrial scale projects.

The Ketzin pilot site for geological storage of CO_2 in the German Federal State of Brandenburg is the longest operating on-shore CO_2 storage pilot site within Europe and is still the only active CO_2 storage project in Germany. It provides an in situ laboratory for on-shore CO_2 storage in a saline aquifer of the Northeast German Basin. The storage complex is located in an anticline structure above a salt pillow and thereby the Ketzin site shares some fundamental geologic characteristics with future CO_2 storage sites within the European Permian Basin, either on-shore in, e.g., Germany or Poland, or off-shore under the North Sea. The Ketzin site is a pure research and development (R&D) driven project and as a research project limited by national legal regulations to a maximum amount of stored CO_2 of 100,000 t. CO_2 storage at the Ketzin site is accompanied by one of the most comprehensive scientific research and development programs worldwide with key objectives being R&D on CO_2 injection operation, monitoring and modeling. These technological objectives are accompanied by an extensive public outreach and dissemination program. This chapter provides a comprehensive review of the main results and experiences gained at the Ketzin pilot site. For additional information and further reading the reader is referred to Martens et al. (2012, 2013) and Liebscher et al. (2013a, b).

8.7.2 Site Location and Geology

The Ketzin pilot site is located about 25 km west of Berlin and Potsdam (Germany) near the town Ketzin within the Northeast German Basin (Fig. 8.22). The Northeast German Basin is part of the European Permian Basin, which extends from the Polish Trough in the East to present day off-shore areas of the North Sea (Fig. 8.22a) and is made off by sedimentary sequences of Permo-Mesozoic to Cenozoic age. The pilot site itself sits on the southeast flank of the "Roskow-Ketzin" double anticline, which formed above a deep seated, elongated salt pillow (Fig. 8.22b, c). The target reservoir sandstone layers for CO_2 storage belong to the Upper Triassic Stuttgart Formation at about 630–650 m depth and are overlain by more than 165 m of the shaly caprocks of the Upper Triassic Weser and Arnstadt Formations (Fig. 8.22d). The final seal of the multi-barrier system at the Ketzin site is formed by the transgressional Oligocene Rupelian Clay at the base of the Tertiary, which separates the post-Rupelian freshwater horizons from the deep, pre-Rupelian saline formations. The reservoir sandstones are well to moderately-well sorted, immature feldspathic litharenites to lithic arkoses, which are composed of 22–43 wt% quartz, 19–32 wt% plagioclase, 4–13 wt% K-feldspar and subordinate mica, illite, mixed-layer silicates and meta-sedimentary and volcanic rock fragments (Förster et al. 2006). Heterogeneously distributed cement phases make up 5–32 vol.% and include analcime and anhydrite with minor dolomite, barite, and celestine (Förster et al. 2006). Due to the heterogeneity of the reservoir sandstone, reservoir porosity ranges from 12 to 26 vol.% with an averaged permeability of around 100 mD (Zemke et al. 2010; Zettlitzer et al. 2010). The initial reservoir conditions were $\sim$33 °C and 61 bar at 630 m depth (Henninges et al. 2011).

8.7.3 Research Infrastructure at the Ketzin Site

To meet the operational and scientific needs of the Ketzin site a total of five wells have been drilled and an injection facility with a pipeline built (Fig. 8.23). Prior to start of injection in summer 2008, the wells Ktzi 200–202 have been drilled in 2007, each to a depth of 750–800 m (Fig. 8.24). The well Ktzi 201 serves as an injection and observation well, whereas the wells Ktzi 200 and Ktzi 202 are exclusively used for monitoring the injection process and subsurface migration and behaviour of the CO_2. The three wells form the corners of a right-angled triangle (Fig. 8.23). In autumn 2012 a fourth deep well Ktzi 203 was drilled in close vicinity to the injection point (Fig. 8.23) to recover rock cores from the caprock and reservoir sandstones that have been in contact with the injected CO_2 for more than four years. Contrary to the wells Ktzi 200–202, which have steel casings throughout, the well Ktzi 203 has been completed with a glass fibre reinforced

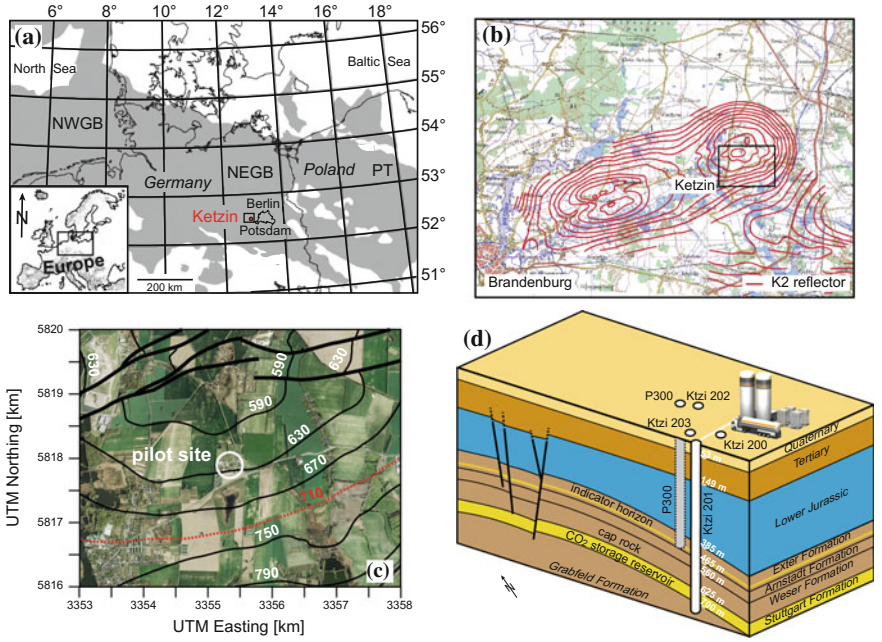

Fig. 8.22 Geographic location and principal geologic environment of the Ketzin pilot site. **a** The Ketzin site is located within the Northeast German Basin (NEGB; NWGB = Northwest German Basin, PT = Polish Trough) (redrawn and modified after Förster et al. 2010) and **b**, **c** sits above the southeast flank of the Roskow-Ketzin double anticline [*red lines* in **b** refer to the depth of the prominent K2 reflector, an anhydrite layer about 80 m above the reservoir; isolines in **c** refer to the depth of top-Stuttgart, *dotted red isoline* at 710 m depth represents the lateral extension of the storage complex. **d** Schematic block diagram showing the general stratigraphic succession at the Ketzin site and the site's infrastructure with four deep wells (Ktzi 200–203) and one shallow observation well (P300) down to the indicator horizon within the Exter Formation (not to scale) [redrawn and modified after Liebscher et al. (2013a, b), Martens et al. (2012)]

plastic casing in the lower-most part to study the applicability of this corrosion resistant material in CO_2 storage operations (Fig. 8.24). To allow for above-zone monitoring within the indicator horizon (Fig. 8.22d) a shallow groundwater observation well P300 was drilled in 2011 to 446 m depth into the lowermost aquifer (Exter Formation) above the caprock.

All four deep wells are completed with a smart casing concept (Prevedel et al. 2009) that allows for quasi-permanent, easily accessible monitoring of the wells and the near-well area (Fig. 8.24). This concept includes behind casing fibre-optic cables for distributed temperature/acoustic sensing (DTS/DAS), behind casing heater cables for heating experiments, permanently installed electrodes (Vertical Electrical Resistivity Array VERA) for electrical resistivity tomography and different pressure and temperature sensors (P-T). The shallow well P300 is equipped with high resolution pressure gauges and a U-tube fluid sampling system to allow for precise pressure and fluid monitoring of the indicator horizon.

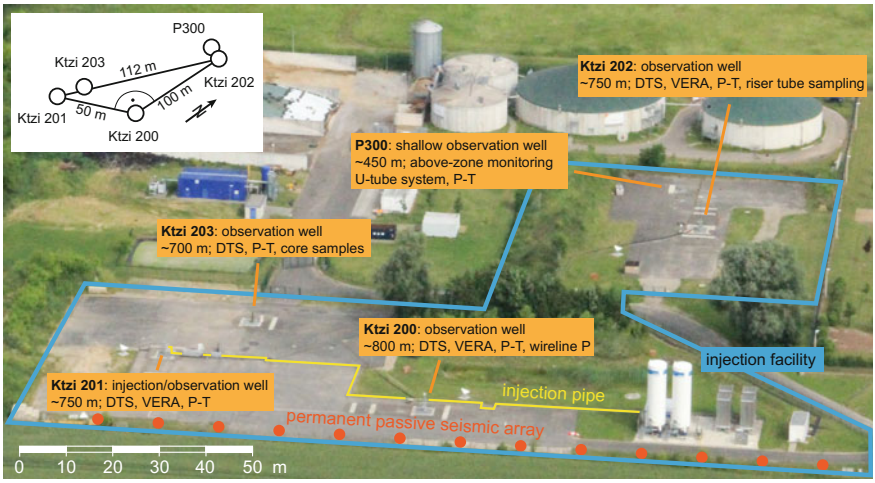

Fig. 8.23 Aerial view of the pilot site Ketzin showing location of the injection and observation wells and the operational and monitoring surface installations

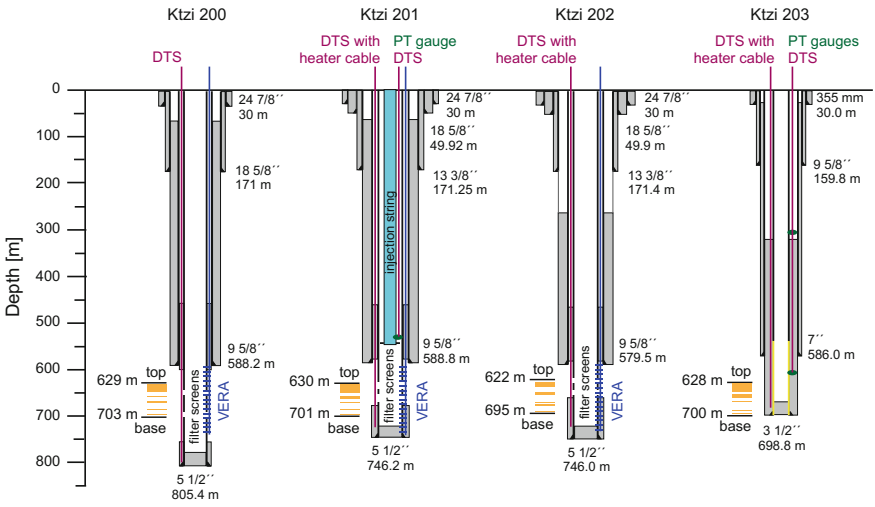

Fig. 8.24 Detailed drawing of the smart casing concept of the four deep wells at the Ketzin site (for location of the four wells see Fig. 8.23). The wells Ktzi 200, 201 and 202 have steel casings throughout whereas Ktzi 203 has a glass fibre reinforced plastic casing in the lower-most part (*yellow*). *Black bars* and *orange boxes left hand side* of the respective wells refer to top and base and main sandstone intervals (=reservoirs) of the Stuttgart Formation (Compiled and re-drawn with additions after Prevedel et al. 2008, 2009; Förster et al. 2010; Liebscher et al. 2013a, b)

8.7.4 Injection Operation and History

Continuous injection of CO_2 at the Ketzin site started on June 30th, 2008 and lasted until August 29th, 2013, when the Ketzin site entered the post-injection phase after more than five years of safe and successful injection of slightly more than 67,000 tons of CO_2. During most time of the injection period, food-grade CO_2 with a purity >99.9 vol.% has been injected at monthly injection rates between 1,000 and 2,300 tons CO_2. From May to June 2011, 1,515 tons of captured CO_2 from the Vattenfall Schwarze Pumpe oxyfuel pilot plant with a purity >99.7 vol.% have been injected. In July and August 2013, a CO_2-N_2 co-injection experiment has been performed to test and demonstrate the technical feasibility of a continuous impure CO_2 injection scenario. A total of 613 tons CO_2 and 32 tons N_2 have been continuously mixed on-site and co-injected resulting in an average CO_2 to N_2 mass ratio of approximately 95:5.

Throughout the entire injection phase, liquid CO_2 was delivered by road tankers and intermediately stored on-site at about −18 °C and 20 bars in two storage tanks with a capacity of 50 t CO_2 each. Prior to injection, the CO_2 was preconditioned in the injection facility to the desired injection conditions. Preconditioning was done in three steps; first up to three plunger pumps for liquid media raised the pressure to the necessary injection pressure, than the CO_2 was heated to the desired injection temperature first by ambient air heaters and afterwards by an electrical heater. The preconditioned CO_2 was transported via the injection pipeline to well Ktzi 201 and injected. Due to the injection process, the reservoir pressure as calculated from the permanently installed pressure sensor increased from initially ∼61 bars to about 76–79 bars already after 8 month of injection. After this initial increase the reservoir pressure slightly decreased and stabilized at about 72–75 bars reflecting a stable injection regime (Fig. 8.25; Liebscher et al. 2013b). With stop of injection and entering the post-injection phase, the reservoir pressure started to continuously decrease and evolves back towards initial reservoir conditions (Fig. 8.25).

8.7.5 Monitoring

8.7.5.1 Integrated Monitoring Concept

Research and Development on monitoring is one of the key objectives of the Ketzin pilot site and a comprehensive, integrated state-of-the-art monitoring concept has been established at the pilot site (Fig. 8.26). This concept combines permanent and periodic geophysical, geochemical, operational and remote sensing monitoring techniques. Geophysical monitoring techniques include active seismic (2D, 3D, VSP, MSP), passive seismic and geoelectric (cross-hole, surface-downhole) methods. Geochemical monitoring techniques focus on surface CO_2 soil-flux measurements and fluid sampling either via permanently installed capillary riser

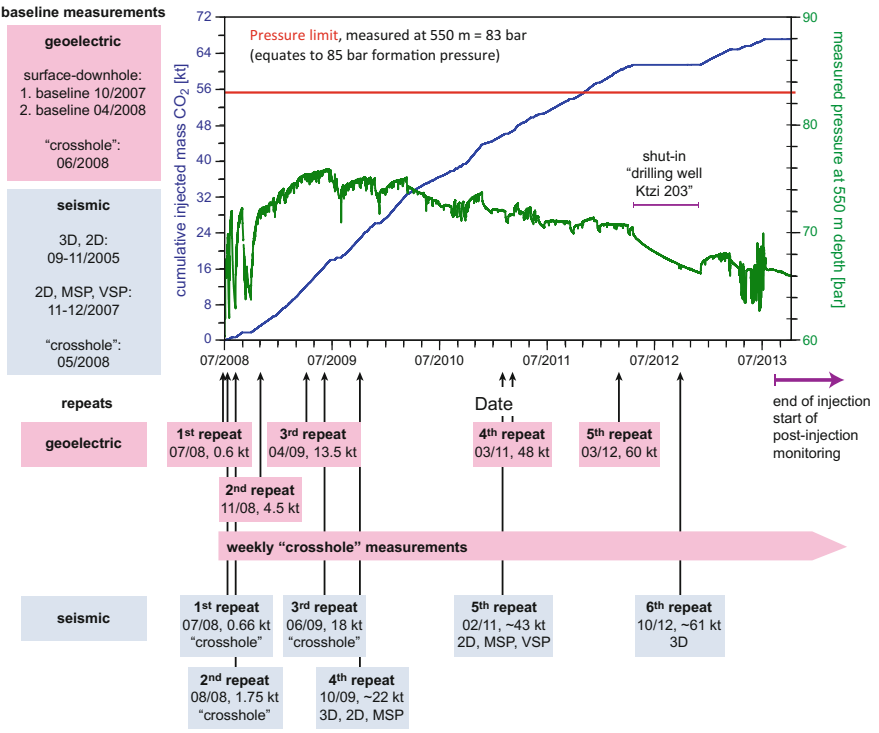

Fig. 8.25 Overall injection history showing cumulative mass of injected CO_2 (*blue*) and measured pressure at 550 m depth in well Ktzi 201 (*green*). The reservoir pressure at 630 m is about 2 bars higher than the measured pressure at 550 m. The *red line* refers to the maximum permitted pressure of 85 bars at reservoir depth. Also shown are the different repeat surveys of the geoelectric and seismic monitoring

tubes or during logging campaigns. These logging campaigns are routinely run and comprise gas-saturation measurements within the reservoir and overburden to test for upward gas migration and magnetic imaging defectoscopy and video logs for casing inspection.

8.7.5.2 Seismic Monitoring

Various active and passive seismic monitoring campaigns were performed during the operational phase at Ketzin (Fig. 8.25). The major part of the active seismic monitoring is the 3D seismic time lapse monitoring with the baseline acquired in 2005 and two repeat surveys in autumn 2009, after the injection of approximately 22,000 tons of CO_2, and in autumn 2012, after the injection of approximately 61,000 tons of CO_2 (Ivanova et al. 2012; Juhlin et al. 2007). The processing and interpretation of the 3D time lapse data delivered amplitude and travel time

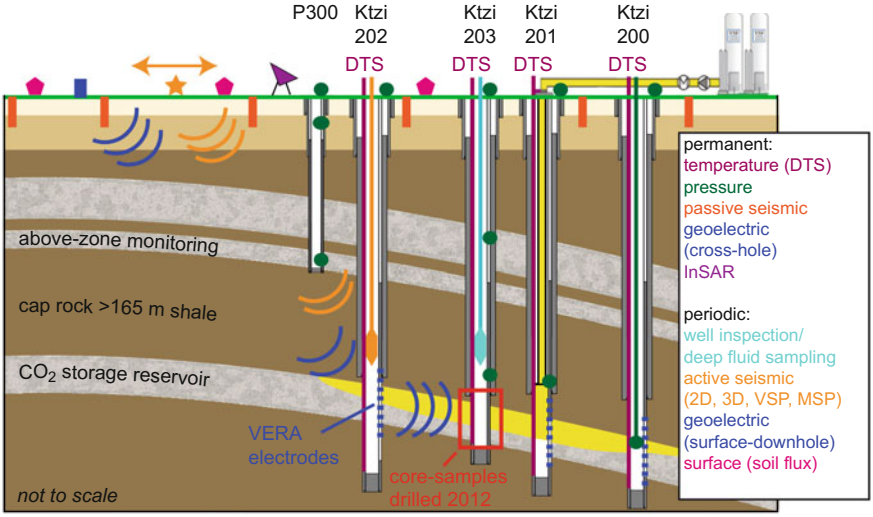

Fig. 8.26 Schematic profile through the Ketzin anticline showing the general geology and the different permanent and periodic monitoring techniques and installations applied at the Ketzin site for an integrated monitoring concept

signatures that could be attributed to the CO_2 stored in the Stuttgart formation and allowed image the lateral spread of the CO_2 plume (Fig. 8.27). The lateral extension of the CO_2 plume as estimated based on the 3D time lapse data was $\sim$0.08 km^2 after approximately 22,000 tons of CO_2 and $\sim$0.15 km^2 after approximately 61,000 tons of CO_2 (Fig. 8.27). The CO_2 plume shows a slightly west-northwest to east-southeast elongated shape with an indicated preferred migration towards west-northwest. The results from the 3D repeat surveys also allowed for an update of the reservoir model with a more realistic description of lateral heterogeneities of physical parameters within the storage formation. Additional experiments include repeat surveys using a focused surface and surface-downhole acquisition pattern in order to achieve an enhanced resolution close to and in the depth range of the injection level (Ivandic et al. 2012).

8.7.5.3 Geoelectric Monitoring

A comprehensive geoelectric surveillance concept has been developed and implemented at the Ketzin pilot site. This concept includes permanent cross-hole measurements and periodic large-scale surface-downhole surveys (Fig. 8.25). Main objectives of the surveillance concept were detection of the early CO_2 migration phase, imaging of the CO_2 plume by electrical resistivity tomography ERT, determination of relative CO_2 and brine saturations as well as correlation between injection operation and geoelectric signal (Bergmann et al. 2012; Kiessling et al.

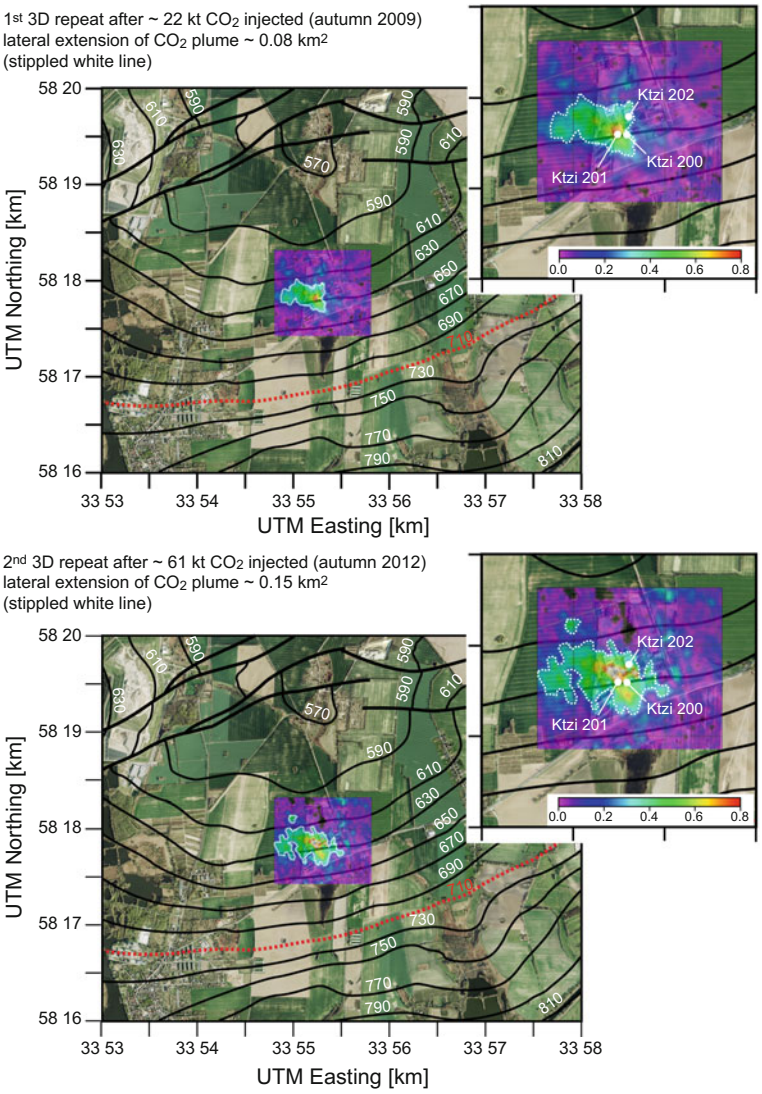

Fig. 8.27 Subsurface extension of the CO_2 plume (*white dotted lines*) as imaged by the 1st and 2nd 3D seismic repeat surveys. *Colour coding* refers to normalized changes in reflection amplitude. *Dotted white lines* are drawn by eye to show changes in normalized reflection amplitude >0.3. (*black lines* refer to top of Stuttgart Formation; *dotted red line* refers to lateral boundary of storage complex as defined by deepest closed top-Stuttgart isobath)

2010; Schmidt-Hattenberger et al. 2011). During the whole CO_2 injection period, a continuous series of time-lapse results based on weekly-measured crosshole data at near-wellbore scale and surface-downhole measurements in 2008, 2009, 2011 and 2012 at a scale of up to 1.5 km was acquired (Fig. 8.25). In the geoelectrical

tomographies a noticeable resistivity signature within the target storage zone was observed and could be attributed to the CO_2 plume (Schmidt-Hattenberger et al. 2011) and has been interpreted in terms of the relative CO_2 saturations (Bergmann et al. 2012; Fig. 8.28). The results are very encouraging and show the potential of geoelectric monitoring methods. Especially the relative CO_2 saturations derived for the near-wellbore area correlate well with borehole saturation logs and support the quantitative estimation of injected CO_2 in the near-wellbore area.

8.7.5.4 Surface and Gas Monitoring

To monitor upward migration of CO_2 with potential leakage to the surface, surface soil gas monitoring has been established at the Ketzin pilot site since 2005. The soil gas monitoring network consists of 20 sampling locations for soil gas flux, soil

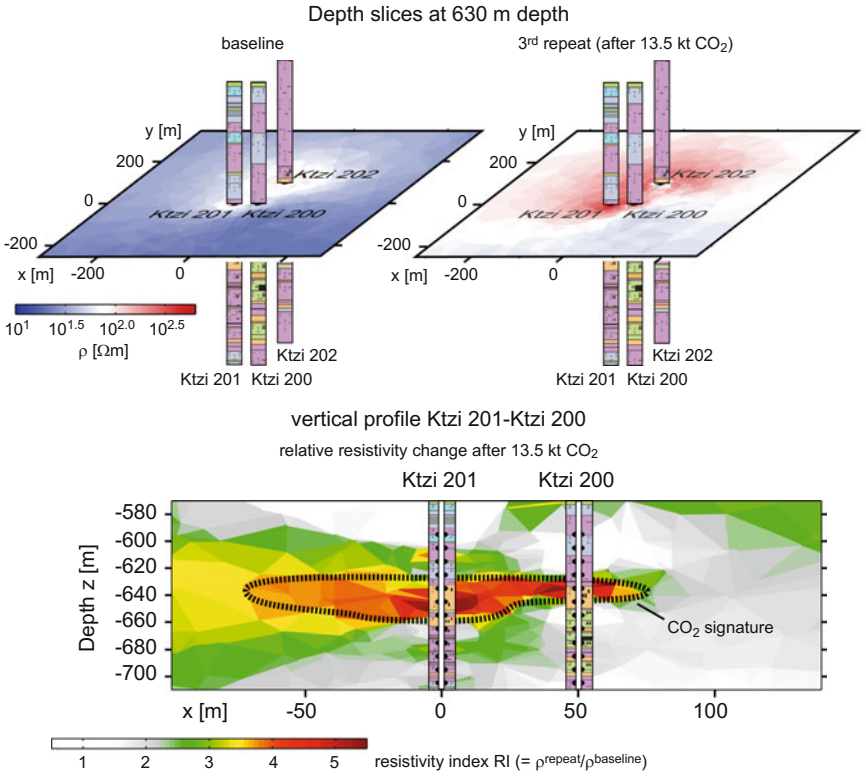

Fig. 8.28 Results from geoelectric surface-downhole monitoring. Resistivity distribution at 630 m depth as estimated for the baseline and repeat survey after 13.5 kt CO_2 injected (*upper part*) and calculated time-lapse signal (*lower part*). Electrical resistivity tomography shows a clear CO_2 signature with up to four to fivefold increase in resistivity within the target reservoir horizon (redrawn and compiled after Bergmann et al. 2012)

moisture and temperature measurements distributed over an approximately 4 km^2 large area around the pilot site. In 2011, the installation of additional eight permanent stations with automated soil gas samplers in the direct vicinity of the injection and monitoring wells expanded the monitoring network. Since the start of injection in June 2008, no change in soil CO_2 gas flux could be detected in comparison to the pre-injection baseline from 2005 to 2007 (Zimmer et al. 2011).

8.7.6 Public Outreach Activities

Public acceptance is a key issue for the Ketzin project as it is for any other CO_2 storage project. From the very beginning, the research activities were therefore accompanied by a factual, open and transparent dialogue with the general public, scientists, industry and decision makers. Public outreach activities focus on the local public from the nearby town of Ketzin but also interested people from all over Germany and worldwide. The visitor centre at the Ketzin site is the most important contact point. Here, a computer-based info terminal enables visitors to inform themselves easily and interactively. Weekly visitor tours are offered by GFZ on site. In addition, an annual open house day at the Ketzin pilot site is carried out in close cooperation with the local community of the town of Ketzin and warmly received. Project status and progress are covered and disseminated in brochures and a public website in German and English (www.co2ketzin.de). The Ketzin project is also presented in a broader context in a film entitled "The geological storage of CO_2" made up of six five-minute segments. The research activities at the pilot site are supported by the town of Ketzin, and the regulatory authority has been involved and cooperative since the start of the Ketzin project (Martens et al. 2011). The experience from the Ketzin pilot site shows that an honest, open and factual target group oriented communication and dissemination program is able to overcome critical public perception even for highly debated technologies.

8.7.7 Conclusions and Outlook

The Ketzin project demonstrates successful and safe CO_2 storage in a saline aquifer on a pilot scale. The results show that:

- the geological storage of CO_2 at the Ketzin pilot site runs reliably and without any risks for people and environment,
- a meaningful, site related combination of geophysical and geochemical monitoring techniques is able to detect even small amounts of CO_2 and to image its spatial distribution, and
- a targeted communication and dissemination program is able to overcome critical public perception even for highly debated technologies.

Although the CO_2 injection at Ketzin ceased in August 2013, R&D activities on CO_2 storage continues at Ketzin in order to address and close the entire life cycle of a storage site. Well abandonment, post-injection monitoring and transfer of liability are major objectives of the on-going post-injection phase at the Ketzin site. Because the Ketzin site has been permitted under the German Mining Law, transfer of liability will follow the regulations set out by the German Mining Law. The R&D work in the post-closure phase will nevertheless address the three high-level criteria for transfer of liability set out by the EU Directive:

- observed behaviour of the injected CO_2 conforms with the modeled behaviour,
- no detectable leakage, and
- site is evolving towards a situation of long-term stability.

During the post-injection phase, further field-experiments like controlled back-production of CO_2 as reservoir pressure management measure and small-scale brine injection as wellbore leakage mitigation measure are performed. By these experiments, the Ketzin site meets the demands made for pilot sites to perform field-scale experiments on specific technical and operational aspects that may not be executable at demonstration or industrial scale projects.

References

Aki K, Richards PG (1980) Quantitative seismology, 2nd edn

Alnes H, Eiken O, Nooner S, Sasagawa G, Stenvold T, Zumberge M (2011) Results from Sleipner gravity monitoring: updated density and temperature distribution of the CO_2 plume. Energy Procedia. In: 10th international conference on greenhouse gas control technologies, vol 4, pp 5504–5511

Archie GE (1942) The electrical resistivity log as an aid in determining some reservoir characteristics. Trans AIME 146:54–62

Arts R, Chadwick A, Eiken O, Thibeau S, Nooner S (2008) Ten years' experience of monitoring CO_2 injection in the Utsira Sand at Sleipner, offshore Norway. First Break 26:65–72

Assayag N, Matter J, Ader M, Goldberg D, Agrinier P (2009) Water–rock interactions during a CO_2 injection field-test: implications on host rock dissolution and alteration effects. Chem Geol 265(1):227–235

Asveth P (2009) Explorational rock physics: the link between geological processes and geophysical observables. In: Petroleum geoscience. Springer

Bachu S, Bennion B (2007) Effects of in-situ conditions on relative permeability characteristics of CO_2-brine systems. Environ Geol 54:1707–1722

Bakke NE, Ursin B (1998) Thin-bed AVO effects. Geophys Prospect 46:571–587

Batzle ML, Wang Z (1992) Seismic properties of pore fluids. Geophysics 57:1396–1408

Behrens H, Ghergut J, Bensabat J, Niemi A, Sauter M (2014) Merging single- and inter-well tracer tests into one forced-gradient dipole test, at the Heletz site within the MUSTANG project. Energy Procedia 59:249–255

Benson S, Doughty C (2006) Estimation of field-scale relative permeability from pressure transient tests. In: Presented at the CO2SC symposium. Lawrence Berkeley National Laboratory, Berkeley, CA

Bergmann P, Schmidt-Hattenberger C, Kiessling D, Rücker C, Labitzke T, Henninges J, Baumann G, Schütt H (2012) Surface-downhole electrical resistivity tomography applied to monitoring of CO_2 storage at Ketzin, Germany. Geophysics 77:B253–B267

Berryman JG, Milton GW (1991) Exact results for generalized Gassmann's equations in composite porous media with two constituents. Geophysics 56:1950–1960

Bickle M, Chadwick A, Huppert HE, Hallworth M, Lyle S (2007) Modelling carbon dioxide accumulation at Sleipner: Implications for underground carbon storage. Earth Planet Sci Lett 255:164–176

Biondi BL (2006) Three dimensional seismic imaging. Investigation in Geophysics. Society of Exploration Geophysicists

Boait FC, White NJ, Bickle MJ, Chadwick RA, Neufeld JA, Huppert HE (2012) Spatial and temporal evolution of injected CO_2 at the Sleipner Field, North Sea. J Geophys Res Solid Earth 117

Boreham C, Underschultz J, Stalker L, Kirste D, Freifeld B, Jenkins C, Ennis-King J (2011) Monitoring of CO_2 storage in a depleted natural gas reservoir: gas geochemistry from the CO2CRC Otway Project, Australia. Int J Greenh Gas Control 5:1039–1054

Borgos H, Skov T, Randen T, Sonneland L (2003) Automated geometry extraction from 3D seismic data. In: SEG technical program expanded abstracts 2003, SEG technical program expanded abstracts. Society of Exploration Geophysicists, pp 1541–1544

Bortfeld R (1961) Approximations to the reflection and transmission coefficients of plane longitudinal and transverse waves. Geophys Prospect 9:485–502

Butler DB, Knight RJ (1988) Electrical conductivity of steam-flooded, clay-bearing geologic materials. Geophysics 63:1137–1149

Carbon Sequestration Leadership Forum (CSLF) (2013) 2013 Annual report by the CSLF Task force on reviewing best practices and standards for geologic storage and monitoring of CO_2. www.cslforum.org. Oct 2013

Carcione JM, Picotti S, Gei D, Rossi G (2006) Physics and seismic modeling for monitoring CO_2 storage. Pure appl Geophys 163:175–207

Castagna J, Backus M (1993) Offset-dependent reflectivity? Theory and practice of AVO analysis. Investigations in Geophysics. Society of Exploration Geophysicists

Cavanagh A (2013) Benchmark calibration and prediction of the Sleipner CO_2 plume from 2006 to 2012. Energy Procedia. In: GHGT-11 proceedings of the 11th international conference on greenhouse gas control technologies, 18–22 Nov 2012, Kyoto, Japan vol 37, pp 3529–3545

Chadwick RA, Noy DJ (2010) History-matching flow simulations and time-lapse seismic data from the Sleipner CO_2 plume. Geol Soc Lond Pet Geol Conf Ser 7:1171–1182

Chadwick RA, Holloway S, Kirby G, Gregersen U, Johannessen P (2000) The Utsira Sand, Central North Sea—an assessment of its potential for regional CO_2 disposal. In: Presented at the proceedings of 5th international conference on greenhouse gas control technologies. IEA Greenhouse Gas Programme, Cairns, Australia

Chadwick A, Williams G, Delepine N, Clochard V, Labat K, Sturton S, Buddensiek M, Dillen M, Nickel M, Lima A, Arts R, Neele F, Rossi G (2010) Quantitative analysis of time-lapse seismic monitoring data at the Sleipner CO_2 storage operation. Lead Edge 29:170–177

Christensen NB, Sherlock D, Dodds K (2006) Monitoring CO_2 injection with cross-hole electrical resistivity tomography. Explor Geophys 37:44–49

CO_2 Capture Project, CCP CO_2 STORAGE PROGRAM fact sheet, modular borehole monitoring design and field test [WWW Document] (2013) http://www.co2captureproject.org/reports/FACTSHEET_MBM.pdf

Corey AT (1954) The interrelation between gas and oil relative permeabilities. Prod Mon 19:38–41

Crow W, Carey JW, Gasda S, Williams DB, Celia M (2010) Wellbore integrity analysis of a natural CO_2 producer. Int J Greenhouse Gas Control 4(2):186–197

Daley TM, Myer LR, Peterson JE, Majer EL, Hoversten GM (2008) Time-lapse crosswell seismic and VSP monitoring of injected CO_2 in a brine aquifer. Environ Geol 54:1657–1665

Daley TM, Ajo-Franklin JB, Doughty C (2011) Constraining the reservoir model of an injected CO_2 plume with crosswell CASSM at the Frio-II brine pilot. Int J Greenh Gas Control 5:1022–1030

Daley TM, Hendrickson J, Queen JH (2013) Monitoring CO_2 Storage at Cranfield, Mississippi with Time-Lapse Offset VSP—Using Integration and Modeling to Reduce Uncertainty. Energy Procedia 63:4240–4248

De Witte L (1955) A study of electric log interpretation methods in Shaly formations

Deregowski SM (1986) What is DMO? First break 4

Domes F (2010) The influence of overburden on quantitive time-lapse seismic interpretation (Thesis). Heriot-Watt University

Doughty C (2007) Modeling geologic storage of carbon dioxide: comparison of non-hysteretic and hysteretic characteristic curves. Energy Convers Manag. In: Geologic carbon sequestration and methane hydrates research from the TOUGH symposium 2006, vol 48, pp 1768–1781

Doughty C, Pruess K, Benson S, Hovorka SD, Knox PR, Green CT (2001) Capacity investigation of brine-bearing sands of the Frio Formation for geologic sequestration of CO_2. In: Presented at the first national conference on carbon sequestration, Washington, DC

Doughty C, Freifeld BM, Trautz RC (2008) Site characterization for CO_2 geologic storage and vice versa: the Frio brine pilot, Texas, USA as a case study. Environ Geol 54:1635–1656

Dwarakanath V, Pope GA (1998) New approach for estimating alcohol partition coefficients between nonaqueous phase liquids and water. Environ Sci Technol 32:1662–1666

Eberhart-Phillips D, Han DH, Zoback MD (1989) Empirical relationships among seismic velocity, effective pressure, porosity, and clay content in sandstone. Geophysics 54:82–89

Eiken O, Ringrose P, Hermanrud C, Nazarian B, Torp TA, Høier L (2011) Lessons learned from 14 years of CCS operations: Sleipner. In: Salah and Snøhvit. Energy Procedia. In: 10th international conference on greenhouse gas control technologies, vol 4, pp 5541–5548

Elodie J, Philippe S (2012) The relevance of geochemical tools to monitor deep geological CO_2 storage sites. In: Panagiotaras D (ed) Geochemistry—earth's system processes. InTech

Emberley S, Hutcheon I, Shevalier M, Durocher K, Mayer B, Gunter WD, Perkins EH (2005) Monitoring of fluid–rock interaction and CO_2 storage through produced fluid sampling at the Weyburn CO_2-injection enhanced oil recovery site, Saskatchewan, Canada. Appl Geochem 20:1131–1157

Estublier A, Fornel A, Parra T, Deflandre J-P (2013) Sensitivity study of the reactive transport model for CO_2 injection into the Utsira Saline formation using 3D fluid flow model history matched with 4D seismic. Energy Procedia 37:3574–3582

Fabriol H, Bitri A, Bourgeois B, Delatre M, Girard JF, Pajot G, Rohmer J (2011) Geophysical methods for CO_2 plume imaging: comparison of performances. Energy Procedia. In: 10th international conference on greenhouse gas control technologies, vol 4, pp 3604–3611

Fagerlund F, Niemi A, Bensabat J, Shtivelman V (2013a) Design of a two-well field test to determine in situ residual and dissolution trapping of CO_2 applied to the Heletz CO_2 injection site. Int J Greenhouse Gas Control 19:642–651

Fagerlund F, Niemi A, Bensabat J, Shtivelman V (2013b) Interwell field test to determine in situ CO_2 trapping in a deep saline aquifer: Modelling study of the effects of test design and geological parameters. Energy Procedia 40:554–563

Fornel A, Estublier A (2013) To a dynamic update of the Sleipner CO_2 storage geological model using 4d seismic data. Energy Procedia. In: GHGT-11 proceedings of the 11th international conference on greenhouse gas control technologies, 18–22 Nov 2012, Kyoto, Japan 37, pp 4902–4909

Förster A, Norden B, Zinck-Jørgensen K, Frykman P, Kulenkampff J, Spangenberg E, Erzinger J, Zimmer M, Kopp J, Borm G, Juhlin C, Cosma C-G, Hurter S (2006) Baseline characterization of the CO_2SINK geological storage site at Ketzin, Germany. Environ Geosci 13:145–161

Förster A, Schöner R, Förster H-J, Norden B, Blaschke A-W, Luckert J, Beutler G, Gaupp R, Rhede D (2010) Reservoir characterization of a CO_2 storage aquifer: the upper Triassic Stuttgart formation in the Northeast German Basin. Mar Pet Geol 27(10):2156–2172

Freifeld BM, Trautz RC (2006) Real-time quadrupole mass spectrometer analysis of gas in borehole fluid samples acquired using the U-tube sampling methodology. Geofluids 6:217–224
Freifeld BM, Trautz RC, Kharaka YK, Phelps TJ, Myer LR, Hovorka SD, Collins DJ (2005) The U-tube: a novel system for acquiring borehole fluid samples from a deep geologic CO_2 sequestration experiment. J Geophys Res Solid Earth 110
Freifeld BM, Finsterle S, Onstott TC, Toole P, Pratt LM (2008) Ground surface temperature reconstructions: using in situ estimates for thermal conductivity acquired with a fiber-optic distributed thermal perturbation sensor. Geophys Res Lett 35:L14309
Frohlich RK, Parke CD (1989) The electrical resistivity of the vadose zone—field survey. Ground Water 27:524–530
Gassmann F (1951) Über die Elastizität poröser Medien. Inst. für Geophysik an der ETH, Zürich
Gelchinsky B (1988) The common reflecting element (CRE) method (non-uniform asymmetric multifold system). Explor Geophys 19:71–75
Gelchinsky B, Berkovitch A, Keydar S (1999) Multifocusing homeomorphic imaging: part 2. Multifold data set and multifocusing. J Appl Geophys 42:243–260
Gemmer L, Hansen O, Iding M, Leary S, Ringrose P (2012) Geomechanical response to CO_2 injection at Krechba, In Salah, Algeria. First Break 30:79–84
Ghergut J, Bensabat J, Niemi A, Licha T, Ptak T, Sauter M (2013) CCS site characterization by single-well and inter-well tracer tests. Stanford Geothermal Program Workshop Report SGP-TR-198:316–325
Giese R, Henninges J, Lüth S, Morozova D, Schmidt-Hattenberger C, Würdemann H, Zimmer M, Cosma C, Juhlin C (2009) Monitoring at the CO_2 SINK site: a concept integrating geophysics, geochemistry and microbiology. Energy Procedia 1:2251–2259
Gochioco LM (1991) Tuning effect and interference reflections from thin beds and coal seams. Geophysics 56:1288–1295
Guéguen Y, Palciauskas V (1994) Introduction to the physics of rocks. Princeton University Press, New Jersey
Gunter B, Perkins E (2004) Geochemical monitoring and modeling. In: Presented at the 7th international conference on greenhouse gas control technologies, IEA Greenhouse Gas Programme, Vancouver, Canada
Guy E, Radzevicius S, and Conroy J (2003) Computer programs for application of equations describing elastic and electromagnetic wave scattering from planar interfaces, Comput Geosci 29:569–575
Han M, Youssef S, Rosenberg E, Fleury M, Levitz P (2009) Deviation from Archie's law in partially saturated porous media: Wetting film versus disconnectedness of the conducting phase. Phys Rev E 79:31127
Hantush MS, Jacob CE (1955) Non-steady radial flow in an infinite leaky aquifer. EOS Trans Am Geophys Union 36:95–100
Henninges J, Liebscher A, Bannach A, Brandt W, Hurter S, Köhler S, Möller F, CO2SINK Group (2011) P–T–rho and two-phase fluid conditions with inverted density profile in observation wells at the CO_2 storage site at Ketzin (Germany). Energy Procedia 4:6085–6090
Hesse M, Tchelepi HA, Orr FM (2006) Scaling analysis of the migration of CO_2 in saline aquifers. Soc Petrol Eng
Hill R (1963) Elastic properties of reinforced solids: some theoretical principles. J Mech Phys Solids 11:357–372
Holtz MH (2002) Residual gas saturation to aquifer influx: a calculation method for 3-D computer reservoir model construction. Soc Petrol Eng
Holtz MH (2005) Reservoir characterization applying residual gas saturation modeling, example from the Starfak (MSc). University of Texas, Austin
Hoversten GM, Gasperikova E (2005) Chapter 23—non-seismic geophysical approaches to monitoring A2 In: Thomas DC (ed) Carbon dioxide capture for storage in deep geologic formations. Elsevier Science, Amsterdam, pp 1071–1112

Hoversten G, Gritto R, Washbourne J, Daley T (2003) Pressure and fluid saturation prediction in a multicomponent reservoir using combined seismic and electromagnetic imaging. Geophysics 68:1580–1591

Hovorka SD, Benson SM, Doughty C, Freifeld BM, Sakurai S, Daley TM, Kharaka YK, Holtz MH, Trautz RC, Nance HS, Myer LR, Knauss KG (2006) Measuring permanence of CO_2 storage in saline formations: the Frio experiment. Environ Geosci 13:105–121

Hunkeler D, Hoehn E, Höhener P, Zeyer J (1997) 222Rn as a partitioning tracer to detect diesel fuel contamination in aquifers: laboratory study and field observations. Environ Sci Technol 31:3180–3187

Iding M, Ringrose P (2009) Evaluating the impact of fractures on the long-term performance of the In Salah CO_2 storage site. Energy Procedia. In: Proceedings of the 9th international conference on greenhouse gas control technologies 9 (GHGT-9), 16–20 Nov 2008, Washington DC, USA 1, pp 2021–2028

IEAGHG (2013) The process of developing a CO_2 test injection: experience to date and best practice. Report 2013/13. Oct 2013

Ivandic M, Yang C, Lüth S, Cosma C, Juhlin C (2012) Time-lapse analysis of sparse 3D seismic data from the CO_2 storage pilot site at Ketzin, Germany. J Appl Geophys 84:14–28

Ivanova A, Kashubin A, Juhojuntti N, Kummerow J, Henninges J, Juhlin C, Lüth S, Ivandic M (2012) Monitoring and volumetric estimation of injected CO_2 using 4D seismic, petrophysical data, core measurements and well logging: a case study at Ketzin, Germany. Geophys Prospect 60:957–973

Jäger R, Mann J, Höcht G, Hubral P (2001) Common-reflection-surface stack: image and attributes. Geophysics 66:97–109

Javandel I, Doughty C, Tsang C-F (1984) Groundwater transport: handbook of mathematical models. Am Geophys Union

Jenkins CR, Cook PJ, Ennis-King J, Undershultz J, Boreham C, Dance T, de Caritat P, Etheridge DM, Freifeld BM, Hortle A, Kirste D, Paterson L, Pevzner R, Schacht U, Sharma S, Stalker L, Urosevic M (2012) Safe storage and effective monitoring of CO_2 in depleted gas fields. Proc Natl Acad Sci 109:E35–E41

Johnson G, Mayer B, Nightingale M, Shevalier M, Hutcheon I (2011a) Using oxygen isotope ratios to quantitatively assess trapping mechanisms during CO_2 injection into geological reservoirs: the Pembina case study. Chem Geol 283:185–193

Johnson G, Mayer B, Shevalier M, Nightingale M, Hutcheon I (2011b) Tracing the movement of CO_2 injected into a mature oilfield using carbon isotope abundance ratios: the example of the Pembina Cardium CO_2 monitoring project. Int J Greenh Gas Control 5:933–941

Jones DG, Lister TR, Smith DJ, West JM, Coombs P, Gadalia A, Brach M, Annunziatellis A, Lombardi S (2011) In Salah gas CO_2 storage JIP: surface gas and biological monitoring. Energy Procedia. In: 10th international conference on greenhouse gas control technologies, vol 4, pp 3566–3573

Juhlin C, Young R (1993) Implications of thin layers for amplitude variation with offset (AVO) studies. Geophysics 58:1200–1204

Juhlin C, Giese R, Zinck-Jørgensen K, Cosma C, Kazemeini H, Juhojuntti N, Lüth S, Norden B, Förster A (2007) 3D baseline seismics at Ketzin, Germany: the project. Geophysics 72:B121–B132

Kashubin A, Juhlin C, Malehmir A, Lüth S, Ivanova A, Juhojuntti N (2011) A footprint of rainfall on land seismic data repeatability at the CO_2 storage pilot site, Ketzin, Germany. In: Presented at the 2011 SEG annual meeting, Society of Exploration Geophysicists

Kazemeini SH, Juhlin C, Fomel S (2010) Monitoring CO_2 response on surface seismic data; a rock physics and seismic modeling feasibility study at the CO_2 sequestration site, Ketzin, Germany. J Appl Geophys 71:109–124

Kearey P, Brooks M, Hill I (2002) An introduction to geophysical exploration, 3rd edn. Wiley, Hoboken

Kharaka YK, Hanor JS (2003) Deep fluids in the continents: I. Sedimentary basins. Treatise Geochem 5:605

Kharaka YK, Cole DR, Hovorka SD, Gunter WD, Knauss KG, Freifeld BM (2006) Gas-water-rock interactions in Frio Formation following CO_2 injection: Implications for the storage of greenhouse gases in sedimentary basins. Geology 34:577–580

Kiessling D, Schmidt-Hattenberger C, Schuett H, Schilling F, Krueger K, Schoebel B, Danckwardt E, Kummerow J (2010) Geoelectrical methods for monitoring geological CO_2 storage: first results from cross-hole and surface–downhole measurements from the CO_2SINK test site at Ketzin (Germany). Int J Greenh Gas Control 4:816–826

Kirsch DR (2006) Petrophysical properties of permeable and low-permeable rocks. In: Kirsch DR (ed) Groundwater geophysics. Springer, Berlin, pp 1–22

Kragh E, Christie P (2002) Seismic repeatability, normalized rms, and predictability. Lead Edge 21:640–647

LaForce T, Ennis-King J, Boreham C, Paterson L (2014) Residual CO_2 saturation estimate using noble gas tracers in a single-well field test: the CO2CRC Otway project. Int J Greenhouse Gas Control 26:9–21

Landrø M (2001) Discrimination between pressure and fluid saturation changes from time-lapse seismic data. Geophysics 66:836–844

Lange G (1997) Gleichstromgeoelektrik. In: Knödel K, Krummel H, Lange G (eds) Handbuch zur Erkundung des Untergrundes von Deponien und Altlasten. Band 3: Geophysik. Springer, Berlin

Lay T, Wallace TC (1995) Modern global seismology, 1st edn. Academic Press, San Diego

Lee M (2011) Connectivity equation and Shaly-Sand correction for electrical resistivity (USGS scientific investigations report 2011–5005)

Liebscher A, Martens S, Moller F, Kuhn M (2013a) 12-on-shore CO_2 storage at the Ketzin pilot site in Germany. Geological storage of carbon dioxide (CO_2). Woodhead Publishing, Sawston, pp 278–300

Liebscher A, Möller F, Bannach A, Köhler S, Wiebach J, Schmidt-Hattenberger C, Weiner M, Pretschner C, Ebert K, Zemke J (2013b) Injection operation and operational pressure–temperature monitoring at the CO_2 storage pilot site Ketzin, Germany—design, results, recommendations. Int J Greenh Gas Control 15:163–173

Liu Y, Schmitt DR (2003) Amplitude and AVO responses of a single thin bed. Geophysics 68:1161–1168

Luquot L, Gouze P (2009) Experimental determination of porosity and permeability changes induced by massive injection of CO_2 into carbonate reservoirs. Chem Geol 265(1–2):148–159

Martens S, Kempka T, Liebscher A, Lüth S, Möller F, Myrttinen A, Norden B, Schmidt-Hattenberger C, Zimmer M, Kühn M, Group TK (2012) Europe's longest-operating on-shore CO_2 storage site at Ketzin, Germany: a progress report after three years of injection. Environ Earth Sci 67:323–334

Martens S, Liebscher A, Möller F, Würdemann H, Schilling F, Kühn M (2011) Progress report on the first european on-shore CO_2 storage site at ketzin (Germany)—second year of injection. Energy Procedia. In: 10th international conference on greenhouse gas control technologies, vol 4, pp 3246–3253

Martens S, Liebscher A, Möller F, Henninges J, Kempka T, Lüth S, Norden B, Prevedel B, Szizybalski A, Zimmer M, Kühn M, Group K (2013) CO_2 storage at the Ketzin pilot site, Germany: fourth year of injection, monitoring, modelling and verification. Energy Procedia. In: GHGT-11 proceedings of the 11th international conference on greenhouse gas control technologies, 18–22 Nov 2012, Kyoto, Japan 37, pp 6434–6443

Mathieson A, Midgely J, Wright I, Saoula N, Ringrose P (2011) In Salah CO_2 storage JIP: CO_2 sequestration monitoring and verification technologies applied at Krechba, Algeria. Energy Procedia. In: Proceedings of 10th international conference on greenhouse gas control technologies. IEA Greenhouse Gas Programme, Amsterdam, The Netherlands, vol 4, pp 3596–3603

Matter JM, Takahashi T, Goldberg D (2007) Experimental evaluation of in situ CO_2–water–rock reactions during CO_2 injection in basaltic rocks: implications for geological CO_2 sequestration. Geochem Geophys Geosyst 8:Q02001

Mavko G, Mukerji T (1998) Bounds on low-frequency seismic velocities in partially saturated rocks. Geophysics 63:918–924

Mavko G, Mukerji T, Dvorkin J (2003) The rock physics handbook: tools for seismic analysis of porous media. Cambridge University Press, Cambridge

Mayne WH (1962) Common reflection point horizontal data stacking techniques. Geophysics 27:927–938

McCallum SD, Riestenberg DE, Cole DR, Freifeld BM, Trautz RC, Hovorka SD, Phelps TJ (2005) Monitoring geologically sequestered CO_2 during the Frio Brine pilot test using perfluoro-carbon tracers

Meadows MA (2013) 4D rock and fluid properties analysis at the Weyburn Field, Saskatchewan. Int J Greenh Gas Control. The IEAGHG Weyburn-Midale CO_2 monitoring and storage project 16(Suppl 1):S134–S145

Meadows MA, Cole SP (2013) 4D seismic modeling and CO_2 pressure-saturation inversion at the Weyburn Field, Saskatchewan. Int J Greenh Gas Control. The IEAGHG Weyburn-Midale CO_2 monitoring and storage project 16(Suppl 1):S103–S117

Meissner R, Meixner E (1969) Deformation of seismic wavelets by thin layers and layered boundaries. Geophys Prospect 17:1–27

Michael K, Golab A, Shulakova V, Ennis-King J, Allinson G, Sharma S, Aiken T (2010) Geological storage of CO_2 in saline aquifers—a review of the experience from existing storage operations. Int J Greenh Gas Control 4:659–667

Myers M, Stalker L, Ross A, Dyt C, Ho K-B (2012) Method for the determination of residual carbon dioxide saturation using reactive ester tracers. Appl Geochem 27:2148–2156

Myers M, Stalker L, Pejcic B, Ross A (2013a) Tracers—past, present and future applications in CO_2 geosequestration. Appl Geochem 30:125–135

Myers M, White C, Pejcic B, Stalker L, Ross A (2013b) Chemical tracer partition coefficients for CCS (no. EP133018). Chemical Tracer Partition Coefficients for CCS, CSIRO

Nakatsuka Y, Xue Z, Garcia H, Matsuoka T (2010) Experimental study on CO_2 monitoring and quantification of stored CO_2 in saline formations using resistivity measurements. Int J Greenh Gas Control. The ninth international conference on greenhouse gas control technologies 4:209–216

NETL (2012) BEST PRACTICES for monitoring, verification, and accounting of CO_2 stored in deep geologic formations—2012 update. DOE/NETL-2012/1568 second edition. US National Energy Technology Laboratory www.netl.doe.gov

Niemi A, Bensabat J, Shtivelman V, Edlmann K, Gouze P, Luquot L, Hingerl F, Benson SM, Pezard PA, Rasmusson K, Liang T, Fagerlund F, Gendler M, Goldberg I, Tatomir A, Lange T, Sauter M, Freifeld B (2016) Heletz experimental site overview, characterization and data analysis for CO_2 injection and geological storage. Int J of Greenhouse Gas Control 48:3–23

Nilsen MH, Herrera PA, Ashraf M, Ligaarden I, Iding M, Hermanrud C, Lie K-A, Nordbotten JM, Dahle HK, Keilegavlen E (2011) Field-case simulation of CO_2-plume migration using vertical-equilibrium models. Energy Procedia. In: 10th international conference on greenhouse gas control technologies, vol 4, pp 3801–3808

Njiekak G, Schmitt DR, Yam H, Kofman RS (2013) CO_2 rock physics as part of the Weyburn-Midale geological storage project. Int J Greenh Gas Control. The IEAGHG Weyburn-Midale CO_2 monitoring and storage project 16(Suppl 1):S118–S133

Nooner SL, Eiken O, Hermanrud C, Sasagawa GS, Stenvold T, Zumberge MA (2007) Constraints on the in situ density of CO_2 within the Utsira formation from time-lapse seafloor gravity measurements. Int J Greenh Gas Control. In: 8th international conference on greenhouse gas control technologies GHGT-8 1, pp 198–214

Noordman WH, De Boer GJ, Wietzes P, Volkering F, Janssen DB (2000) Assessment of the use of partitioning and interfacial tracers to determine the content and mass removal rates of nonaqueous phase liquids. Environ Sci Technol 34:4301–4306

Norden B, Förster A, Vu-Hoang D, Marcelis F, Springer N, Le Nir I (2010) Lithological and petrophysical core-log interpretation in CO2SINK, the European CO_2 onshore research storage and verification project. SPE Reserv. Eval, Eng 13

Nottebohm M, Licha T, Sauter M (2012) Tracer design for tracking thermal fronts in geothermal reservoirs. Geothermics 43:37–44

Oye V, Aker E, Daley TM, Kühn D, Bohloli B, Korneev V (2013) Microseismic monitoring and interpretation of injection data from the in Salah CO_2 storage site (Krechba), Algeria. Energy Procedia. In: GHGT-11 proceedings of the 11th international conference on greenhouse gas control technologies, 18–22 Nov 2012, Kyoto, Japan 37, pp 4191–4198

Park J, Fawad M, Viken I, Aker E, Bjørnaråa TI (2013) CSEM sensitivity study for Sleipner CO_2-injection monitoring. Energy Procedia. In: GHGT-11 proceedings of the 11th international conference on greenhouse gas control technologies, 18–22 Nov 2012, Kyoto, Japan 37, pp 4199–4206

Picard G, Bérard T, Chabora E, Marsteller S, Greenberg S, Finley RJ, Rinck U, Greenaway R, Champagnon C, Davard J (2011) Real-time monitoring of CO_2 storage sites: application to illinois Basin–Decatur project. Energy Procedia. In: 10th international conference on greenhouse gas control technologies, vol 4, pp 5594–5598

Poupon A, Loy ME, Tixier MP (1954) A contribution to electrical log interpretation in Shaly Sands. J Pet Technol 6:27–34

Preston C, Monea M, Jazrawi W, Brown K, Whittaker S, White D, Law D, Chalaturnyk R, Rostron B (2005) IEA GHG Weyburn CO_2 monitoring and storage project. Fuel Process Technol 86:1547–1568

Prevedel B, Wohlgemuth L, Henninges J, Krüger K, Norden B, Förster A, CO2SINK Drilling Group (2008) The CO2SINK boreholes for geological storage testing. Sci Drill

Prevedel B, Wohlgemuth L, Legarth B, Henninges J, Schütt H, Schmidt-Hattenberger C, Norden B, Förster A, Hurter S (2009) The CO_2SINK boreholes for geological CO_2-storage testing. Energy Procedia. In: Proceedings of the 9th international conference on greenhouse gas control technologies 9 (GHGT-9), 16–20 Nov 2008, Washington DC, USA 1, pp 2087–2094

Pruess K, Oldenburg CM, Moridis GJ (1999) TOUGH2 user's guide version 2. Lawrence Berkeley National Laboratory, Berkeley

Rasmusson K, Rasmusson M, Fagerlund F, Bensabat J, Tsang Y, Niemi A (2014) Analysis of alternative push–pull-test-designs for determining in situ residual trapping of carbon dioxide. Int J Greenh Gas Control 27:155–168. doi:10.1016/j.ijggc.2014.05.008

Rassenfoss S (2012) Fiber optic sensing—learning how it really feels downhole. J Pet Technol 64:36–43

Rhoades JD, Manteghi NA, Shouse PJ, Alves WJ (1989) Soil electrical conductivity and soil salinity: new formulations and calibrations. Soil Sci Soc Am J 53:433

Ringrose P, Atbi M, Mason D, Espinassous M, Myhrer Ø, Iding M, Mathieson A, Wright I (2009) Plume development around well KB-502 at the In Salah CO_2 storage site. First Break 27

Ringrose PS, Mathieson AS, Wright IW, Selama F, Hansen O, Bissell R, Saoula N, Midgley J (2013) The in Salah CO_2 storage project: lessons learned and knowledge transfer. Energy Procedia 37:6226–6236

Ross C (2000) Effective AVO crossplot modeling: a tutorial. Geophysics 65:700–711

Rutqvist J, Vasco DW, Myer L (2010) Coupled reservoir-geomechanical analysis of CO_2 injection and ground deformations at In Salah, Algeria. Int J Greenh Gas Control. The ninth international conference on greenhouse gas control technologies, vol 4, pp 225–230

Sakurai S, Ramakrishnan TS, Boyd A, Mueller N, Hovorka S (2006) Monitoring saturation changes for CO_2 sequestration: petrophysical support of the Frio brine pilot experiment. Petrophysics 47

Schaffer M, Maier F, Licha T, Sauter M (2013) A new generation of tracers for the characterization of interfacial areas during supercritical carbon dioxide injections into deep saline aquifers: kinetic interface-sensitive tracers (KIS tracer). Int J Greenh Gas Control 14:200–208

Schmidt-Hattenberger C, Bergmann P, Kießling D, Krüger K, Rücker C, Schütt H, Group K (2011) Application of a vertical electrical resistivity array (VERA) for monitoring CO_2 migration at the Ketzin site: first performance evaluation. Energy Procedia. In: 10th International conference on greenhouse gas control technologies, vol 4, pp 3363–3370

Shevalier M, Nightingale M, Mayer B, Hutcheon I, Durocher K, Perkins E (2013) Brine geochemistry changes induced by CO_2 injection observed over a 10 year period in the Weyburn oil field. Int J Greenh Gas Control. The IEAGHG Weyburn-Midale CO_2 monitoring and storage project 16(Suppl 1):S160–S176

Shuey R (1985) A simplification of the Zoeppritz equations. Geophysics 50:609–614

Singh VP, Cavanagh A, Hansen H, Nazarian B, Iding M, Ringrose PS (2010) Reservoir modeling of CO_2 plume behavior calibrated against monitoring data from Sleipner. Society of Petroleum Engineers, Norway

Strazisar BR, Wells AW, Diehl JR, Hammack RW, Veloski GA (2009) Near-surface monitoring for the ZERT shallow CO_2 injection project. Int J Greenh Gas Control 3:736–744

Tatomir A, Maier F, Schaffer M, Licha T, Sauter M (2013) Modelling of Kinetic Interface Sensitive Tracers for Two-Phase Systems. In: Hou MZ, Xie H, Were P (eds) Clean energy systems in the subsurface: production, storage and conversion. Springer Series in Geomechanics and Geoengineering, Berlin, pp 65–74

Tatomir AB, Schaffer M, Kissinger A, Hommel J, Nuske P, Licha T, Helmig R, Sauter M (2015) Novel approach for modeling kinetic interface-sensitive (KIS) tracers with respect to time-dependent interfacial area change for the optimization of supercritical carbon dioxide injection into deep saline aquifers. Int J Greenhouse Gas Control 33:145–153

Telford WM, Telford WM, Geldart LP, Sheriff RE (1990) Applied geophysics. Cambridge University Press, Cambridge

Theis CV (1935) The relation between the lowering of the Piezometric surface and the rate and duration of discharge of a well using ground-water storage. EOS Trans Am Geophys Union 16:519–524

Todd T, Simmons G (1972) Effect of pore pressure on the velocity of compressional waves in low-porosity rocks. J Geophys Res 77:3731–3743

Tomich JF, Dalton RL, Deans HA, Shallenberger LK (1973) Single-well tracer method to measure residual oil saturation. J Pet Technol 25:211–218. doi:10.2118/3792-PA

Tong F, Niemi A, Yang Z, Fagerlund F, Licha T, Sauter M (2013) A numerical model of tracer transport in a non-isothermal two-phase flow system for CO_2 geological storage characterization. Transp Porous Media 98:173–192

Underschultz J, Boreham C, Dance T, Stalker L, Freifeld B, Kirste D, Ennis-King J (2011) CO_2 storage in a depleted gas field: an overview of the CO_2CRC Otway Project and initial results. Int J Greenh Gas Control 5:922–932

van Genuchten MT (1980) A closed-form equation for predicting the hydraulic conductivity of unsaturated soils 1. Soil Sci Soc Am J 44:892

Vandeweijer V, van der Meer B, Hofstee C, Mulders F, D'Hoore D, Graven H (2011) Monitoring the CO_2 injection site: K12-B. Energy Procedia 4:5471–5478

Vasco D, Ferretti A, Novali F (2008) Reservoir monitoring and characterization using satellite geodetic data: interferometric synthetic aperture radar observations from the Krechba field, Algeria. GEOPHYSICS 73, WA113-WA122

Vasco DW, Rucci A, Ferretti A, Novali F, Bissell RC, Ringrose PS, Mathieson AS, Wright IW (2010) Satellite-based measurements of surface deformation reveal fluid flow associated with the geological storage of carbon dioxide. Geophys Res Lett 37:L03303

Verdon JP, Kendall J-M, White DJ, Angus DA (2011) Linking microseismic event observations with geomechanical models to minimise the risks of storing CO_2 in geological formations. Earth Planet Sci Lett 305:143–152

Verdon JP, Kendall J-M, Stork AL, Chadwick RA, White DJ, Bissell RC (2013) Comparison of geomechanical deformation induced by megatonne-scale CO_2 storage at Sleipner, Weyburn, and In Salah. Proc Natl Acad Sci 110:E2762–E2771

Vulava VM, Perry EB, Romanek CS, Seaman JC (2002) Dissolved gases as partitioning tracers for determination of hydrogeological parameters. Environ Sci Technol 36:254–262

Wang Y (1999) Approximations to the Zoeppritz equations and their use in AVO analysis. Geophysics 64:1920–1927

Watts M (2003) High temperature circuit reliability testing. Quartzdyne, Inc, Salt Lake City

Waxman MH, Thomas EC (1974) Electrical conductivities in Shaly Sands-I. The relation between hydrocarbon saturation and resistivity index; II. The temperature coefficient of electrical conductivity. J Pet Technol 26:213–225

Wells AW, Diehl JR, Bromhal G, Strazisar BR, Wilson TH, White CM (2007) The use of tracers to assess leakage from the sequestration of CO_2 in a depleted oil reservoir, New Mexico, USA. Appl Geochem 22:996–1016

Wells A, Strazisar B, Diehl JR, Veloski G (2010) Atmospheric tracer monitoring and surface plume development at the ZERT pilot test in Bozeman, Montana, USA. Environ Earth Sci 60:299–305

White DJ (2011) Geophysical monitoring of the Weyburn CO_2 flood: results during 10 years of injection. Energy Procedia. In: 10th international conference on greenhouse gas control technologies, vol 4, pp 3628–3635

White D (2013a) Seismic characterization and time-lapse imaging during seven years of CO_2 flood in the Weyburn field, Saskatchewan, Canada. Int J Greenh Gas Control. The IEAGHG Weyburn-Midale CO_2 monitoring and storage project 16(Suppl 1):S78–S94

White DJ (2013b) Toward quantitative CO_2 storage estimates from time-lapse 3D seismic travel times: an example from the IEA GHG Weyburn–Midale CO_2 monitoring and storage project. Int J Greenh Gas Control. The IEAGHG Weyburn-Midale CO_2 monitoring and storage project 16(Suppl 1):S95–S102

Whittaker (2004) Geological framework. In: Presented at the 7th international conference on greenhouse gas control technologies, Vancouver, Canada

Widess MB (1973) How thin is a thin bed? Geophysics 38:1176–1180

Wildgust N, Gilboy C, Tontiwachwuthikul P (2013) Introduction to a decade of research by the IEAGHG Weyburn-Midale CO_2 monitoring and storage project. Int J Greenh Gas Control 16: S1–S4

Wood AB (1941) A textbook of sound: being an account of the physics of vibrations with special reference to recent theoretical and technical developments. Bell, London

Worthington PF (1985) The evolution of Shaly-sand concepts in reservoir evaluation. Log Anal 26

Xu T, Kharaka YK, Doughty C, Freifeld BM, Daley TM (2010) Reactive transport modeling to study changes in water chemistry induced by CO_2 injection at the Frio-I Brine Pilot. Chem Geol 271:153–164

Yilmaz Ö (2001) Seismic data analysis. Investigations in Geophysics. Society of Exploration Geophysicists

Zemke K, Liebscher A, Wandrey M (2010) Petrophysical analysis to investigate the effects of carbon dioxide storage in a subsurface saline aquifer at Ketzin, Germany (CO2SINK). Int J Greenh Gas Control. CO_2 storage at the EGU general assembly 2009 4:990–999

Zettlitzer M, Moeller F, Morozova D, Lokay P, Würdemann H (2010) Re-establishment of the proper injectivity of the CO_2-injection well Ktzi 201 in Ketzin, Germany. Int J Greenh Gas Control. CO_2 storage at the EGU general assembly 2009 4:952–959

Zhang Y, Freifeld B, Finsterle S, Leahy M, Ennis-King J, Paterson L, Dance T (2011) Single-well experimental design for studying residual trapping of supercritical carbon dioxide. Int J Greenh Gas Control 5:88–98

Zimmer M, Erzinger J, Kujawa C (2011) The gas membrane sensor (GMS): a new method for gas measurements in deep boreholes applied at the CO2SINK site. Int J Greenh Gas Control 5:995–1001. doi:10.1016/j.ijggc.2010.11.007

Zoeppritz K (1919) VII b. Über Reflexion und Durchgang seismischer Wellen durch Unstetigkeitsflächen. Nachrichten Von Ges. Wiss Zu Gött Math Phys Kl 1919:66–84